AER/AGS Open File Report 2025-04

Alberta Energy Regulator

Origin of Lithium and Other Alkali Metals in Devonian Oil Brines of Alberta

AGS
ALBERTA GEOLOGICAL SURVEY

AER/AGS Open File Report 2025-04

Origin of Lithium and Other Alkali Metals in Devonian Oil Brines of Alberta

N.F. Bernal

Alberta Energy Regulator
Alberta Geological Survey

January 2026

ISBN 978-1-4601-5736-7

If you use information from this publication in other publications or presentations, please acknowledge the AER/AGS. We recommend the following reference format:

Bernal, N.F. (2026): Origin of lithium and other alkali metals in Devonian oil brines of Alberta; Alberta Energy Regulator / Alberta Geological Survey, AER/AGS Open File Report 2025-04, 67 p.

Publications in this series have undergone only limited review and are released essentially as submitted by the author.

Published January 2026 by:
Alberta Energy Regulator
Alberta Geological Survey
Suite 205
4999 – 98 Avenue NW
Edmonton, AB T6B 2X3
Canada

Tel: 780.638.4491
Email: AGS-Info@aer.ca
Website: ags.aer.ca

Contents

Tables

Figures

Acknowledgements

This research is a contribution to the Alberta Geological Survey's Mineral Mapping Program, which has been made possible through funding from the Government of Alberta. The program plays a crucial role in supporting the implementation of the province's mineral strategy and action plan released in 2021. The AGS also acknowledge the oil and gas operators for their cooperation and consent in allowing brine sampling from their wells. The author gratefully acknowledges Dan Palombi for his thorough scientific review.

Abstract

The increasing demand for electrified transportation and the need for energy storage solutions to support intermittent renewable energy generation, such as solar and wind power, have sparked significant interest in essential critical minerals and metals, including lithium (Li). Traditional battery technologies rely heavily on lithium, and alternative sources, such as the oil brines of the Alberta Basin, are now being considered more than ever before due to economic improvements in Li extraction methods and reduced environmental impacts when compared to traditional technologies such as hard rock mining and salar evaporation ponds. Therefore, these brines have the potential to become a sustainable and accessible option for battery manufacturers in North America. To explore this mineral development opportunity further, the Alberta Geological Survey (AGS) conducted a comprehensive brine sampling program in collaboration with oil and gas industry operators. Previous studies evaluated the occurrence of lithium in Devonian oil brines of Alberta; however, there is still much to understand about the origin, accumulation, and transport mechanisms of this metal in the Alberta Basin. The chemistry of these brines provides evidence of processes involved in the removal, transport, and accumulation of lithium. Identifying these processes is crucial for developing known existing deposits and locating new areas that have not been explored by oil and gas wells but may contain economically viable lithium concentrations.

For this study, 178 Devonian oil brine samples were investigated, representing a subset of 288 samples reported from the 2021–2024 AGS brine sampling program. In addition, AGS selected 81 Devonian samples from previous publications based on the availability of isotopic and halogen data to complement the dataset. The samples were collected from the Granite Wash, Keg River Formation, Gilwood Member of the Watt Mountain Formation, Beaverhill Lake Group (including the Swan Hills and Slave Point formations), Cooking Lake, Leduc, and Nisku formations, and the Wabamun Group. Given the complex history of these brines, conservative species were analyzed to gather geochemical information while accounting for the effects of evaporation, diagenesis, mixing, precipitation, dissolution, and reprecipitation. Apart from major ions and dissolved metals, the analysis included halogens (chlorine and bromine), alkali metals (rubidium, cesium, lithium, potassium, and sodium), and isotopes of oxygen ($\delta^{18}O$), hydrogen ($\delta^{2}H$), lithium ($\delta^{7}Li$), boron ($\delta^{11}B$), sulphur ($\delta^{34}S$), and strontium ($^{87}Sr/^{86}Sr$).

The Devonian oil brines of the Alberta Basin can be classified into two primary groups: Lower–Middle Devonian and Middle–Upper Devonian. The differentiation between these groups is based on their distribution of $\delta^{2}H$ and $\delta^{18}O$ values and their rubidium/cesium molar ratios. Additionally, their $\delta^{7}Li$ and $\delta^{11}B$ compositions indicate that Li may have been adsorbed from seawater and accumulated within fine-grained marine sediments that may have also been enriched in Li. The $^{87}Sr/^{86}Sr$ values derived from these samples reveal the migration paths taken by these Li-enriched fluids, which may have been expelled from clays and other fine-grained lithologies during the Laramide orogeny and were subsequently mixed with residual evaporitic brines and low Li fluids related to the basement. These brines have undergone further alterations due to diagenetic processes, evaporation, water-rock interactions, and different degrees of mixing with meteoric waters.

This work was completed under the Mineral Grant provided by the Government of Alberta on June 22, 2021.

1 Introduction

Lithium (Li) is one of the elements currently in high demand due to its application in battery technology. Part of the interest in Li stems from its outstanding capabilities to store and transmit electricity, as well as its applications in ceramics, polymers, pharmaceuticals, and glass. The demand for Li batteries has increased dramatically over the last few years, driven by the global push to electrify transportation. The success of pioneering electric vehicles (EVs) has spurred many car manufacturers to focus on developing a model line of EVs, with some planning to phase out internal combustion engines within a decade. On the other hand, without energy storage systems, the now massively adopted green energy technologies of solar and wind will not be able to advance the energy transition due to their intermittent energy generation limitation. Despite considerable efforts to develop new battery technologies, Li batteries remain the most reliable option for energy storage. According to Bradley et al. (2017), the estimated availability of the Li resource is 39 million tonnes, which is sufficient to meet demand until the end of the 21st century. However, most of this Li remains underground, and there is concern that new mining projects will take too long to meet increasing demand (International Energy Agency, 2021).

Lithium has been traditionally extracted from pegmatites, continental brines, and hydrothermally altered clays, which can contain Li concentrations from 100s to 1000s of mg/L (Munk et al., 2016). Brines reached by deep oil and gas wells, which are usually a waste product of the hydrocarbon extraction process, are not included in the three main Li-deposit groups because commercially exploitable Li (>80 mg/L) is not common in these forms of brines. These oilfield brines and formation waters in aquifers and reservoirs associated with petroleum will be referred to as 'oil brines' in this report.

In Alberta, Li is anomalously high in Devonian oil brines. Several studies (Bachu et al., 1995; Eccles and Jean, 2010; Hitchon et al., 1995) have reported Li concentrations between 10 and 40 mg/L in most Devonian brine samples, but some areas, also reported in these studies, are well-known for brines with Li concentrations above 70 mg/L. Continental brine mines, such as those currently exploited in the ABC triangle (i.e., Argentina, Bolivia, and Chile), contain the largest Li reserves in the world, accounting for 43.6% of total reserves (Grosjean et al., 2012). However, Li extraction from these deposits is expensive as the mines are in remote locations and difficult to access. In addition, lithium extraction from salars is criticized for its significant water usage and waste generation (Flexer et al., 2018; Jiang et al., 2020; Kaunda, 2020). Mining operations secure large quantities of fresh water from groundwater wells, which exacerbates the naturally arid conditions of these regions. This environmental stress is further aggravated by the creation of evaporation waste, which can threaten freshwater aquifers and harm the local ecosystems (flora and fauna). Pegmatites and hydrothermally altered clay deposits, which require intensive mining operations, also demand considerable land and energy for extracting and processing the Li ore. In contrast, oil brines are accessed through deep wells and are typically a by-product of the hydrocarbon extraction process.

Mining oil brines in Alberta can leverage existing infrastructure for extracting and transporting the product. Also, after Li extraction, the remaining brines can be injected into suitable reservoirs, minimizing environmental impact. This resource holds significant economic potential for Alberta, given the increasing demand for Li, a predicted market of scarcity, proximity to centres of consumption, the relatively low environmental impact of the Li extraction process from oil brines compared to Li ore mining operations, and the potential availability of this element in Alberta.

This study presents a geochemical interpretation of oil brine samples from Devonian formations collected during the Alberta Geological Survey (AGS) brine sampling program (2021–2024; Reimert et al., 2025) and earlier sampling events. The data comprise major ion, halogen, and alkali metal concentrations, and $\delta^{18}O$, $\delta^{2}H$, $\delta^{11}B$, $\delta^{7}Li$, $\delta^{34}S$, and $^{87}Sr/^{86}Sr$ isotope values. This information was collected to better understand the chemical evolution of these brines in more detail and identify the potential source(s) of Li and other economically valuable elements.

2 Study Area

The study area is a large region spanning from central to northwestern Alberta (Figure 1). In total, 259 oil brine samples sourced from Devonian strata were available for this report (Appendix 1, Tables 2 and 3), 178 of which were collected during the 2021–2024 AGS brine sampling program (Reimert et al., 2025), and the remaining 81 samples were reported in previous AGS publications (Huff et al., 2011, 2012; Lyster et al., 2022; Reimert et al., 2022).

The oil brine samples used for this investigation are from the diachronous Lower–Upper Devonian Granite Wash, the Middle Devonian Keg River Formation and Gilwood Member (Watt Mountain Formation) of the Elk Point Group, the Middle–Upper Devonian Beaverhill Lake Group (including the Slave Point and Swan Hills formations), and Upper Devonian Cooking Lake and Leduc formations (Woodbend Group), Nisku Formation (Winterburn Group), and Wabamun Group (Figures 1 and 2).

3 Background

There is considerable literature regarding the origin and evolution of oil brines in the Western Canada Sedimentary Basin (WCSB). These studies have been dedicated to a wide range of topics, including the origin of water in these brines, using stable isotope compositions ($\delta^{18}O$ and $\delta^{2}H$), and the relationship between salinity and diagenetic mineral alteration. Perhaps the earliest investigation into the origin of water in these brines was conducted by Clayton et al. (1966). The study found that the $\delta^{2}H$ and $\delta^{18}O$ compositions of oil brines from the Illinois, Michigan, and Alberta sedimentary basins have a meteoric origin. Clayton et al. (1966) also suggested oxygen exchange between the formation water and the reservoir rocks, as evidenced by the $\delta^{18}O$ compositions of the oil brines. However, given the regional character of the data used in Clayton et al. (1966), a description of the results for the Alberta formations was not provided.

Billings et al. (1969) identified five types of formation waters based on the chemistry of a set of samples from the WCSB, including those investigated by Clayton et al. (1966). According to Billings et al. (1969), two of the five types were the most relevant to explaining the origin of formation waters in the WCSB: (1) a membrane-concentrated formation water and a brine resulting from the mixing of membrane-filtration water and (2) a residual evaporitic brine formed after halite precipitation. This study also suggests that the alkali metals Rb, K, Na, and Li may have been sourced from clays and shales through a membrane-filtration process.

Along with chemical analyses, Hitchon and Friedman (1969) investigated stable isotopes of hydrogen and oxygen in surface waters, shallow potable formation waters, and formation waters from oil and gas fields in Alberta. In this study, the observations of Clayton et al. (1966) were investigated further to conclude that formation waters in the WCSB are diagenetically modified seawater mixed with at least 2.9 times meteoric water recharged at the same latitude. In addition, the authors estimated the isotopic fractionation of $\delta^{2}H$ resulted from water circulation through micropores in shales, which was found to be characteristic of such interaction.

Hitchon et al. (1971) investigated 78 samples from oil and gas fields in Alberta. Their analysis revealed that the primary factors influencing the chemistry of these brines were dilution by freshwater recharge and ion concentration through membrane filtration. This study proposed clays as an additional source of the Br and I in the oil brines. Also, as Billings et al. (1969) pointed out earlier, some alkali and alkali-earth metals are redistributed between rocks and fluids due to ion exchange on clays. In this work, the evolution of brines in the WCSB is summarized according to the following processes: solution of evaporites, mineral formation, cation exchange on clays, desorption of ions from clays and organic matter, and control by the solubility of minerals.

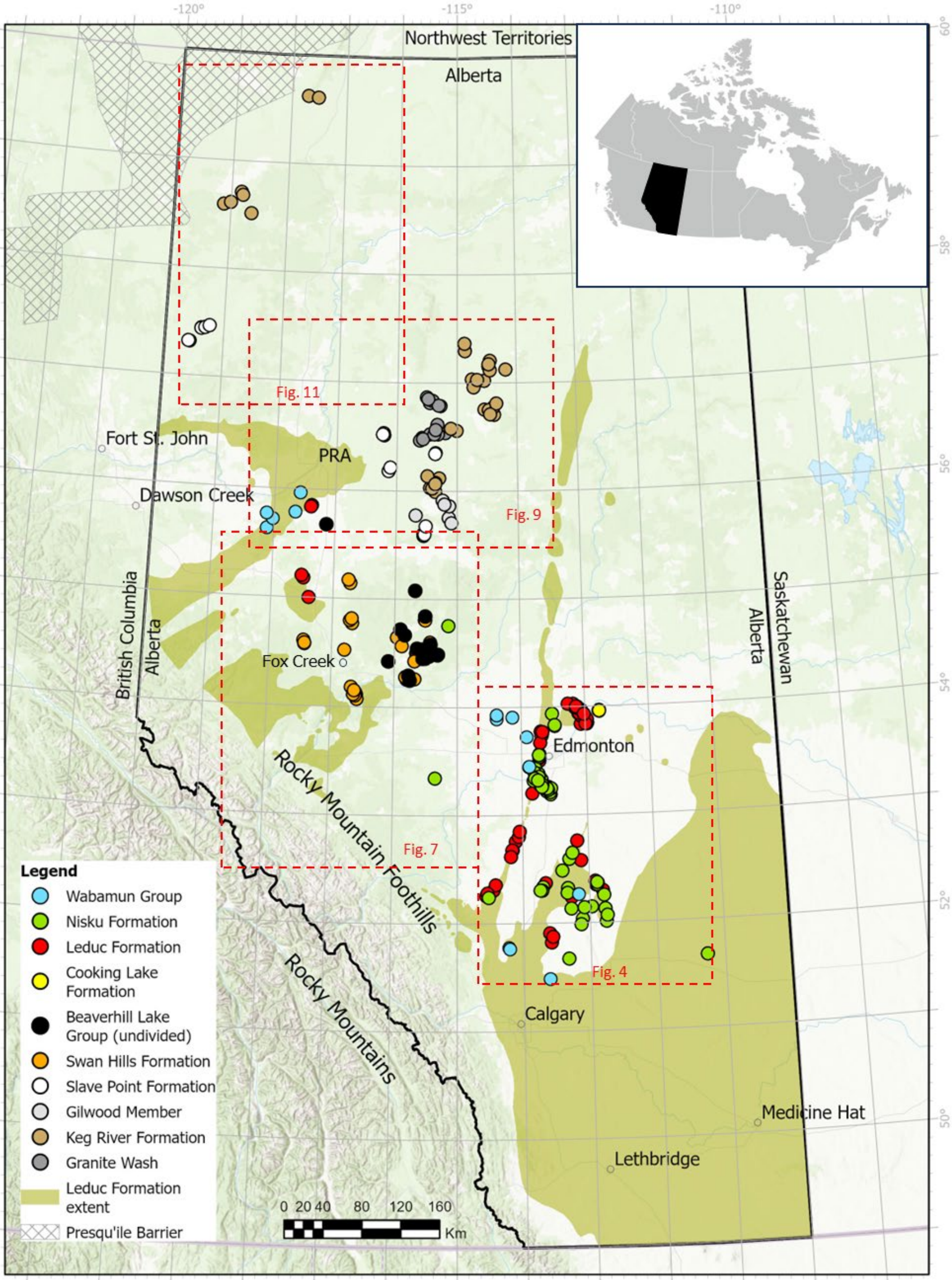

Figure 1. General locations of sampled wells in Alberta symbolized by the geological unit from which the oil brine samples were sourced: Lower–Upper Devonian Granite Wash; Middle Devonian Keg River Formation and Gilwood Member; Middle–Upper Devonian Beaverhill Lake Group (undivided and Swan Hills and Slave Point formations); Upper Devonian Cooking Lake and Leduc formations (Woodbend Group), Nisku Formation (Winterburn Group), and Wabamun Group. The dashed lines represent the study area boundaries and associated figures (Fig.) are noted. Abbreviation: PRA, Peace River Arch.

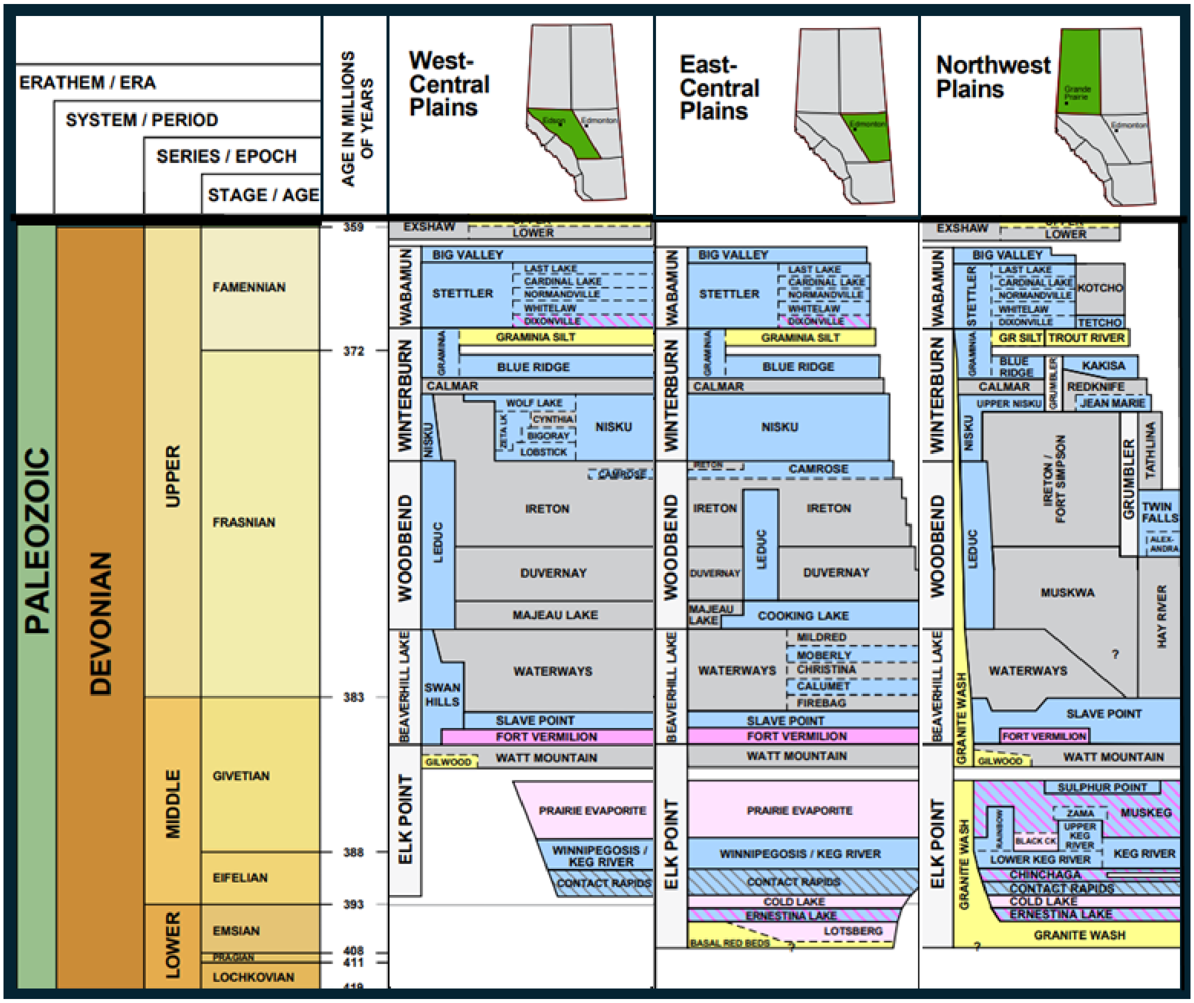

Figure 2. Table of formations for the Devonian in northern and central Alberta (modified after Alberta Geological Survey, 2019).

Spencer (1987) proposed that Cl and Br in the Devonian oil brines of the WCSB were formed after the dilution of residual evaporitic brines with fresh water. These brines reached the basement through a density-driven flux, which reached high temperatures (100°C–300°C). The fluid-rock interaction resulted in the albitization of feldspars and the migration of hot brines through faults and fractures to upper units, where dolomitization of carbonate rocks occurred.

Connolly et al. (1990a) investigated the origin and evolution of oil brines in the WCSB using alkalinity, anions, cations, H_2S contents, S isotopes, and short-chain aliphatic acids data. The authors distinguished three main brine groups in the WCSB, including those in Devonian to Cretaceous formations. Groups I and II corresponded to carbonate reservoirs where a seawater evaporitic brine was diluted 50% to 80% by meteoric water. Group III brines had lower salinity and were found in clastic reservoirs. This study argues that the chemistry of Group I brines was modified by clay mineral transformations in surrounding shale units. Significant leaching reactions from feldspar and clay minerals characterized Group II brines. Connolly et al. (1990b) performed Sr, O, and H isotope analyses on samples from formation waters in the WCSB and based on this information, proposed two different hydrogeological regimes in the basin: (1) Devonian–Lower Cretaceous aquifers, and (2) Upper Cretaceous and more recent sedimentary aquifer systems. They suggested that upward-directed cross-formational flow was superimposed on a predominantly lateral fluid flow system in the Devonian–Lower Cretaceous aquifers. In this investigation, brines from Devonian carbonate rocks returned $^{87}Sr/^{86}Sr$ values higher than those from younger formations. The source(s) of these high Sr isotope values were attributed to Devonian or Cambrian shales.

Hitchon et al. (1995) analyzed 130 000 samples from formation waters collected from drillstem tests in Alberta oil and gas reservoirs and saline aquifers. These data were combined with reported thickness, porosity, and permeability data for aquifers with Ca, Mg, K, Br, and Li concentrations that exceeded predefined exploration-level thresholds. The study concluded that the Leduc–Beaverhill Lake aquifer system in the Windfall–Swan Hills carbonate complex had the most potential for economic Li concentrations.

Using hydrochemical and hydrogeological mapping, Rostron and Tóth (1997) identified two large-scale cross-formational flow systems affecting the Mannville Group, the Upper Devonian Hydrogeologic Group and the Upper Jurassic–Lower Cretaceous flow regime. A high total dissolved solids (TDS) plume was detected in the Mannville Group, above the Bashaw reef complex (BRC). This was interpreted to be the result of changes in aquitard thickness, allowing mixing between ambient Mannville Group waters and ascending Upper Devonian oil brines and hydrocarbons. This agrees with previous conclusions in Connolly et al. (1990a) regarding cross-formational flow in Devonian–Lower Cretaceous aquifers. According to Rostron and Tóth (1997), their findings demonstrate that the Mannville Group is not isolated from adjacent strata in west-central Alberta.

Based on the increasing interest in Li, the AGS conducted a geochemical study to establish the origins of Li-enriched brines in the Swan Hills, Leduc, and Nisku formations (Eccles and Berhane, 2011). This study concluded that brines in the Swan Hills Formation were derived from halite dissolution and mixed with Li-enriched fluids from the Precambrian crystalline basement. In contrast, the study argues that salinity in the brines of the Nisku and Leduc formations is of evaporitic origin, and their Li enrichment is due to the dissolution of late-stage evaporite minerals. Huff (2016, 2019) further explored some of these ideas to explain the observed Li concentrations in the Leduc and Swan Hills formations. This work attributed high Li and Br concentrations to the remobilization/dissolution of potash minerals. According to their study, these late-stage evaporitic brines migrated from the east to mix with Upper Devonian oil brines in the west. The migration of these heavy brines from the east was explained by gravity-driven flow, which controlled the hydrogeology of the WCSB during the onset of the Laramide orogeny tectonics.

4 Methodology

4.1 Oil and Gas Well Sampling

For the AGS brine sampling program, sampling was conducted by AGAT Laboratories Ltd. (AGAT; Calgary, Alberta). To ensure the 178 samples collected were representative of the formation waters' chemistry and to prevent interference with other wells and contamination of the samples, the following protocol was agreed upon with the laboratory:

- wells were not to be sampled within a 5 km radius of other sampled wells or water flood / injection wells
- no commingled well production
- if samples were required to be taken off a separator, care had to be taken to confirm that there were no other wells in production
- the well was on production for at least 24 hours prior to sampling
- no well treatments had been done within 24 hours of sampling

4.2 Geochemical Analysis

The 178 brine samples retrieved from oil and gas wells were analyzed by AGAT, an accredited laboratory under the Standards Council of Canada (ISO/IEC 17025:2017; ISO Committee on Conformity

Assessment, 2017). AGAT outsourced all the isotope analyses presented in this report to ALS Scandinavia AB (Luleå, Sweden) and InnoTech Alberta (Victoria, British Columbia).

4.2.1 Anions and Cations

Analyses of anions (chloride, sulphate, and bromide) were performed according to Standard Method 4110 B (Standard Methods Committee of the American Public Health Association, American Water Works Association, and Water Environment Federation, 2023b) with one deviation. The eluent matrix was prepared according to the product manual for a Thermo Scientific™ Dionex™ IonPac™ AS22 column. Each sample was diluted to 10, 100, and 1000 times its original concentration. Then, each prepared dilution was injected into an eluent stream and passed through an ion exchanger. The anions of interest were separated based on their affinity to the anion exchanger. The separated anions were converted to their acid forms, and a conductivity detector measured the response; this signal generated a concentration from a prepared linear calibration of each analyte and each dilution. Identification was based on individual retention times, and validation was conducted with a third-party standard.

Analyses of cations (sodium, potassium, calcium, magnesium, and iron) were performed according to U.S. Environmental Protection Agency (EPA) Method 200.7 (U.S. Environmental Protection Agency, 1994) for inductively coupled plasma–atomic emission spectrometry (ICP-AES) with one deviation. The linear calibration range was extended to better accommodate samples with high salinity and minimize the need for excessive dilutions. The intensities of the spectra were monitored by a photosensitive device to yield concentrations based on calibration solutions run under the same conditions. A certified reference material was run to validate the accuracy of the calibration on the ICP-AES unit. A blank was run to confirm that the instrument background was lower than the detection limits for each analyte of interest.

4.2.2 Dissolved Metals

Dissolved metal determinations were performed using a modified version of Standard Method 3125B (Standard Methods Committee of the American Public Health Association, American Water Works Association and Water Environment Federation, 2023a) and EPA 1669 (U.S. Environmental Protection Agency, 1996) in a triple-quad inductively coupled plasma–mass spectrometer (ICP-MS). A certified reference material was run to validate the accuracy of the calibration on the ICP-MS unit. A low-level verification sample was used to verify the linearity of the calibration on the ICP-MS unit. A blank was run to confirm that the instrument background was lower than the detection limits for each analyte of interest. A blank spike and sample spike were also used to verify the instrument response.

4.2.3 Stable Isotopes

Hydrogen and oxygen isotopes in water were analyzed using a Thermo Scientific Delta V Advantage mass spectrometer with a dual inlet setup. Runs with Vienna Standard Mean Ocean Water (VSMOW) and Standard Light Antarctic Precipitation 2 (SLAP2) established the laboratory's in-house standards for properly reporting the isotopic compositions of the samples versus VSMOW. Results accuracy was ±0.1 per mil (‰) for $\delta^{2}H$ and ±0.2‰ for $\delta^{18}O$.

Lithium ($\delta^{7}Li$), boron ($\delta^{11}B$), and strontium ($^{87}Sr/^{86}Sr$) isotopes were measured with a multicollector (MC) ICP-MS instrument (Thermo Scientific Neptune Plus™) with correction for instrumental bias by bracketing standards. In-run precision (2 sigma) is typically better than 0.2‰ for Li and B and 0.03‰ for Sr. Results are within 0.5‰ for Li and B, and 0.1‰ for Sr.

Sulphur and oxygen isotope analyses were conducted by continuous-flow–isotope ratio mass spectrometry (CF-IRMS) employing an elemental analyzer for $\delta^{34}S$ or a Thermo Finnigan high temperature conversion elemental analyzer (TC/EA) for $\delta^{18}O$ linked to a gas source mass spectrometer. The standard reference materials for oxygen and sulphur were the VSMOW and Vienna Canyon Diablo Troilite (V-CDT). Reproducibility for $\delta^{34}S$ and $\delta^{18}O$ was ±0.2‰ and ±0.5‰, respectively.

4.3 Data Analysis

For the geochemical characterization of the Devonian oil brines, residual evaporitic brines and halite dissolution sources in formation waters were evaluated using halogens (Cl and Br). Additional sources of ions were assessed using alkali metals (Li, Na, K, Rb, and Cs). Water isotopes ($\delta^{18}O$ and $\delta^{2}H$) were applied to detect significant mixing trends with meteoric water and to identify water-rock interaction processes. Adsorption, accumulation, and transport of Li and B in Devonian oil brines were evaluated using lithium ($\delta^{7}Li$), boron ($\delta^{11}B$), and strontium ($^{87}Sr/^{86}Sr$) isotopes, as well as the secular variation of $\delta^{7}Li$ in seawater, and the existing fluid inclusion records for dolomites in carbonate reservoirs. In a select group of samples, the potential magmatic input and the effect of thermochemical reactions were assessed by using the isotope pairs chlorine ($\delta^{37}Cl$) and lithium ($\delta^{7}Li$), and oxygen ($\delta^{18}O$) and sulphur ($\delta^{34}S$) in SO_4, respectively.

5 Results

5.1 Origin of Water and the Isotope Record

Earlier work on the water isotope composition of brines in the WCSB recognized the influence of meteoric waters (Clayton et al., 1966). There is also evidence that Neogene meteoric recharge mixed with oil brines in the Devonian sequence of the WCSB (Connolly et al., 1990a). The relationship between $\delta^{18}O$ and $\delta^{2}H$ for the samples investigated (Figure 3) confirms mixing with meteoric waters, which is depicted by the distribution of samples from the Upper Devonian Leduc and Nisku formations and the Wabamun Group and the Middle–Upper Devonian Beaverhill Lake Group, including the Swan Hills Formation, along a straight line (mixing line 1). The distribution of samples from the Middle Devonian Gilwood Member and the Slave Point Formation indicates a second mixing trend (mixing line 2). The heavy isotopic compositions of some oil brines likely evolved from seawater (i.e., $\delta^{18}O$ is 0‰ and $\delta^{2}H$ is 0‰). This evolution follows a two-stage isotopic system, as described in previous studies (Gonfiantini, 1965; Holser, 1979; Pierre et al., 1984).

In Figure 3, stage 1 shows the isotopic enrichment of the oil brines as seawater evaporation increases. Stage 2 depicts the depletion of both isotopes, following a hook-like trajectory towards very negative values due to further evaporation. The arrowhead at the end of stage 2, located inside the 'Endmembers' box in Figure 3, indicates the range of isotopic values for the endmembers. Additionally, mixing with meteoric waters modifies the $\delta^{18}O$ and $\delta^{2}H$ makeup of the oil brines, resulting in mixing lines 1 and 2.

The isotopic compositions ($\delta^{18}O$ and $\delta^{2}H$) of the Devonian oil brines collected during the 2021–2024 AGS brine sampling program differentiate Lower–Middle from Middle–Upper Devonian oil brines. This implies that brines from the Granite Wash, Keg River Formation, Gilwood Member, and Slave Point Formation evolved independently from brines in the Beaverhill Lake Group (undivided), Swan Hills, Cooking Lake, Leduc, and Nisku formations, and Wabamun Group. This observation was based on the distribution of these brines along mixing line 1 and mixing line 2. The mixing trends were identified by deviations from the local meteoric water line (LMWL; Gibson et al., 2011). Mixing line 1 and mixing line 2 were defined by two endmembers, the Edmonton weighted average precipitation (EWAP) value and an isotopically heavier endmember from the Middle–Upper and Lower–Middle Devonian, respectively (Figure 3).

The isotopic composition of Upper Devonian oil brines (Figure 3) suggests the effect of water-rock interaction. This and other relevant geochemical processes will be discussed in more detail, focusing on the samples in the box outlined with a dashed red line in Figure 3 and their geographic and stratigraphic locations.

For ease of representation, the samples presented in this report are labelled with a two-letter code identifying the geological unit and a corresponding reference number. For instance, sample 29 from the

Leduc Formation is represented as LD29. Each sample has its corresponding unique well identifier (UWI) for reference. The label and the corresponding UWI for each sample are listed in Appendix 1, Table 2.

5.1.1 Central Alberta

The geographic distribution of oil brine samples collected from the Cooking Lake, Leduc, and Nisku formations, and Wabamun Group in central Alberta is shown in Figure 4. The isotopic compositions of these samples are shown in Figure 5. The Leduc Formation brine samples provide the most apparent spatial correlation between reef distribution and isotopic compositions. In Figure 5, samples with similar isotopic values are grouped in the Redwater reef (RWR), Homeglen-Rimbey reef (HGR), Golden Spike (GSR), and Wizard Lake reef (WLR), all part of the Rimbey-Meadowbrook reef trend (RMBRT), and BRC. Individual samples from GSR and WLR are used for reference.

Samples LD09, LD16, LD27, LD29, LD30, LD56, and LD57 from the BRC (Figure 4) contain $\delta^{18}O$ values from 6.5‰ to 7.9‰ (Figure 5) and chloride concentrations from 130 000 to 145 300 mg/L (Appendix 1, Table 2). The $\delta^{18}O$ shift in these samples is highest when compared to other Leduc Formation brines. This suggests the emplacement of a high-temperature fluid that exchanged oxygen-18 with the host rocks at these locations. On the other hand, it has been argued that the Cooking Lake and Leduc formations conform to an aquifer in the area of the BRC (Rostron and Tóth, 1997), which is supported by the distribution of $\delta^{18}O$ values and Cl concentrations measured in this study. Based on this hypothesis, it is conceivable that the Cooking Lake Formation in central Alberta contained a high-temperature fluid that reached overlying Devonian units. Based on the observed isotope distribution, this flow appears vertical in the BRC area. This interpretation implies that by the time these deep fluids ascended to shallower depths, considerable transmissivity had developed in the Leduc Formation reefs.

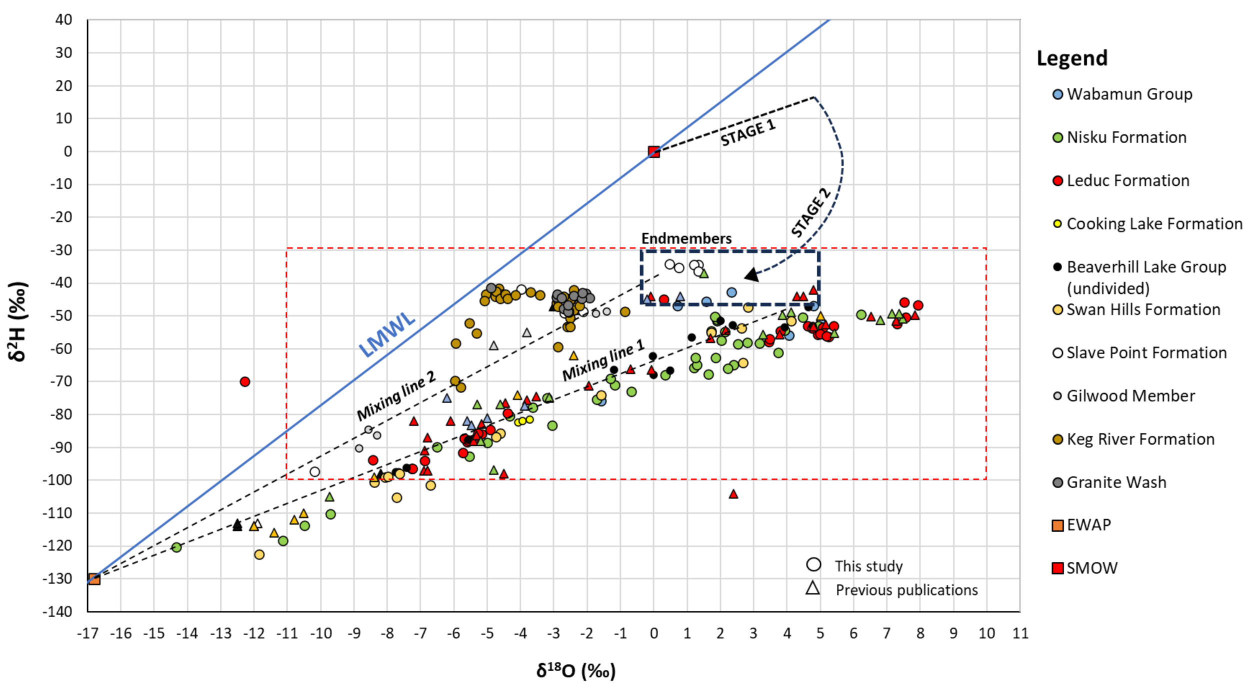

Figure 3. The $\delta^{18}O$ versus $\delta^{2}H$ diagram representing the isotopic compositions of Devonian oil brines in the Western Canada Sedimentary Basin in Alberta. Samples in the box outlined with a dashed red line are discussed in detail in the report. Endmembers are in the box outlined with a dashed blue line. Previously published isotope values were also included for completeness (Huff et al., 2011, 2012; Lyster et al., 2022; Reimert et al., 2022). Abbreviations: EWAP, Edmonton weighted average precipitation; LMWL, local meteoric water line for Edmonton; SMOW, Standard Mean Ocean Water.

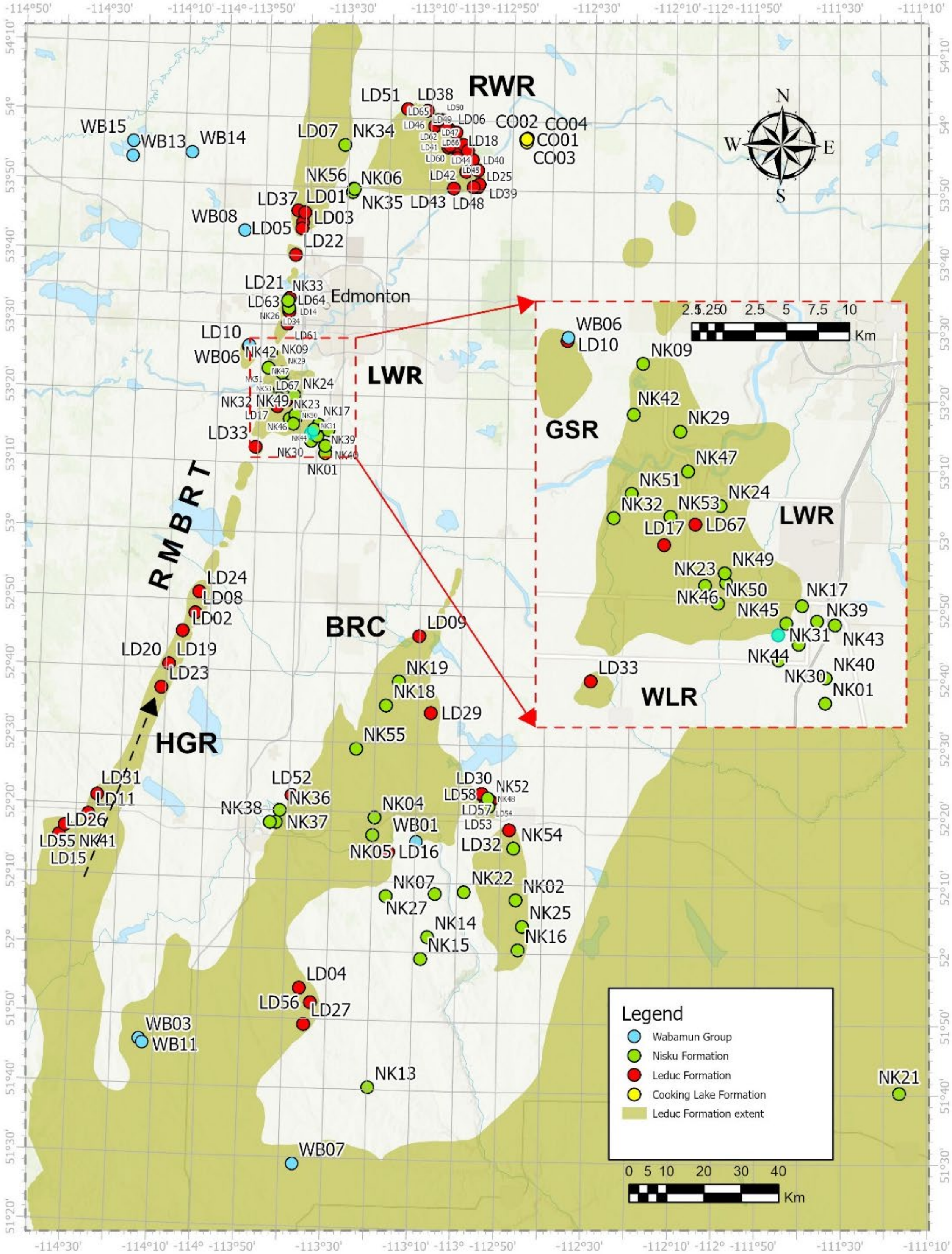

Figure 4. Location of oil brine samples from wells in the Cooking Lake (CL), Leduc (LD), and Nisku (NK) formations and Wabamun Group (WB), central Alberta. Samples were collected from the Redwater reef (RWR), Homeglen-Rimbey reef (HGR), Rimbey-Meadowbrook reef trend (RMBRT), and Bashaw reef complex (BRC). The detailed inset map shows samples collected at the Golden Spike reef (GSR), Wizard Lake reef (WLR), and Leduc-Woodbend reef (LWR). The black arrow indicates the suggested updip direction of fluid flow in the Cooking Lake–Leduc aquifer.

Leduc Formation oil brine samples in the HGR (LD02, LD08, LD11, LD15, LD19, LD20, LD23, LD24, LD26, LD31, and LD55; Figure 4) have $\delta^{18}O$ values from 3.8‰ to 5.4‰ (Figure 5) and chloride concentrations from 139 000 to 161 796 mg/L (Appendix 1, Table 2). In the southwestern segment of the HGR, $\delta^{18}O$ tends to be heavier than in the northeast. This observation suggests the fluid flow was updip in the Cooking Lake–Leduc aquifer, indicated by the arrow on the HGR in Figure 4. Samples with depleted $\delta^{18}O$ are from wells located in the northern segment of the RMBRT, GSR (LD10), and WLR (LD33; Figures 4 and 5). The rest of the wells from the northern segment of the RMBRT and the RWR have $\delta^{18}O$ and $\delta^{2}H$ values that indicate mixing with meteoric waters (samples plotting along mixing line 1 in Figure 5).

For this study, three samples were collected from wells in the Cooking Lake Formation, located east of the RWR (CO01, CO02, and CO03; Figure 4). These samples plot along mixing line 1, very close to the RWR samples (Figure 5), suggesting they were also diluted with meteoric waters. The RWR is isolated from surrounding geological units, with only its west side in communication with the Cooking Lake Platform (Gunter et al., 2009).

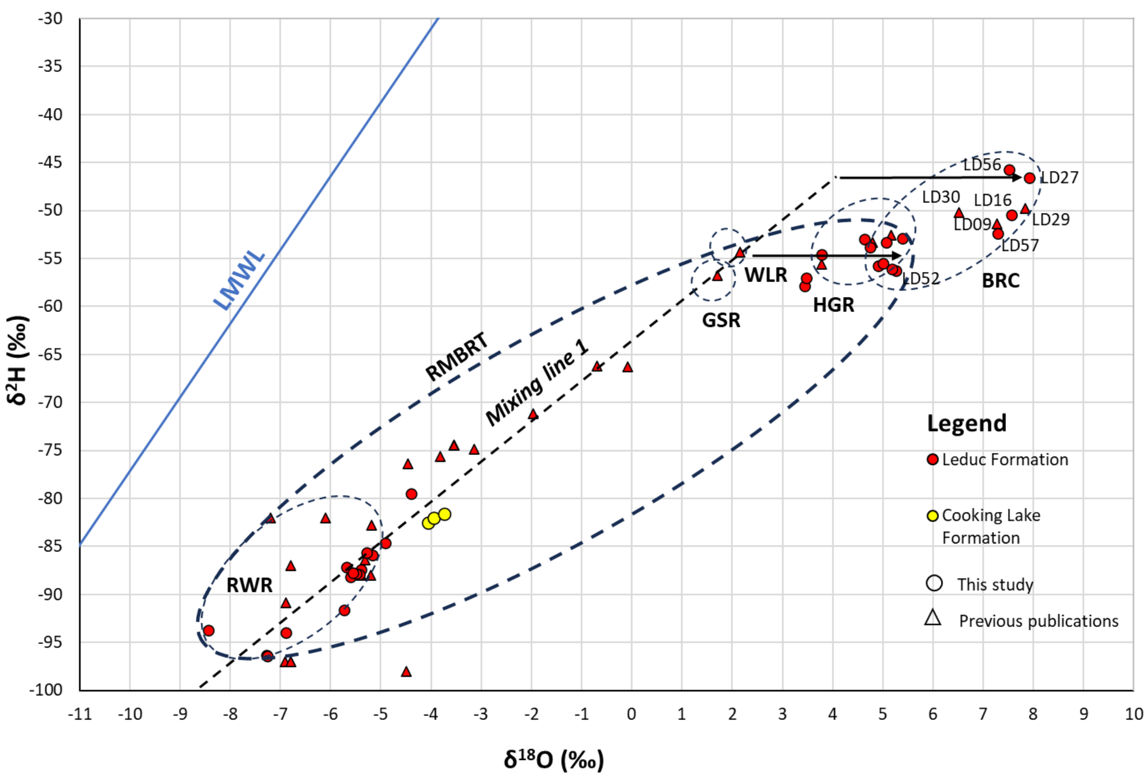

Figure 5. The $\delta^{18}O$ versus $\delta^{2}H$ diagram for oil brine samples from the Cooking Lake and Leduc formations, central Alberta. The dotted ellipses represent isotopic compositions of oil brines in the Leduc Formation reefs, shown as reference. Black arrows represent a shift in the $\delta^{18}O$ composition as a result of oxygen exchange with the reservoir rocks at high temperatures. Previously published isotope values were also included for completeness (Connolly et al., 1990; Eccles and Berhane, 2011; Huff et al., 2011, 2012, 2019; Reimert et al., 2022, 2025). Abbreviations: BRC, Bashaw reef complex; GSR, Golden Spike reef; HGR, Homeglen-Rimbey reef; LMWL, local meteoric water line; RMBRT, Rimbey-Meadowbrook reef trend; RWR, Redwater reef; WLR, Wizard Lake reef.

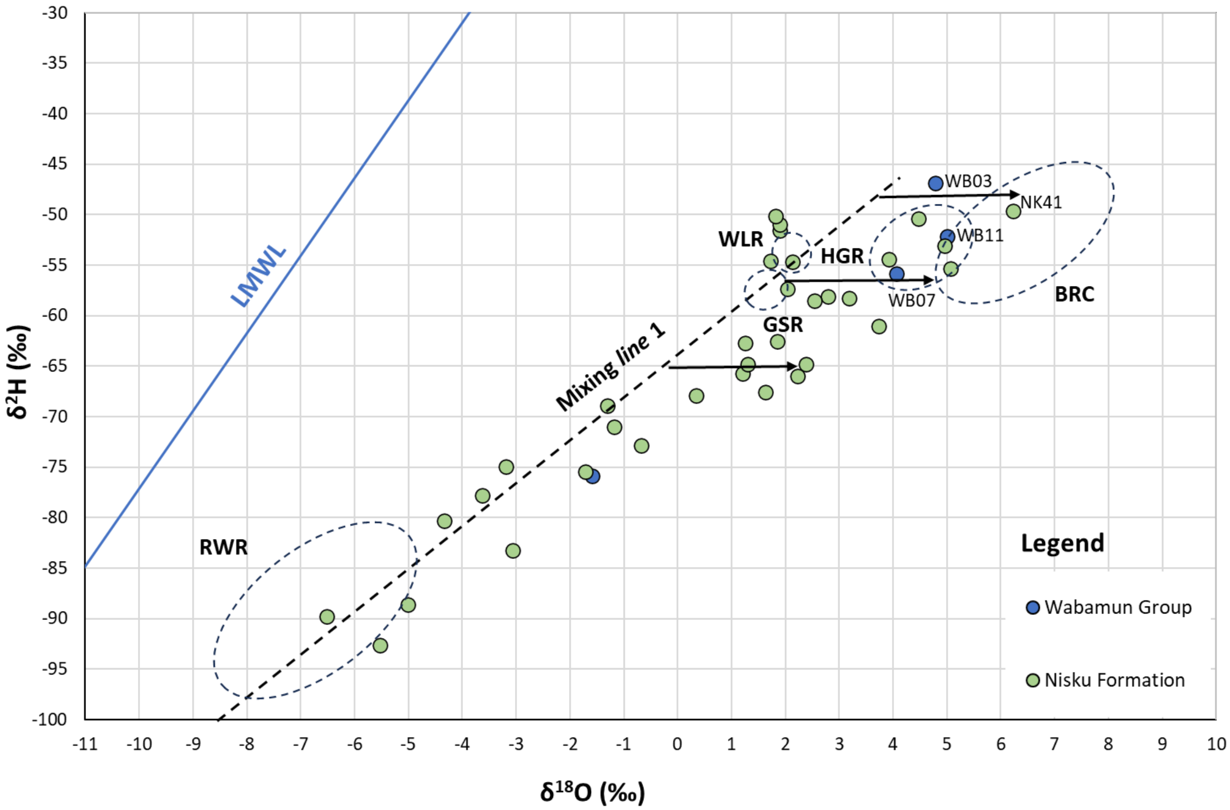

Figure 6. The δ^{18}O versus δ^{2}H diagram for oil brine samples from the Nisku Formation (NK) and Wabamun Group (WB), central Alberta. The dotted ellipses represent isotopic compositions of oil brines in the Leduc Formation reefs, shown as reference. Black arrows represent a shift in the δ^{18}O composition as a result of oxygen exchange with the reservoir rocks at high temperatures. Abbreviations: BRC, Bashaw reef complex; GSR, Golden Spike reef; HGR, Homeglen-Rimbey reef; LMWL, local meteoric water line; RWR, Redwater reef; WLR, Wizard Lake reef.

Figure 6 shows the Nisku Formation and the Wabamun Group well samples. In Figure 6, many oil brines follow mixing line 1, indicating the influence of meteoric waters on their isotopic composition. Other samples plot very close to the Leduc Formation brines with high δ^{18}O values.

Well samples NK04, NK05, NK07, NK18, NK19, and NK52, located stratigraphically above the BRC (Figure 4), have δ^{18}O values between 4.1‰ and 7.5‰, and chloride concentrations between 127 120 and 144 270 mg/L (Appendix 1, Table 2). These values are comparable with chloride and δ^{18}O values from some Leduc Formation brines from the BRC (LD09, LD16, LD27, LD29, LD30, LD52, LD56, and LD57) having chloride concentrations between 122 200 mg/L and 152 600 mg/L (Appendix 1, Table 2), and δ^{18}O values between 5.3‰ and 7.9‰ (Figure 5).

Above the HGR, the Nisku Formation sample NK41 had a chloride concentration of 130 000 mg/L, which is outside the range of Leduc Formation samples LD11, LD15, LD26, and LD31 (139 000 to 155 842 mg/L; Appendix 1, Table 2) from the HGR. The δ^{18}O value for sample NK41 is 6.2‰, higher than other Leduc Formation samples from the HGR (4.9‰ to 5.2‰; Figures 5 and 6). Based on δ^{18}O and Cl concentrations, sample NK41 appears more closely related to Leduc Formation samples from the BRC than samples from the HGR; this suggests that cross-formational flow may have a horizontal component in the Nisku Formation. Paul (1994) proposed the hydraulic continuity of the Cooking Lake, Leduc, and Nisku formations based on water chemistry, potentiometric surface analysis, and pressure-depth correlations. Paul (1994) concluded that thin and permeable areas in the Ireton Formation shales allowed vertical flow from the Cooking Lake Platform to the Leduc and Nisku formations in the area of the BRC. Later work (Rostron and Tóth, 1997) also found that flow regimes in the BRC tend to become vertical at locations where aquitards are thin or absent. These conclusions support a correlation between brines from the Leduc and Nisku formations that exhibit heavy $\delta^{18}O$ values and high chloride contents.

The Wabamun Group oil brine samples WB03, WB07, and WB11, collected in central Alberta, have $\delta^{18}O$ and $\delta^{2}H$ values comparable to those of the Leduc Formation samples from both the HGR and BRC (Figures 5 and 6). However, the chloride concentrations of these Wabamun Group brines are between 44 300 and 55 800 mg/L, much lower than the Leduc Formation samples from the BRC (LD56, 136 700 mg/L; LD27, 134 000 mg/L; LD04, 131 710 mg/L; Appendix 1, Table 2). It would be expected that brines diluted with meteoric water would have a lighter isotopic composition; however, in the case of these Wabamun Group samples, although they contain around one-third of the chloride found in Leduc Formation brines, they still preserve heavy isotopic signatures, particularly in $\delta^{18}O$. This indicates that a high-temperature fluid of low salinity may have reached the Wabamun Group at this location, remaining isolated from meteoric waters after emplacement.

5.1.2 West-Central Alberta

The locations of well samples from the Beaverhill Lake Group (undivided), and Swan Hills, Leduc, and Nisku formations in west-central Alberta are shown in Figure 7. The isotopic compositions ($\delta^{18}O$ versus $\delta^{2}H$) of oil brines from the Beaverhill Lake Group and Swan Hills Formation are presented in Figure 8.

In west-central Alberta, the Middle–Upper Devonian Beaverhill Lake Group and Upper Devonian Woodbend (Leduc Formation), Winterburn (Nisku Formation), and Wabamun groups form regional aquifers (Buschkuehle and Machel, 2002). On the southwest side of the Wild River Basin area, the Ireton Formation is either thin or absent, allowing for the hydraulic interconnection of these four aquifers (Buschkuehle and Machel, 2002). Hydrodynamic analysis of the porous dolostone sequence in the Wild River Basin area concluded that the Swan Hills, Leduc, and Nisku formations, along with the Wabamun Group, form a single flow system that remains operational to this day (Wendte et al., 1998). In other areas of west-central Alberta where the Waterways Formation is not present, the Leduc Formation overlies the Swan Hills Formation directly (Reinson et al., 1993).

Oil brines from the Beaverhill Lake Group (undivided) and the Swan Hills Formation follow mixing line 1 (Figure 8); this is a common characteristic of Upper Devonian oil brines, which appear to have a comparable isotopic composition regardless of their geographic location. For instance, samples from Sturgeon Lake reef (SLR; LD12, LD35, and LD36) seem to represent the endmember of mixing line 1 (Figure 8). Oil brine samples from the Beaverhill Lake Group (BL14, BL06, and BL12) and the Swan Hills Formation (SH22 and SH30) have high $\delta^{18}O$ values comparable to brines from the Leduc and Nisku formations and Wabamun Group in central Alberta (Figures 6 and 8). These characteristics indicate that the brines in the investigated Middle–Upper Devonian geological units have a common origin.

The $\delta^{18}O$ and $\delta^{2}H$ compositions of these oil brines support the previously proposed cross-formational flow within these aquifers, with many brine samples having heavy $\delta^{18}O$ values. This information indicates the Swan Hills Formation served as a gateway for deep hot fluids that moved vertically and horizontally in Upper Devonian formations, mixing with resident brines. The migration of hot saline fluids, followed by several subsequent mixing events and diagenetic reactions, may have influenced the current chemistry of these Devonian oil brines.

Original well records indicate that samples from wells 100/16-18-064-11W5/00 and 102/05-36-065-13W5/02 were initially identified as being from the Slave Point Formation. However, the geographic and stratigraphic locations of these samples, along with their chemical and isotopic compositions, suggest that they were actually collected from the undivided Beaverhill Lake Group. Consequently, these samples have been labeled BL14 and BL15, respectively (Appendix 1, Table 2).

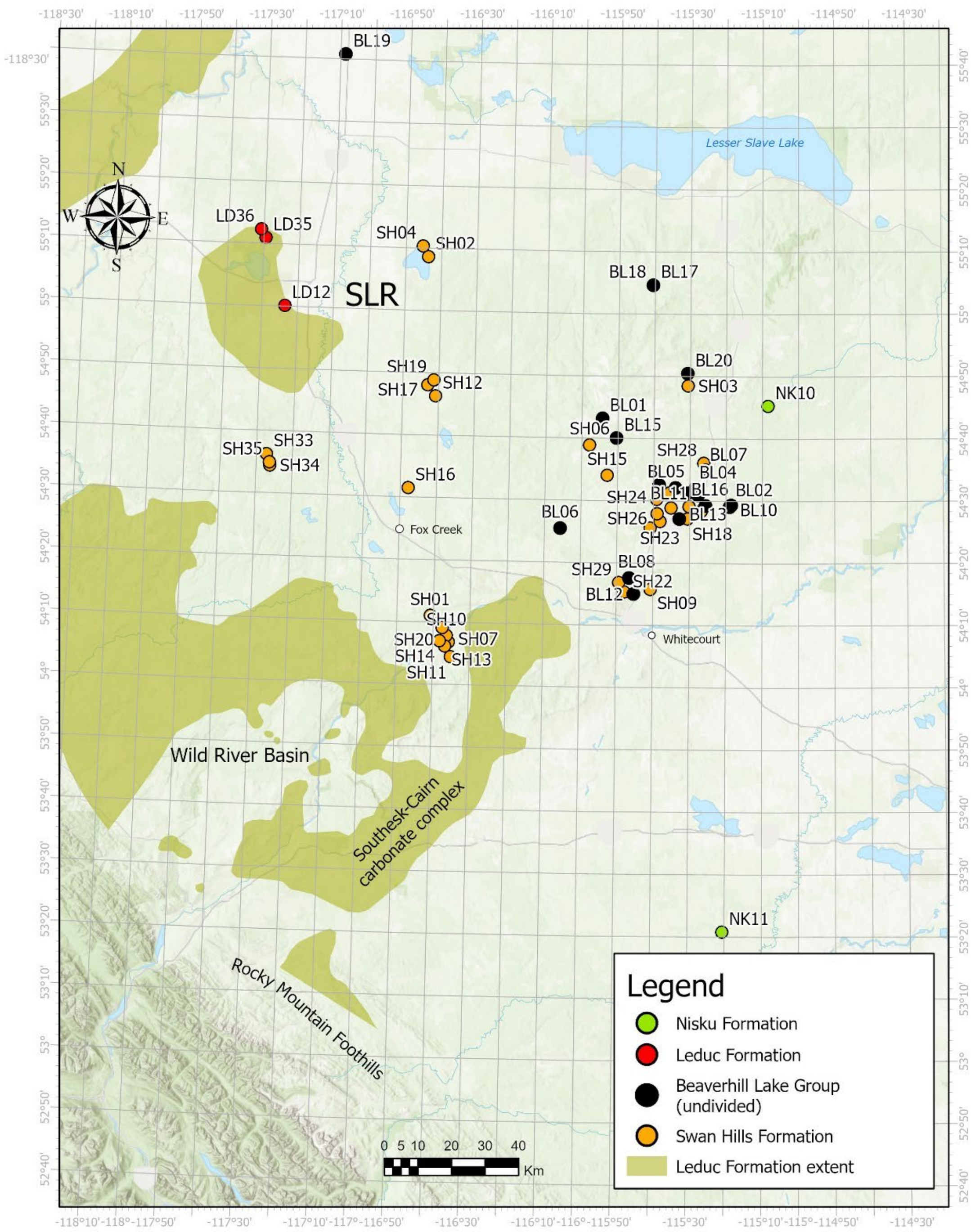

Figure 7. Location of oil brine samples from wells in the Beaverhill Lake Group (undivided; BL), and Swan Hills (SH), Leduc (LD), and Nisku (NK) formations, west-central Alberta. The Leduc Formation samples are in the Sturgeon Lake reef (SLR).

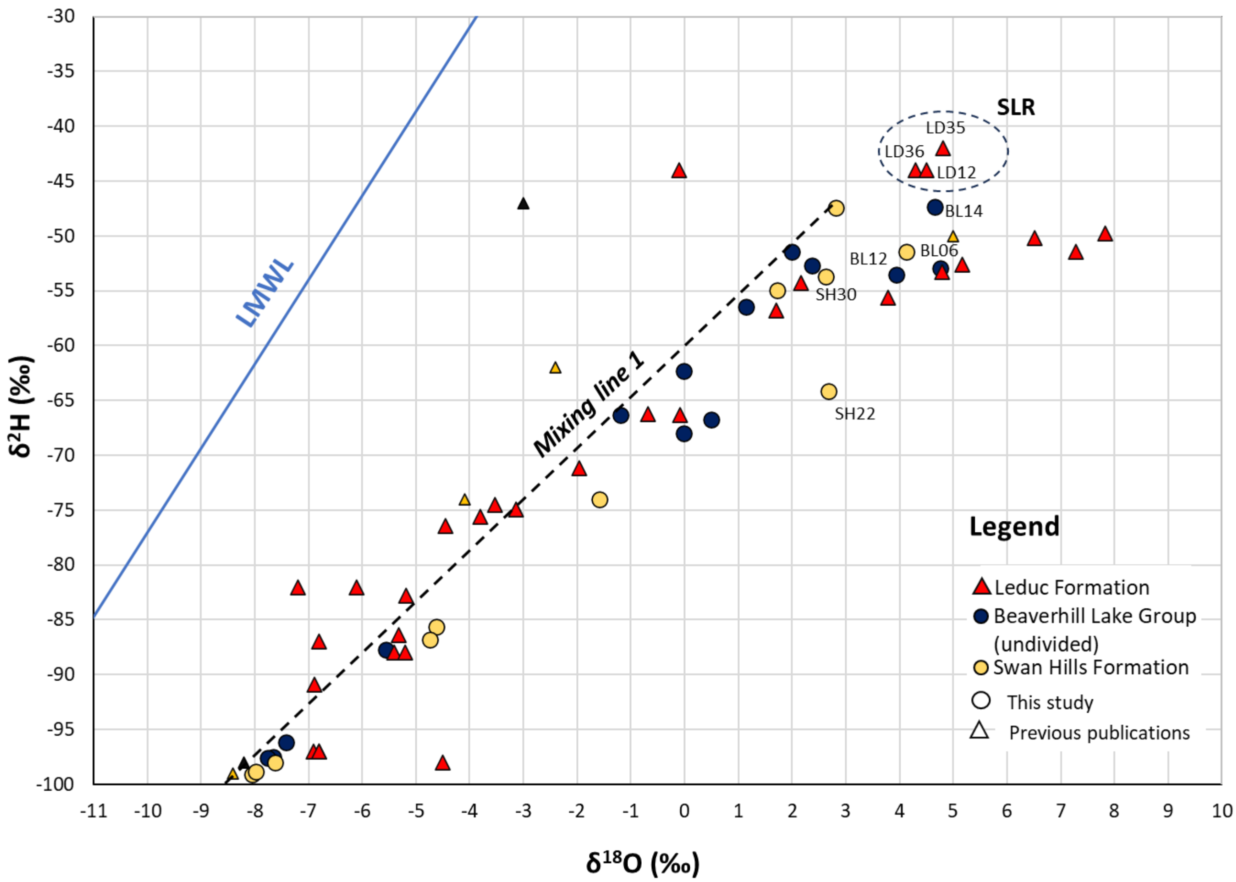

Figure 8. The δ¹⁸O versus δ²H diagram for oil brine samples from the Beaverhill Lake Group (undivided; BL) and Swan Hills (SH) and Leduc (LD) formations, west-central Alberta. The dotted ellipse represents the isotopic composition of oil brines in the Sturgeon Lake reef (SLR). Previously published isotope values were also included for completeness (Huff et al., 2011, 2012; Lyster et al., 2022; Reimert et al., 2022). Abbreviation: LMWL, local meteoric water line.

5.1.3 Peace River Arch Area

Oil brine samples collected from the Peace River Arch (PRA) area are shown in Figure 9. These samples were collected from the Granite Wash, Keg River Formation, Gilwood Member, Slave Point Formation, Leduc Formation, and Wabamun Group. The δ^2H and δ^{18}O values of these brines are shown in Figure 10. Mixing line 2 in this figure was defined by samples from the Gilwood Member collected for this study (GL02, GL03, and GL05 to GL08) and samples from previous studies (GL01 and GL04), as well as samples from the Slave Point Formation (SP03, SP04, SP09, and SP15 and SP12 from northwestern Alberta). According to Reinson et al. (1993), in proximity to the PRA, the Gilwood Member, Keg River sandstone (Keg River Formation), and Chinchaga sandstone (Chinchaga Formation) are undifferentiated and collectively form part of the Granite Wash, which directly overlies the Precambrian basement. This relationship is reflected in the clustering of brine samples from these geological units, which exhibit consistent isotopic values at approximately -45‰ δ^2H and -2‰ δ^{18}O (Figure 10). These similarities suggest that the geological units may function together as a hydraulically connected aquifer system.

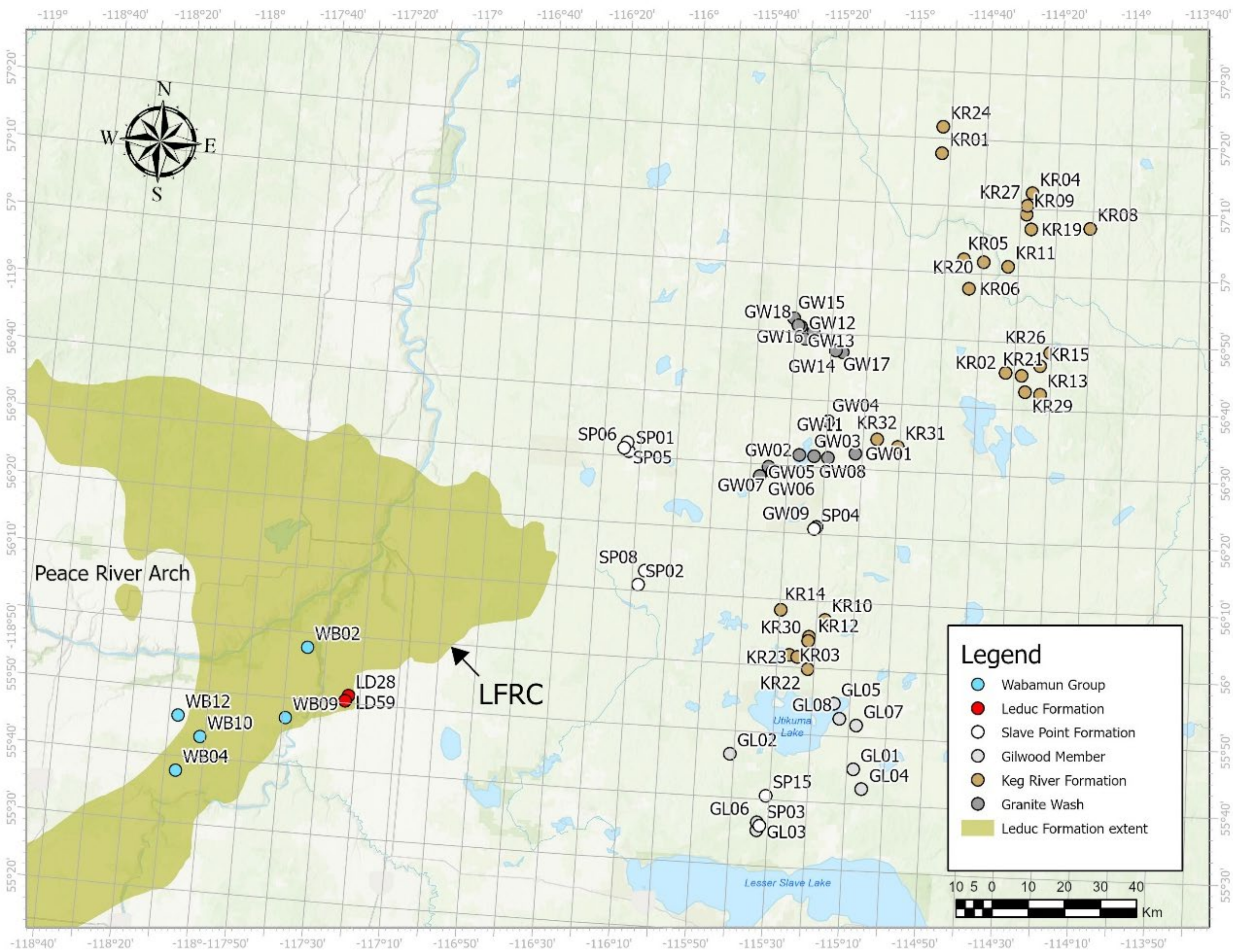

Figure 9. Location of oil brine samples from wells in the Granite Wash (GW), Keg River Formation (KR), Gilwood Member (GL), Slave Point Formation (SP), Leduc Formation (LD), and Wabamun Group (WB), Peace River Arch area, Alberta. Abbreviation: LFRC, Leduc fringing reef complex.

Oil brines from the Leduc Formation (LD28 and LD59) in the Leduc fringing reef complex (LFRC; Figure 9) and the Wabamun Group (WB02, WB04, WB09, WB10, and WB12) form a cluster of samples between mixing lines 1 and 2 (Figure 10). Chloride concentrations in the Wabamun Group samples range from 163 430 to 193 192 mg/L, encompassing the concentrations in the Leduc Formation brines, 172 880 and 189 540 mg/L (Appendix 1, Table 2). These correlations, along with the geographic location of these samples, indicate cross-formational flow occurring in the LFRC (Figure 9). Dix (1993) used plain-light cathodoluminescence and fluorescence microscopy in combination with stable isotopes and trace elements to find that deep burial fracture flow was recorded upsection in carbonate rocks from the Leduc Formation through the Wabamun Group in the PRA area. According to Dix (1993), this fracturing enabled the development of channelized flow, which began in the Mississippian and continued into the Paleogene.

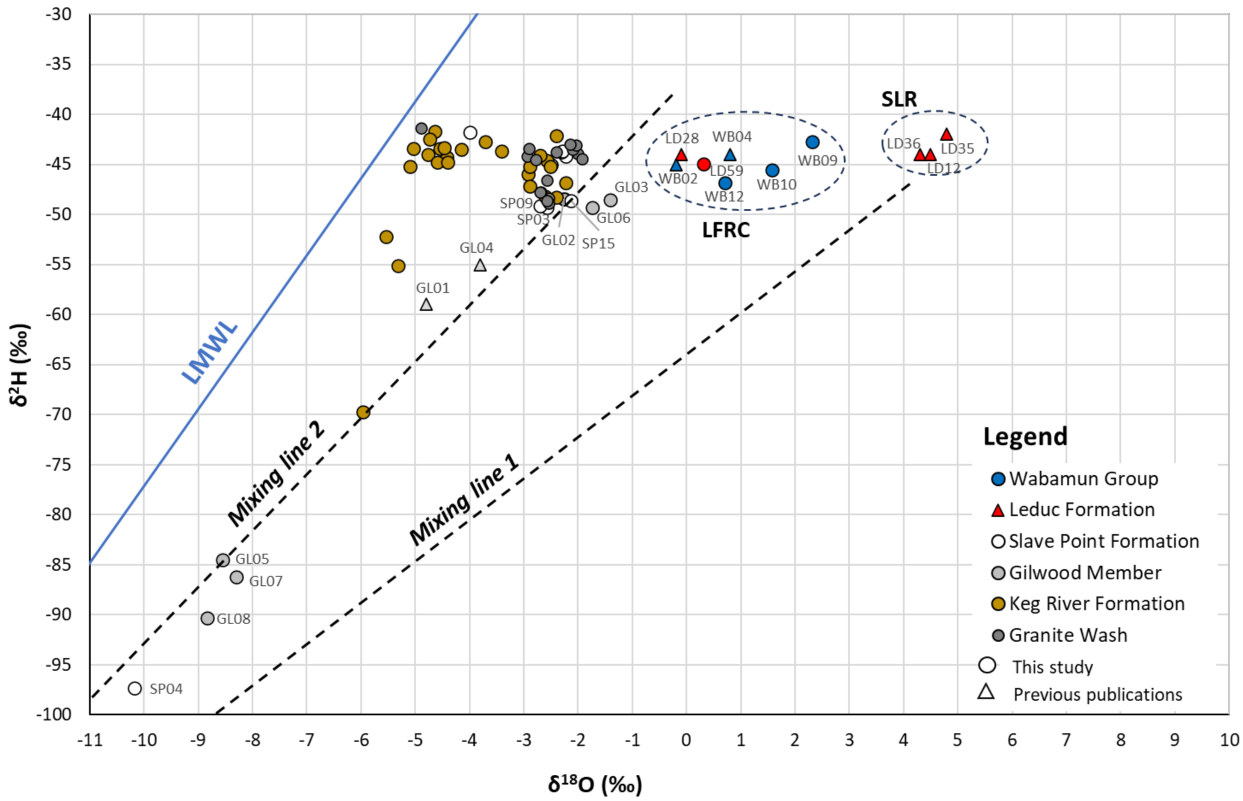

Figure 10. The δ^{18}O versus δ^{2}H diagram for oil brine samples from the Granite Wash (GW), Keg River Formation (KR), Gilwood Member (GL), Slave Point Formation (SP), Leduc Formation (LD), and Wabamun Group (WB), Peace River Arch (PRA) area, Alberta. Brine samples in the Sturgeon Lake reef (SLR; west-central Alberta) are provided for comparison to lower δ^{18}O values in brine samples from the PRA area. The dotted ellipses represent isotopic compositions of oil brines in the Leduc Formation reefs, shown as reference. Previously published isotope values were also included for completeness (Huff et al., 2011, 2012; Lyster et al., 2022; Reimert et al., 2022). Abbreviations: LFRC, Leduc fringing reef complex; LMWL, local meteoric water line.

If the Leduc Formation samples in the SLR (LD12, LD35, and LD36; Figure 10) in west-central Alberta represent the endmember of mixing line 1, a shift to lower δ^{18}O values emerges as a pattern for brines in the PRA area. This will be discussed in more detail in Section 5.2.

5.1.4 Northwestern Alberta

Figure 11 includes samples collected from the Keg River and Slave Point formations in northwestern Alberta, and their isotopic compositions are presented in Figure 12.

The Keg River Formation oil brines belong to the Rainbow (samples KR17, KR18, KR25, KR33, and KR34) and Shekilie (samples KR07 and KR28) basins. Brine samples from the Slave Point Formation (SP09 to SP14) are in the Cranberry and Chinchaga Slave Point reef complexes (CCSPRC; Figure 12), as defined in Reinson et al. (1993). Based on the data available for this report, there is no apparent isotopic correlation between brines in the Keg River and Slave Point formations that suggests cross-formational flow.

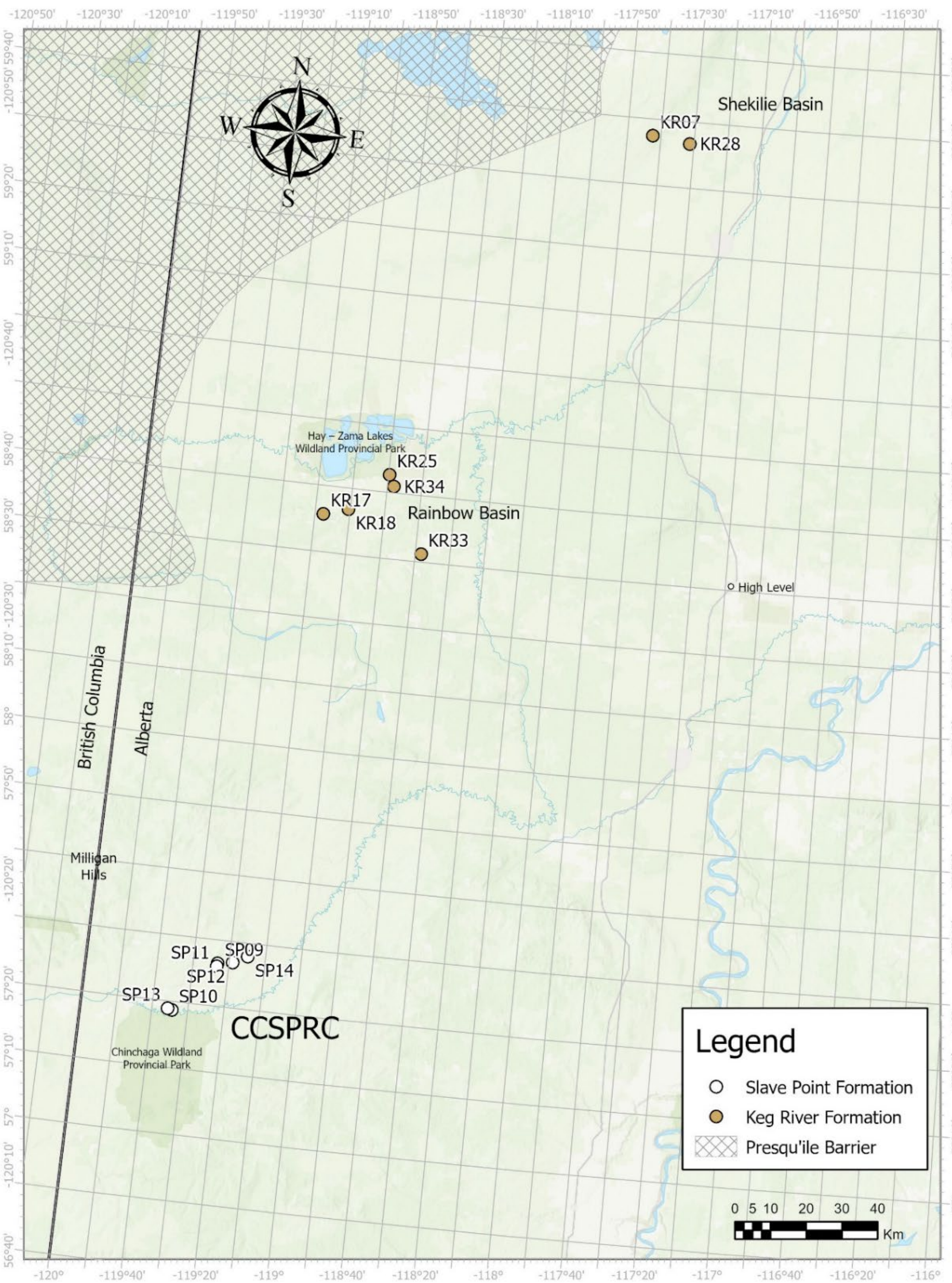

Figure 11. Location of oil brine samples from wells in the Keg River Formation (KR) in the Rainbow and Shekilie basins and Slave Point Formation (SP) in the Cranberry and Chinchaga Slave Point reef complexes (CCSPRC), northwestern Alberta.

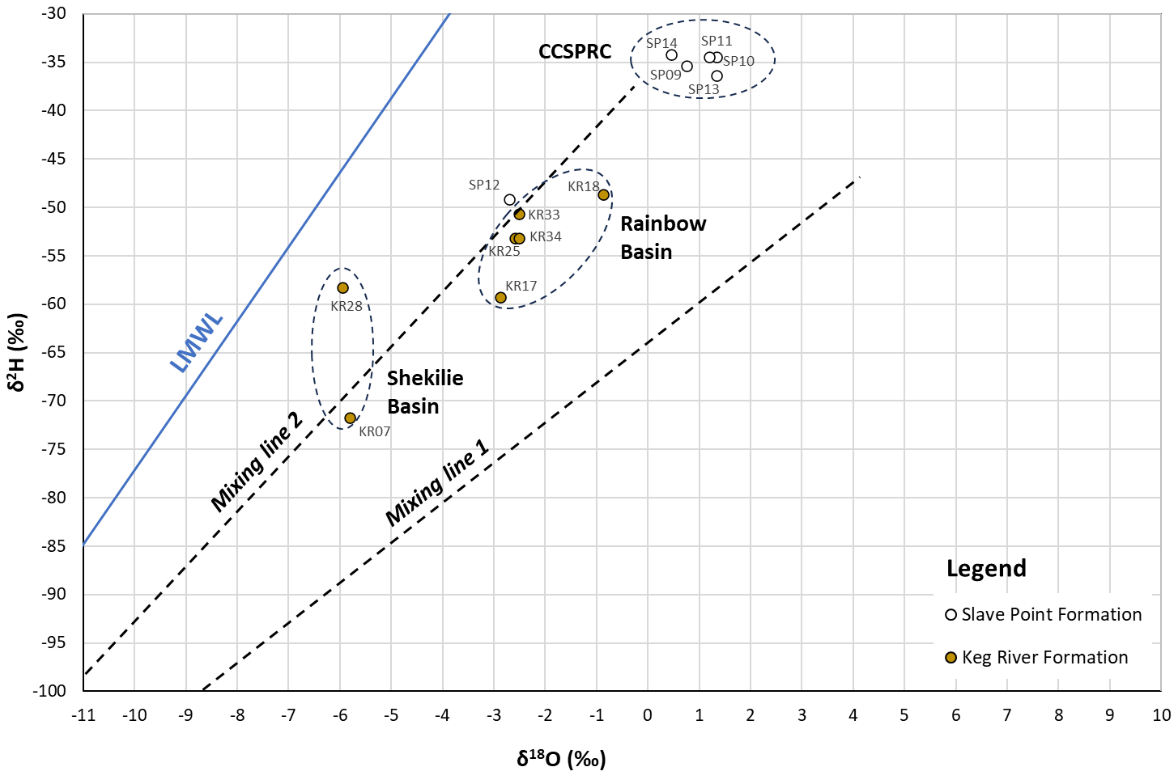

Figure 12. The δ^{18}O versus δ^{2}H diagram for oil brine samples from the Keg River (KR) and Slave Point (SP) formations, northwestern Alberta. The dotted ellipses represent isotopic compositions of oil brines in the Shekilie and Rainbow basins and Cranberry and Chinchaga Slave Point reef complex (CCSPRC), shown as reference. Abbreviation: LMWL, local meteoric water line.

Oil brines from both the Rainbow and Shekilie basins plot on or close to mixing line 2 (Figure 12), which indicates they mixed with meteoric waters at some point. As shown in Figure 12, brines from the Slave Point Formation in the CCSPRC, situated north of the Chinchaga Wildland Provincial Park area (Figure 11), do not exhibit a mixing trend. These samples contain the highest δ^{2}H values measured in this study. Samples SP09, SP10, SP11, SP13, and SP14 contain δ^{2}H and δ^{18}O values around -35‰ and 1‰, respectively (Figure 12). However, sample SP12, located on mixing line 2 (Figure 12), represents a diluted brine from the CCSPRC. The projection of mixing line 2 intercepts the CCSPRC sample points (Figure 12). This intersection suggests that the Slave Point Formation brines at the CCSPRC represent the endmember of a dilution trend, which depicts different degrees of mixing between these brines and meteoric waters. Meteoric waters also mixed with brines from the Gilwood Member, Slave Point Formation, and Keg River Formation in the PRA and northwestern areas. This process imparts an isotopic signature that differentiates these brines from those related to mixing line 1, which is defined by the dilution of Middle–Upper Devonian oil brines with meteoric water. Processes, such as mixing, water-rock interactions, diagenesis, and changes in temperature due to burial, may have modified the isotopic composition of the residual brines. On the other hand, evaporation appears to be the most relevant process controlling the salinity of these oil brines. However, as it will be discussed later, evaporation is not the main process responsible for the concentration of Li in these samples.

5.2 Chemical Evolution of Devonian Oil Brines

Since the early Devonian (~400 Ma), the oil brines of Alberta have undergone several geochemical and hydrogeological processes that have defined their current chemistry. These processes have been documented in the past and include evaporation, burial, diagenesis, mineral precipitation, water-rock interaction, large-scale migration, mixing, mineral dissolution, and reprecipitation.

For the AGS brine sampling program, major ions, and dissolved and trace metals were analyzed in addition to the isotopes of O, H, Sr, Li, B, and Sr. These analyses were selected to better understand water-rock interaction (Li, B, δ^{7}Li, δ^{11}B, ^{87}Sr/^{86}Sr, δ^{18}O, and δ^{2}H) and thermochemical sulphate reduction (δ^{18}O and δ^{34}S in SO_4), evaporation (δ^{18}O, δ^{2}H, Br, Na, and Cl), and diagenesis and fluid temperatures (Li, Rb, Cs, K, and Mg).

5.2.1 Water-Rock Interaction and Thermochemical Sulphate Reduction

5.2.1.1 Central Alberta

Oil brines from the Leduc Formation in the HGR and BRC tend to contain higher δ^{18}O, as indicated by the black arrows in Figure 5. These arrows represent a shift in the δ^{18}O composition of the fluid towards higher values due to oxygen exchange with the reservoir rocks at high temperatures. The extent of δ^{18}O shift in the high-temperature water-rock interaction brines is approximately 4.0‰, measured from the intersection of the black arrow with mixing line 1 to sample LD27 (Figure 5). The isotopic exchange found in Leduc Formation brines is higher than what has been measured in some high-temperature geothermal systems (>200°C), where the δ^{18}O shift reaches up to 3‰ (Bernal et al., 2014). Significant isotopic shifts in the brines can be attributed to the higher availability of exchangeable oxygen in carbonate rocks compared to igneous or metamorphic rocks, which are commonly found in high-temperature geothermal reservoirs. Water-rock interaction is a thermodynamic process that requires the fluid-rock equilibrium to operate for thousands or even millions of years. In the case of the Leduc Formation reefs, brines with high δ^{18}O shifts imply an efficient entrapment mechanism operating at these locations. Water-rock interaction may have also shifted the isotopic composition of the Wabamun Group samples WB03, WB07, and WB11 (Figure 6). Similar to the samples from the Wabamun Group, some brines from the Nisku Formation show significant oxygen exchange with the rocks (black arrow in Figure 6). As will be explained later, brine samples with high δ^{18}O shifts strongly correlate with high alkali metal contents, including Li.

5.2.1.2 West-Central Alberta

Oil brines from the Beaverhill Lake Group (undivided) and the Swan Hills Formation in west-central Alberta follow mixing line 1 (Figure 8). The same mixing line that brine samples from the Leduc Formation in the RMBRT and BRC follow. This is a remarkable characteristic, considering the geographic distance between the Leduc Formation in central Alberta and the Swan Hills Formation reefs in west-central Alberta, approximately 150 km (Figure 2). Additionally, some samples from the Beaverhill Lake Group (e.g., BL06, BL12, and BL14) and the Swan Hills Formation (e.g., SH22 and SH30) exhibit heavy δ^{18}O values. This suggests that these brines have undergone similar water-rock interactions with aquifers and reservoir rocks, comparable to those brines from the Leduc and Nisku formations, and Wabamun Group in central Alberta.

5.2.1.3 Peace River Arch

In the PRA area, oil brines from the Leduc Formation and Wabamun Group in the LFRC appear to be shifted towards lighter δ^{18}O values (Figure 10), which is the opposite of what has been previously described for the same units in central Alberta (Figures 5 and 6). Also, several samples from the Keg River Formation, one sample from the Granite Wash (GW09), and one sample from the Slave Point Formation (SP02) plot close to the LMWL (Figure 13), indicating a progressive decrease in ^{18}O.

A group of 17 samples from the Keg River Formation located southeast of the Buffalo Head Hills (Figure 9) forms a cluster in the δ^{18}O versus δ^{2}H diagram of Figure 13. Except for KR01, KR04, KR08, and KR24, the rest of the samples from this group are characterized by lighter δ^{18}O values. Of the seven samples collected north of Utikuma Lake (Figure 9), five samples (KR03, KR10, KR12, KR22, and KR23) form a cluster (Figure 13) characterized by heavier δ^{18}O values; sample KR14 has a lower δ^{18}O value and sample KR30 also has a low isotopic value but it plots on mixing line 2 indicating that this sample was clearly affected by mixing with meteoric water. Samples KR31 and KR32, located geographically between the Buffalo Head Hills and Utikuma Lake groups (Figure 9), are also located between the isotopic values of these two clusters (Figure 13). The $\delta^{18}O$ and $\delta^{2}H$ composition and geographic location of the Granite Wash samples are very similar to those of samples KR31 and KR32.

The above description suggests the existence of a geochemical process or processes that modified the $\delta^{18}O$ and $\delta^{2}H$ composition of the brines in the Granite Wash, Keg River Formation, Gilwood Member, and Slave Point Formation. One possibility for producing this effect in the brines is through interaction with acid gases, such as CO_2 and H_2S, at high temperatures. The occurrence of CO_2 and H_2S in the WCSB has been attributed to thermochemical sulphate reduction (TSR; Orr, 1974; Eliuk, 1984; Eliuk and Hunter, 1987; Krause et al., 1988; Reinson et al., 1993). Thermochemical sulphate reduction has been documented in reservoirs within the Leduc and Nisku formations (Amthor et al., 1994; Cole and Machel, 1994; Machel et al., 1995; Riciputi et al., 1996; Drivet and Mountjoy, 1997).

This study's isotopic analyses of $\delta^{18}O$ and $\delta^{34}S$ in SO_4 suggest that redox reactions occurred in the Granite Wash, the Keg River Formation, and the Gilwood Member. Figure 14a shows a consistent increase in both isotopes ($\delta^{18}O$ and $\delta^{34}S$ in SO_4) in samples from these geological units, with the Granite Wash samples exhibiting the highest values.

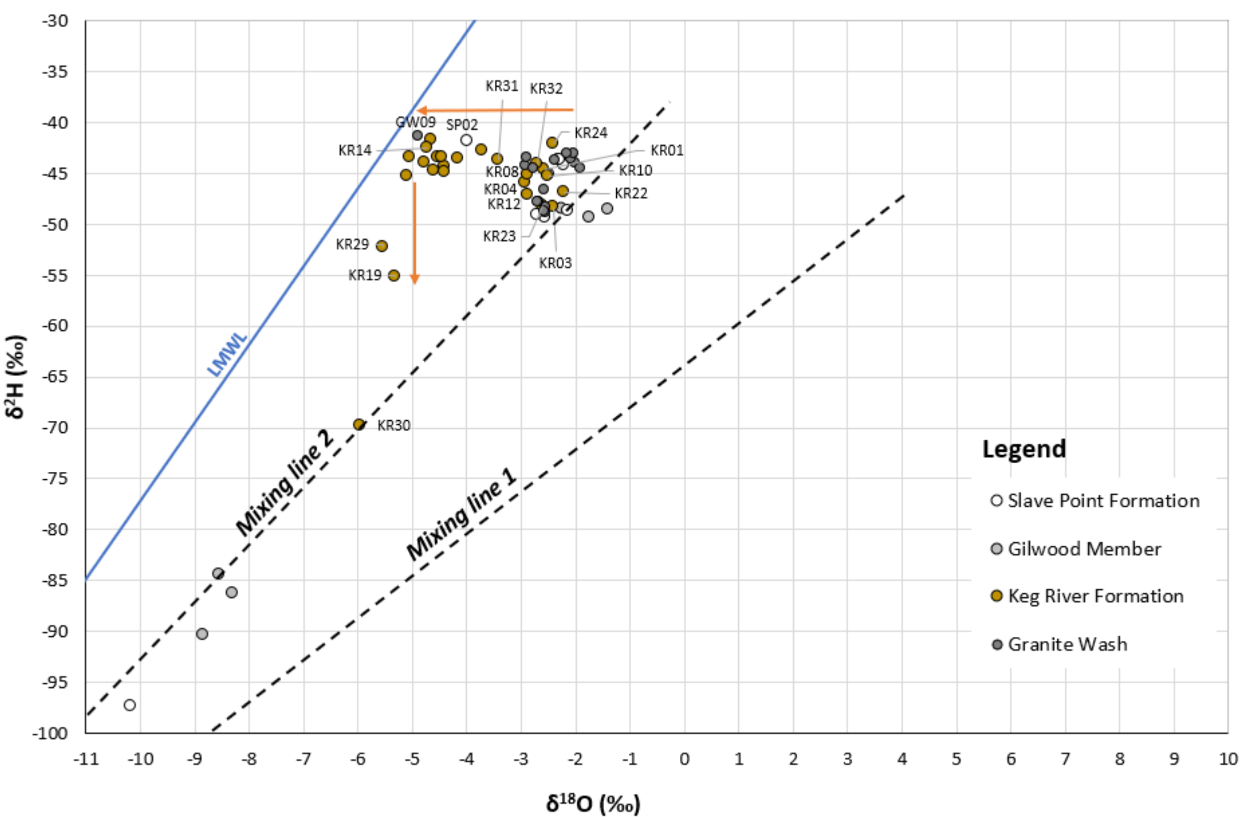

Figure 13. The $\delta^{18}O$ versus $\delta^{2}H$ diagram for oil brine samples from the Granite Wash (GW), Keg River Formation (KR), Gilwood Member (GL), and Slave Point Formation (SP), Peace River Arch area, Alberta. Orange arrows indicate interaction of oil brines with isotopically depleted pore waters. Abbreviation: LMWL, local meteoric water line.

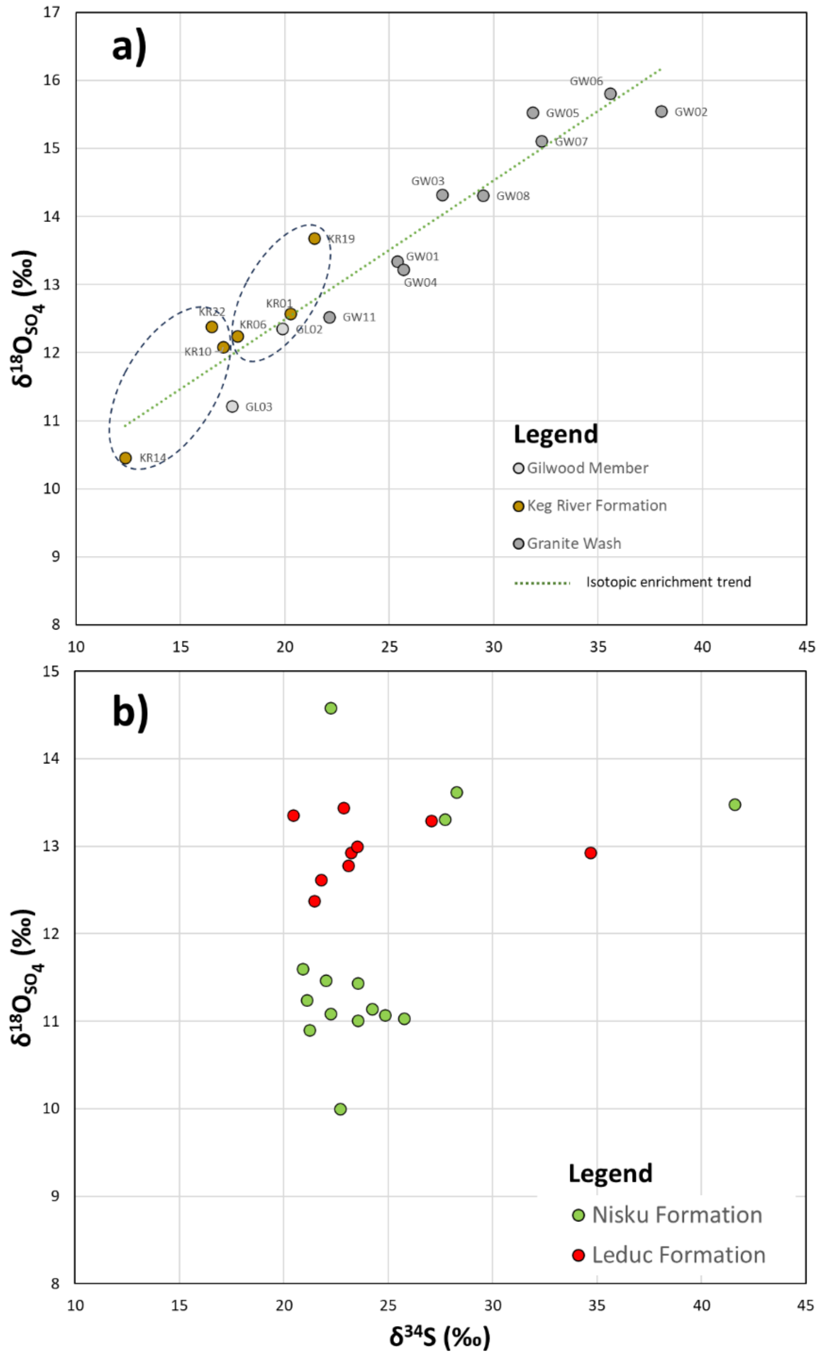

Figure 14. Comparison of oxygen and sulphur isotopes in sulphate compositions of oil brine samples from the Peace River Arch area, Alberta: (a) Granite Wash (GW), Keg River Formation (KR), and Gilwood Member (GL); (b) Leduc and Nisku formations. The dotted ellipses represent isotopic compositions of oil brines in the Utikuma Lake and Buffalo Head Hills areas, shown as reference.

The data for oil brines in the Leduc and Nisku formations (Figure 14b) are inconclusive; the effects of TSR on their isotopic composition remain unclear. However, even if TSR was a dominant process in the Granite Wash, Keg River Formation, and Gilwood Member, according to Clark and Fritz (1997), the volume of gas produced may not have been enough to deplete the isotopic composition of the brines to the extent observed for most samples (i.e., ~3‰ $\delta^{18}O$ and ~6‰ δ^2H; Figure 13) and even lower for samples KR19 and KR29.

The isotopic shifts shown by the orange arrows in Figure 13 suggest interaction with a source depleted in $\delta^{18}O$ and δ^2H. Even though minerals like feldspars or clays can contribute to low $\delta^{18}O$ values (Hitchon and Friedman, 1969), they would not affect δ^2H, as hydrogen exchange is not involved. Given this, mixing with fluids that are depleted in both $\delta^{18}O$ and δ^2H, such as pore waters, offers a more plausible explanation for the isotopic patterns observed in PRA brines.

5.2.1.4 Northwestern Alberta

The isotopic composition of oil brine samples collected from wells in northwestern Alberta does not show evidence of water-rock interaction or isotopic exchange with gases. However, as mentioned earlier, Keg River Formation brines from the Rainbow (KR17, KR18, KR25, KR33, and KR34) and Shekilie (KR07 and KR28) basins (Figure 11) appear to have a meteoric water component indicated by their position near mixing line 2 (Figure 12).

5.2.2 Evaporation

The conservative character of the ions Cl, Br, and Li in aqueous solutions is a useful tool for identifying sources of salinity and mixing processes. The experimental work conducted by McCaffrey et al. (1987) provided a detailed record of the evolution of a residual seawater brine as evaporation progressed. This work showed that Cl, Br, and Li tend to remain in the brine and are incorporated only by a few minerals. Lithium is the most conservative ion in this environment, followed by Br and Cl.

Seawater salinity has varied throughout geological history. During the Devonian period, it is estimated to have ranged between 42‰ and 45‰ (Hay et al., 2006), significantly higher than the modern average of 35‰. This implies that the concentrations of major ions in Devonian seawater were approximately 30% greater than those in today’s oceans. For reference, modern seawater contains about 19 120 mg/L of chloride (Cl), 70 mg/L of bromide (Br), and 0.2 mg/L of lithium (Li). Applying the upper salinity estimate of 45‰ from Hay et al. (2006), these concentrations would increase to approximately 24 858 mg/L for Cl, 91 mg/L for Br, and 0.26 mg/L for Li.

This projection assumes that the relative proportions of major ions in Devonian seawater mirrored those of modern seawater. This assumption may not hold, given that the exact composition of Devonian seawater remains unknown. Notably, a recent study analyzing fluid inclusions in marine halite suggests that around 150 million years ago, Li concentrations in seawater were up to seven times higher than present levels, gradually declining to current values of 0.2–0.3 mg/L (Weldeghebriel and Lowenstein, 2023).

These studies represent a small part of the broader and ongoing effort to reconstruct the evolution of seawater salinity over geological time, a complex and still incomplete endeavour due to natural variability. Given this uncertainty, this study assesses the plausibility of the Devonian salinity values proposed by Hay et al. (2006), rather than relying on estimates from other geological periods. To do so, conservative anions measured in the collected Devonian oil brines were used to infer the maximum degree of evaporation these brines experienced and to estimate the maximum Li concentration from evaporitic origin.

Chloride is recognized as the dominant ion in both modern and Devonian seawater (Hay et al., 2006). However, under extreme evaporation, Cl can be removed from the solution through the formation of evaporite minerals, such as halite. Bromide (Br), in contrast, is more conservative and remains in solution even after Cl has precipitated. The molar Cl/Br ratio in modern seawater is approximately 620, whereas the Na/Br ratio is around 530. These ratios were used to assess whether the relative proportions of Cl, Br, and Na in Devonian seawater differ significantly from those in the modern ocean. For this purpose, the Na-Cl-Br systematics were used (Walter et al., 1990). A Na/Br versus Cl/Br plot using seawater (SW) as the central reference point (Figure 15) shows that most samples plot parallel to the dissolution trend line, indicating a 1:1 molar ratio. Samples plotted below or close to SW on the 1:1 dissolution line are considered influenced by evaporated seawater. Samples plotting above SW on the 1:1 dissolution line indicate a strong influence of halite dissolution by meteoric water (Kesler et al., 1995).

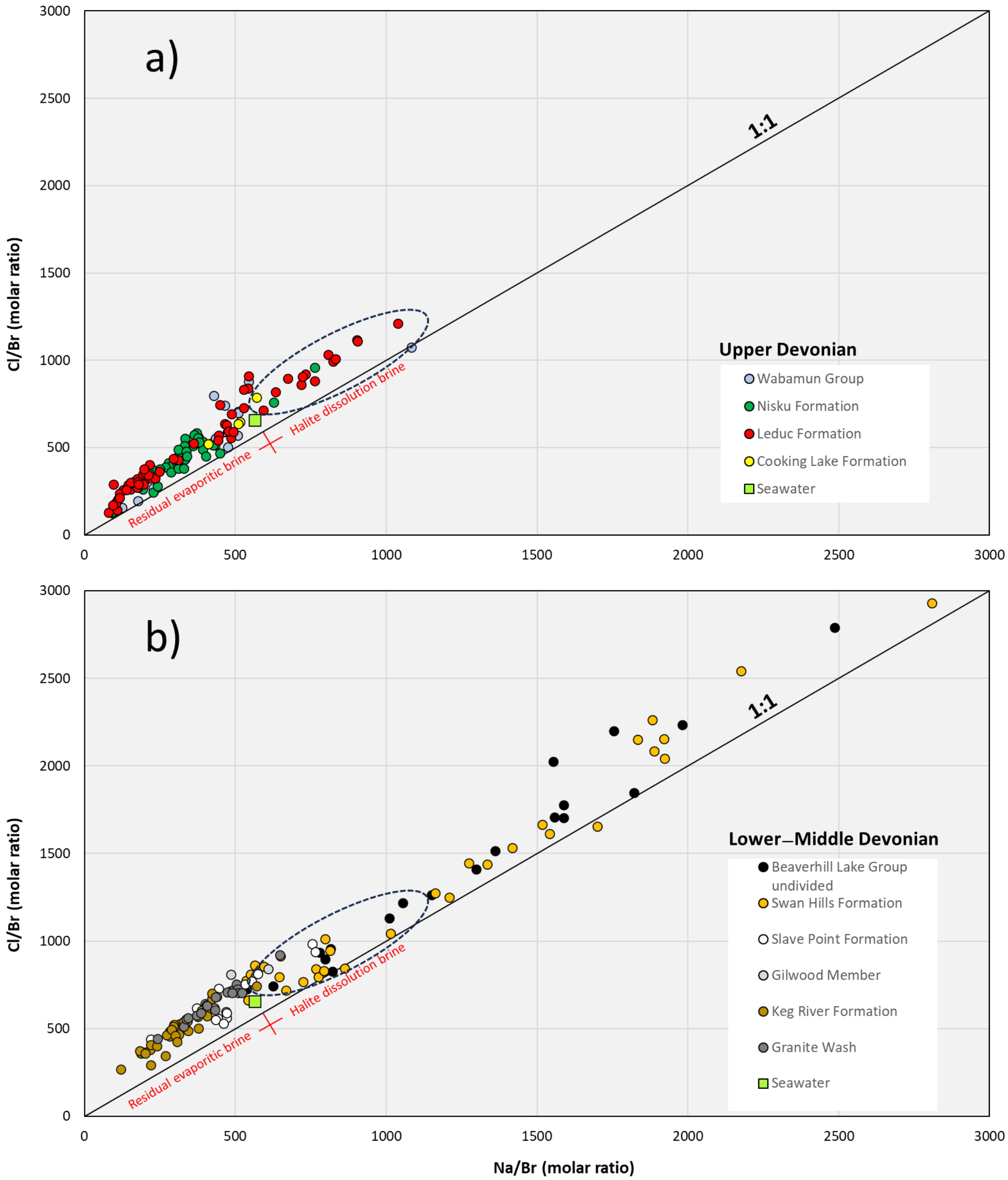

Figure 15. The Na-Cl-Br systematics for oil brine samples from Alberta: (a) Upper Devonian samples. The dotted ellipse primarily includes the samples from the Leduc Formation in the Redwater reef. (b) Lower–Middle Devonian samples. The dotted ellipse primarily includes samples from the Swan Hills Formation in the Fox Creek area. The 1:1 Na/Cl molar ratio represents the dissolution trend line used as a reference. Values above the seawater value on the dissolution line represent oil brines formed from halite dissolution, and values below the seawater value are attributed to seawater evaporation.

The Na-Cl-Br systematics indicate that the molar Cl/Br and Na/Br ratios in the Devonian brine samples behave similarly to those in modern brines. This is evident from the alignment of the data along the 1:1 regression line and their positions relative to the seawater composition (Figure 15). These findings suggest that the molar ratios of Cl/Br and Na/Br in Devonian seawater were likely comparable to present-day values.

Assuming the Devonian seawater salinity reached approximately 45‰, as proposed by Hay et al. (2006), and that the Cl/Br and Na/Br ratios were similar to those of modern seawater, it was possible to estimate Li contributions to Devonian oil brines. Using the previously calculated minimum Li concentration of 0.26 mg/L (approximately 30% higher than in modern seawater), the extent to which seawater evaporation contributed to the Li in these ancient brines can be evaluated by applying the evaporation trends observed in salt production facilities.

The dotted ellipses in Figure 15 enclose samples with Cl/Br molar ratios above SW. Figure 15a includes oil brines from the Leduc Formation in the RWR, the Cooking Lake Formation (CO04), the Nisku Formation in the PRA (NK10) and central Alberta (NK43), and the Wabamun Group (WB07) in central Alberta (Figure 4). Figure 15b includes the brines with Cl/Br molar ratios above SW from the Slave Point Formation (SP01, SP03, SP05, SP06, and SP15), the Gilwood Member (GL03), and the Granite Wash (GW12) located in the PRA area (Figure 9). The rest of the samples from these geological units have a clear residual evaporite component; nonetheless, the halogen compositions of these brines suggest that two fluids of different origins (i.e., evaporated seawater and halite dissolution brines) mixed at these locations.

The Na-Cl-Br systematics indicate that most Devonian brine samples are residual evaporitic brines. In contrast, the Swan Hills Formation and other brines in the Beaverhill Lake Group are the product of halite dissolution. However, samples from the Swan Hills Formation have some of the highest Li concentrations (Appendix 1, Table 3), which supports the hypothesis of a nonevaporitic Li source.

Lithium in modern seawater has a concentration between 0.2 and 0.3 mg/L, and according to data from McCaffrey et al. (1987), the maximum Li concentration obtained from seawater evaporated to ~100 times its original concentration (0.2 to 0.3 mg/L) is ~16 mg/L. The maximum degree of evaporation found in the set of samples analyzed for this study was ~37 times that of seawater, which corresponds to a Li concentration of less than 7 mg/L. According to this, evaporation alone was not the mechanism responsible for accumulating the Li concentrations measured in Middle to Upper Devonian oil brines. It is clear that the Devonian oil brines of Alberta have an anomalously high Li content, which implies the input of an additional Li source(s) and an effective accumulation process, as well as a transport mechanism.

Despite evaporated seawater being discarded as the primary source of Li, it is important to establish its contribution to the brines' salinity and to identify the formations in which evaporitic brines or dissolved halite are predominant sources.

5.2.3 Diagenesis and Fluid Temperatures

In the Alberta Basin, dolomitization has been studied in detail to understand the origin and characteristics of fluids involved in this process (e.g., Sun, 1994; Drivet and Mountjoy, 1997; Potma et al., 2001; Machel, 2004; Green and Mountjoy, 2005; Davies and Smith, 2006). One of the most extensively investigated areas is the RMBRT, a part of the Leduc Formation. Drivet and Mountjoy (1997) identified two different generations of dolomites in the southern part of this reef, one produced by pervasive replacement dolomitization and the other, of reduced extent, formed during cementation. In the Drivet and Mountjoy (1997) study, fluid inclusion data indicated the occurrence of two distinct events involving two different types of fluids, one at approximately 117°C and a later one at around 150°C. Similar characteristics have been observed at other locations within the Leduc Formation reefs, which led Drivet and Mountjoy (1997) to conclude that a large-scale fluid flow of evaporitic brines, expelled tectonically during the Antler orogeny, was responsible for the dolomitization of the Leduc Formation.

As seen in Figure 5, some samples from the Leduc Formation in the BRC and the HGR in the RMBRT exhibit high $\delta^{18}O$ values and plot to the right of mixing line 1, suggesting that they have not mixed with recent meteoric waters. In addition, these samples have some of the highest concentrations of halogens (Cl and Br) and alkali metals (Li, Na, K, Rb, and Cs). The $\delta^{18}O$ composition of these brines suggests that the fluid was at some point in thermodynamic equilibrium with the surrounding rocks at its current location. The $\delta^{18}O$ and $\delta^{2}H$ values suggest that initial thermodynamic equilibrium conditions can be estimated, assuming these oil brines have been isolated from meteoric waters.

In the literature, most aqueous geothermometers have been proposed based on exchange reactions that occur under a thermodynamic equilibrium of chemical species in magmatic environments. However, few aqueous geothermometers have been successfully applied to sedimentary basins, including Na-Li, Na-K-Ca with Mg correction, and Mg-Li geothermometers (Kharaka and Mariner, 1989). These three geothermometers were evaluated for the Devonian oil brines; however, the Mg-Li geothermometer was found to be the most accurate, reflecting the range of temperatures measured in fluid inclusions by Drivet and Mountjoy (1997), 117°C to 150°C in the RMBRT.

The Mg-Li geothermometer developed by Kharaka and Mariner (1989) is defined by

$$t = \frac{2200}{\log\left(\frac{\sqrt{Mg}}{Li}\right) + 5.47} - 273 \qquad (1)$$

where *t* is temperature (°C) and Li and Mg are expressed in mg/L.

The Mg-Li geothermometer and fluid inclusion data indicate that fluids around 150°C interacted with the host rocks. However, the Mg-Li exchange may have happened at higher temperatures, perhaps in a deeper part of the basin. Aqueous geothermometers are not precise tools but are very useful for explaining thermodynamic conditions. Table 1 shows that the highest temperatures were estimated for Leduc Formation oil brines in the BRC, reaching up to 145°C, compared to the HGR ones, which reached a maximum of 128°C.

Table 1. The $\delta^{18}O$ and Mg-Li geothermometer temperatures for oil brine samples from the Leduc Formation, central Alberta. Abbreviations: BRC, Bashaw reef complex; HGR, Homeglen-Rimbey reef.

UWI	Label	Leduc Formation	$\delta^{18}O$ (‰)	Mg-Li Geothermometer Temperature (°C)
100/02-05-044-01W5/00	LD02	HGR	4.6	122
100/05-36-038-04W5/00	LD11	HGR	4.9	127
100/10-01-043-02W5/00	LD20	HGR	4.8	124
100/11-14-042-02W5/00	LD23	HGR	5.4	125
100/12-02-045-01W5/00	LD24	HGR	3.8	119
100/14-07-038-04W5/00	LD26	HGR	5.1	127
100/06-20-038-04W5/00	LD55	HGR	5.2	126
102/10-18-039-03W5/00	LD31	HGR	5.0	128
100/09-06-038-23W4/00	LD16	BRC	7.6	140
103/09-22-039-26W4/00	LD52	BRC	5.3	145
100/06-36-033-26W4/02	LD56	BRC	7.5	137
100/09-26-039-21W4/00	LD57	BRC	7.3	132
100/15-13-039-21W4/00	LD58	BRC	3.5	129

In addition, if these fluids were in thermodynamic equilibrium with the Mg-Li system, a correlation between high Li concentrations and high temperatures is indicated by Equation 1. This correlation has been previously documented in fluids interacting with clays, showing that Li desorption increases with fluid temperature (Munk et al., 2011, 2016; Decarreau et al., 2012; Araoka et al., 2014). Based on these studies, the Devonian oil brines of Alberta may have been enriched in Li through interaction with clays at high fluid temperatures; however, given that the reservoir rocks containing these brines are mostly dolomitized with relatively low clay contents, significant Mg-Li exchange may have occurred elsewhere. If that is the case, at least a portion of the fluids making up the current composition of the brines migrated to their current locations after being desorbed from clays and mixed with Li of evaporitic origin contained in resident brines. This is an initial clue to establish the source of Li and other alkali metals in the Devonian oil brines; therefore, further geochemical characteristics were investigated to support or discard this hypothesis. It is also necessary to consider that diagenesis modifies the original chemical composition of the brines. For this reason, to identify the source(s) of Li, the following sections will focus on the behaviour of species that are unaffected by this process.

6 Discussion

6.1 Alkali Metals and the Origin of Regional Fluids

Lithium belongs to the alkali metals group, which also includes Na, K, Rb, and Cs. The alkali metals group is characterized by low electronegativities (0.79 to 0.98), a measure of an atom's ability to attract electrons in a chemical bond. During mineralization, some alkali metals, such as Li, Rb, and Cs, are rarely retained by the solid phase and, therefore, tend to be concentrated in the liquid phase. In sedimentary environments, Na and K are common elements that can be found in multiple minerals; these characteristics make them unreliable for identifying alkali metal sources. In contrast, given its small ionic radius, Li is the most conservative element of the five alkali metals in aqueous systems. Rubidium and Cs are the most reactive elements of this group; however, they are several orders of magnitude scarcer in the crust than Na and K. Therefore, the scarcity of Rb and Cs, in combination with the tracer applicability of Li, is ideal for helping identify their source(s). Figure 16 shows the distribution of Cs and Rb concentrations in oil brine samples from the Leduc Formation. These samples were selected based on their high alkali metal content and low or no dilution with meteoric waters, as determined by their $\delta^{18}O$ and $\delta^{2}H$ compositions. A strong linear correlation ($R^2 = 0.9865$) suggests that these two alkali metals exhibit similar behaviour and perhaps a common origin.

Three main observations can be extracted from Figure 16. The first one is the positive correlation between Cs and Rb ($R^2 = 0.9875$), suggesting that the sources of both alkali metals are related. The second is the spatial distribution of the samples. The samples with the highest concentrations of Cs and Rb are found in the BRC (LD16, LD27, LD52, LD56, and LD57), and those with the second-highest concentrations are from the HGR, part of the RMBRT. Thirdly, recalling the relationship between $\delta^{18}O$ and temperature, it is safe to conclude that the concentration of alkali metals is a temperature-dependent variable in the Leduc Formation samples and, by extension, in the remaining Upper Devonian oil brines. This is confirmed by the strong Cs versus Rb correlation ($R^2=0.9876$) obtained for oil brine samples from the Swan Hills, Leduc, and Nisku formations, and the Wabamun and Beaverhill Lake groups (Figure 17).

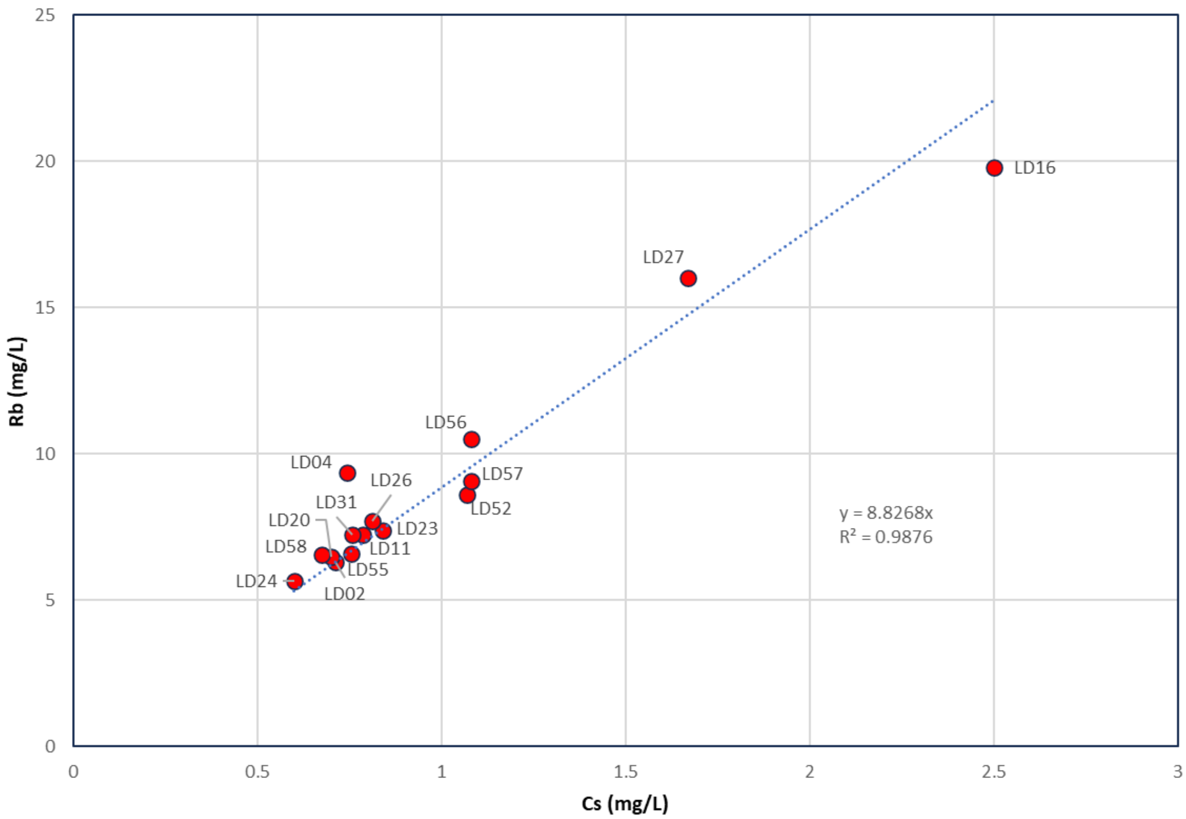

Figure 16. Distribution of Cs and Rb concentrations in oil brine samples from the Leduc Formation in central Alberta. Samples LD04, LD16, LD27, LD52, LD56, LD57, and LD58 belong to the Bashaw reef complex.

The results indicate that in Upper Devonian reef structures, brines evolved from high to low temperatures and alkali metal concentrations increased. Spatially, this correlation depicts a trend in the northeastern direction, suggesting that the fluids were sourced in southwest-central Alberta, close to the deformation belt (Figure 1), which is supported by previous studies (Qing and Mountjoy, 1992; Bachu, 1995, 1997; Drivet and Mountjoy, 1997). The strong correlation between Cs and Rb, as shown in Figure 16, allows the use of molar ratios to characterize these brines. Figure 18a shows the Li concentration versus the Rb/Cs molar ratio for all the samples and depicts two trends in opposite directions. A vertical trend characterized by Lower–Middle Devonian oil brines (Granite Wash, Keg River Formation, and Gilwood Member with some samples from the Slave Point Formation), and a horizontal trend primarily formed by Middle–Upper Devonian oil brines (Beaverhill Lake Group [undivided], Swan Hills, Leduc, and Nisku formations, and Wabamun Group with some samples from the Slave Point and Keg River formations).

Figure 18a shows that, in general, Lower–Middle Devonian oil brines differ significantly in their alkali metal compositions from Middle–Upper Devonian oil brines, implying that these brines have a distinctive alkali metal composition that can be used to identify their source.

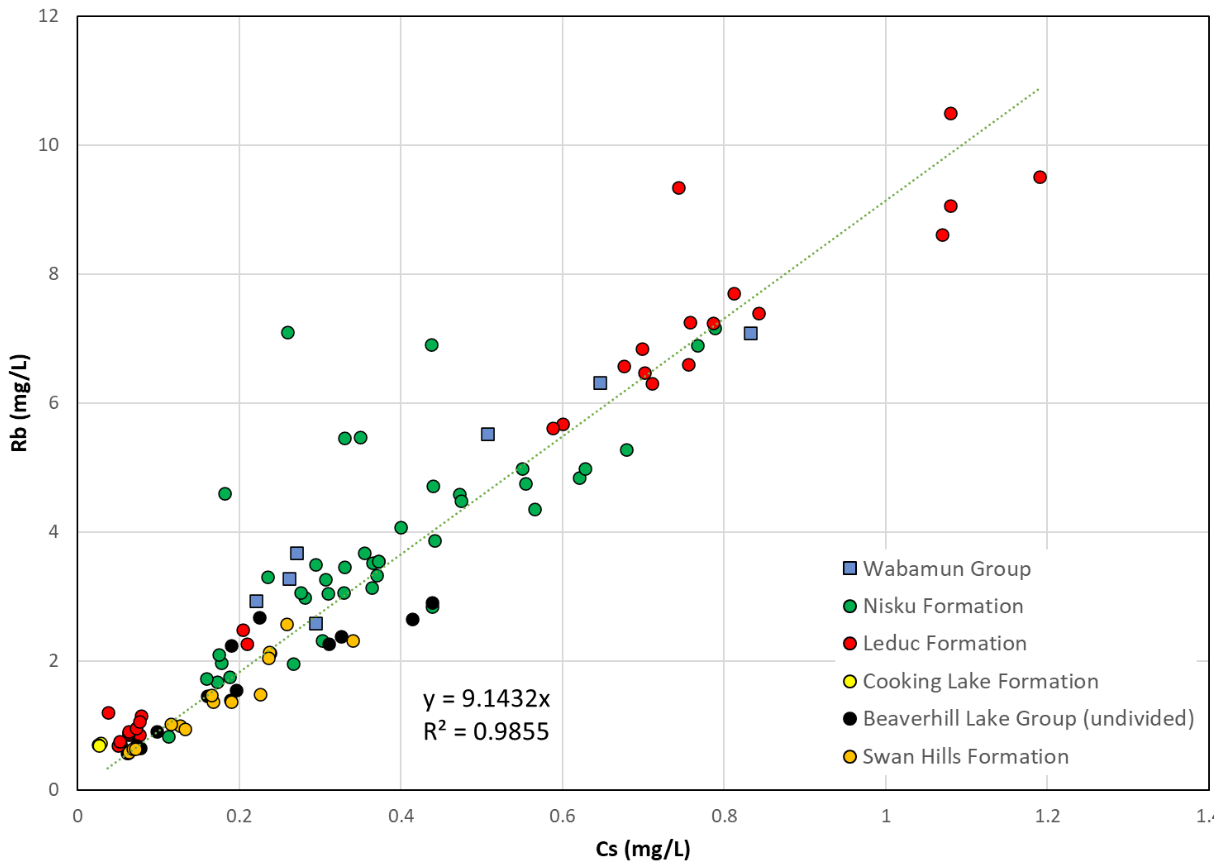

Figure 17. Alkali metal (Cs and Rb) compositions of Middle–Upper Devonian oil brines in Alberta. Despite a wide variation in Li concentrations, Rb and Cs exhibit a high correlation in most samples.

Figure 18b shows details of the horizontal trend, which includes most of the Upper Devonian oil brine samples, except for three samples from the Cooking Lake Formation, two samples from the Nisku Formation, and one from the Leduc Formation with anomalous Rb/Cs molar ratios. The Rb/Cs molar ratios for the brine samples in the horizontal trend range from 7 to 26. Upper Devonian samples from the Nisku and Leduc formations and Wabamun Group with Li concentrations of economic interest (above 40 mg/L) have Rb/Cs molar ratios between 12 and 26. Interestingly, the horizontal trend predominantly encloses samples from the Swan Hills, Leduc, and Nisku formations and Wabamun Group but also includes samples from the Keg River and Slave Point formations. These brine samples from the Keg River Formation also come from reef structures, those in the Rainbow (KR17, KR18, KR25, KR33, and KR34) and Shekilie (KR07 and KR28) basins (Figure 11). The brine samples from the Slave Point Formation (SP09 to SP14) come from the CCSPRC (Figure 11). This characteristic is shared by the Middle–Upper Devonian oil brines, all of which are related to dolomitized reservoirs in reef structures. In the samples analyzed, Li does not correlate with any other elements except for the alkali metals. The Rb/Cs molar ratios are important because, as shown in Figure 18, a molar ratio between 7 and 26 appears to identify samples related to reef structures, which are characterized by high Li contents.

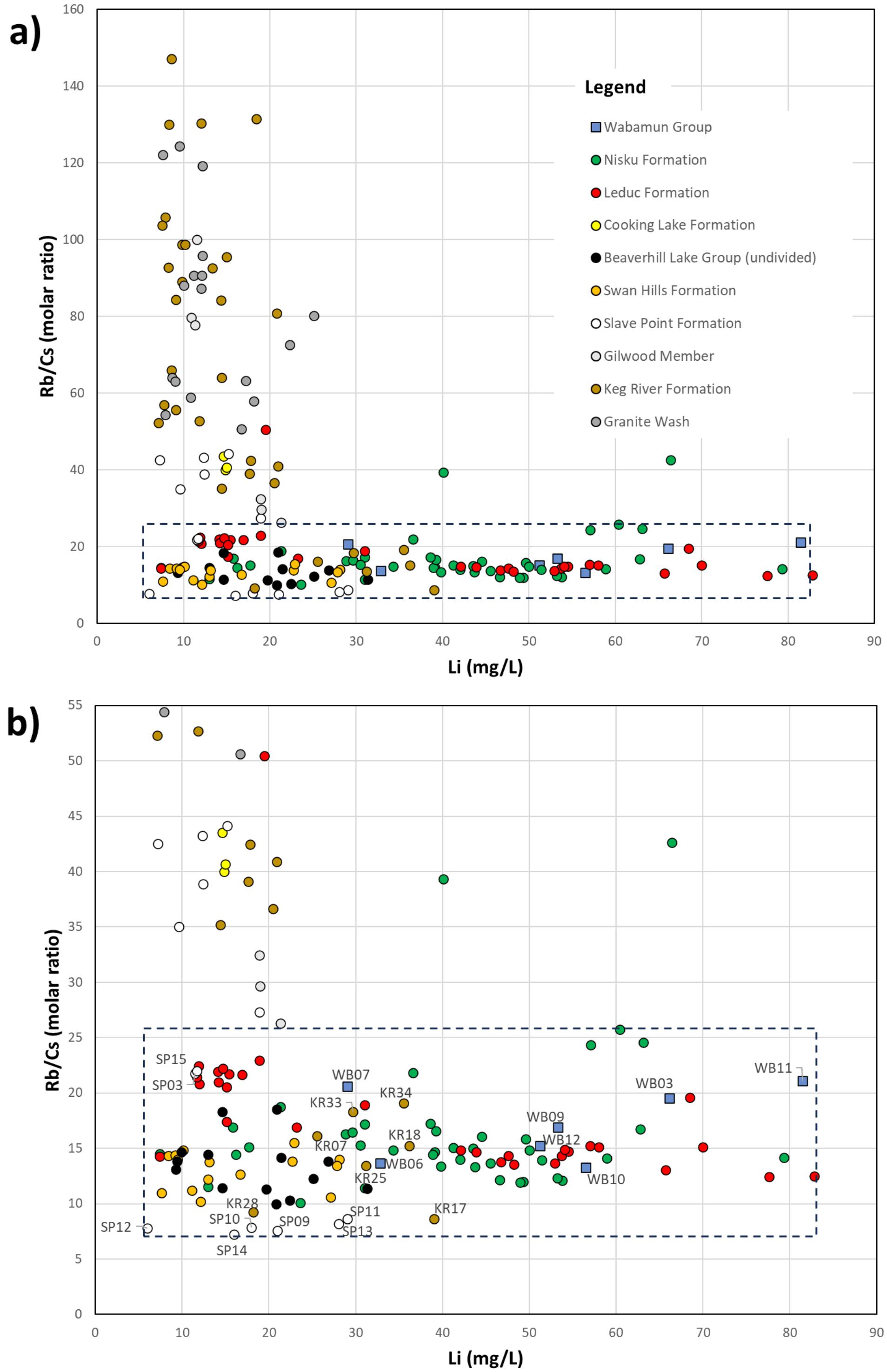

Figure 18. A Li concentration versus Rb/Cs molar ratio diagram for (a) Devonian oil brines in Alberta and (b) selected Devonian oil brines—detailed view of the rectangular area in Figure 18a to illustrate geochemical differences and similarities between Lower–Middle (Granite Wash, Keg River Formation, Gilwood Member, and Slave Point Formation) and Middle–Upper Devonian (Beaverhill Lake Group [undivided], Swan Hills, Cooking Lake, Leduc, and Nisku formations, and Wabamun Group) oil brines.

The Keg River Formation oil brines in the Rainbow and Shekilie basins exhibit a southwest to northeast decrease in Li concentrations comparable to what was observed in brines from the Leduc Formation reefs (Figure 11; Appendix 1, Table 3). Brines from the Rainbow Basin contain higher Li concentrations than brines in the Shekilie Basin. Lewchuck et al. (2000) found that geochemical, paleomagnetic, and petrographic data advocate for the involvement of deep basinal brines at high temperatures during the dolomitization of the Rainbow Basin reefs. Qing and Mountjoy (1992) conducted a detailed fluid inclusion study of the Presqu'ile Barrier, a Middle Devonian carbonate barrier 400 km wide located northwest of the sampling locations (Figure 1). Their research found that the $^{87}Sr/^{86}Sr$ ratio, homogenization temperatures, and calculated $\delta^{18}O$ values of dolomitizing fluids in dolomite cement decrease towards the northeast. Qing and Mountjoy (1992) attributed these progressive temperature and isotopic variations to advective heat transported by the regional migration of hot fluids that originated after tectonic thrusting and compression during the evolution of the WCSB. These studies and their correlations suggest that high-temperature fluids may have been regionally distributed in the Alberta Basin, transporting alkali metals to locations where secondary permeability allowed brine storage.

6.2 Lithium and Boron Sources

Due to its chemical characteristics, Li is useful for identifying geological processes that affect fluids, minerals, and rocks. Lithium isotopes are not affected by redox reactions or atmospheric, biological, or hydrogeological cycles (Burton and Vigier, 2011). However, natural Li reservoirs have a wide variability in Li isotopic composition, represented by a range of about 60‰ (Tomascak et al., 2016). For this reason, many studies have been dedicated to understanding Li isotope fractionation. The conclusions of these studies agree on three main factors controlling Li isotope fractionation: coordination number (bond strength), temperature, and chemistry of the solution, including pH (Hindshaw et al., 2019).

Figure 19 shows a compilation of Li isotopic compositions from various reservoirs, enabling a preliminary comparison with the δ^7Li values obtained in this study, which range from 8.3‰ to 29.1‰, and the lowest value (5.8‰) reported by Eccles and Berhane (2011) for the Alberta Basin. This range is identified by the blue contoured box in Figure 19. Considering the geological environment of the Alberta Basin, its depth, the $\delta^{18}O$ and δ^2H compositions of the oil brines, and their chemistry, these are the isotopic ranges of some potential Li sources: seawater from 30.6‰ to 30.8‰ (Brand et al., 2014), altered mid-ocean ridge basalt (MORB) from 6.6‰ to 20.8‰ (Chan et al., 2002a), river waters from 2‰ to 43‰ (Huh et al., 1998; Dellinger et al., 2015; Murphy et al., 2019), cold seep pore waters from 7.5‰ to 45.7‰ (Scholz et al., 2010), marine sediments from -4.3‰ to 14.5‰ (Chan et al., 2006), general soils from -5‰ to 15‰ (Penniston-Dorland et al., 2017), continental volcanic rocks from 0‰ to 7‰ (Meixner et al., 2020), gneisses from -17.9‰ to 15.7‰ (Teng, 2005), and granites from -3‰ to 7‰ (Teng et al., 2006).

However, it is also necessary to consider factors that can further modify the isotopic composition of oil brines, such as meteoric and marine burial diagenesis (Dellinger et al., 2020), weathering, the availability of dolomites with high Li detrital composition (Taylor et al., 2019), or sourcing of Li from deep marine sedimentary deposits (Chan et al., 1994). Therefore, it is helpful to introduce a second element, B, and its isotopes, that may have a similar origin to Li and a comparable isotopic behaviour. Figure 20 shows the relationship of δ^7Li versus $\delta^{11}B$ and the distribution of Lower to Upper Devonian oil brines. The sizes of the bubbles represent Li concentrations.

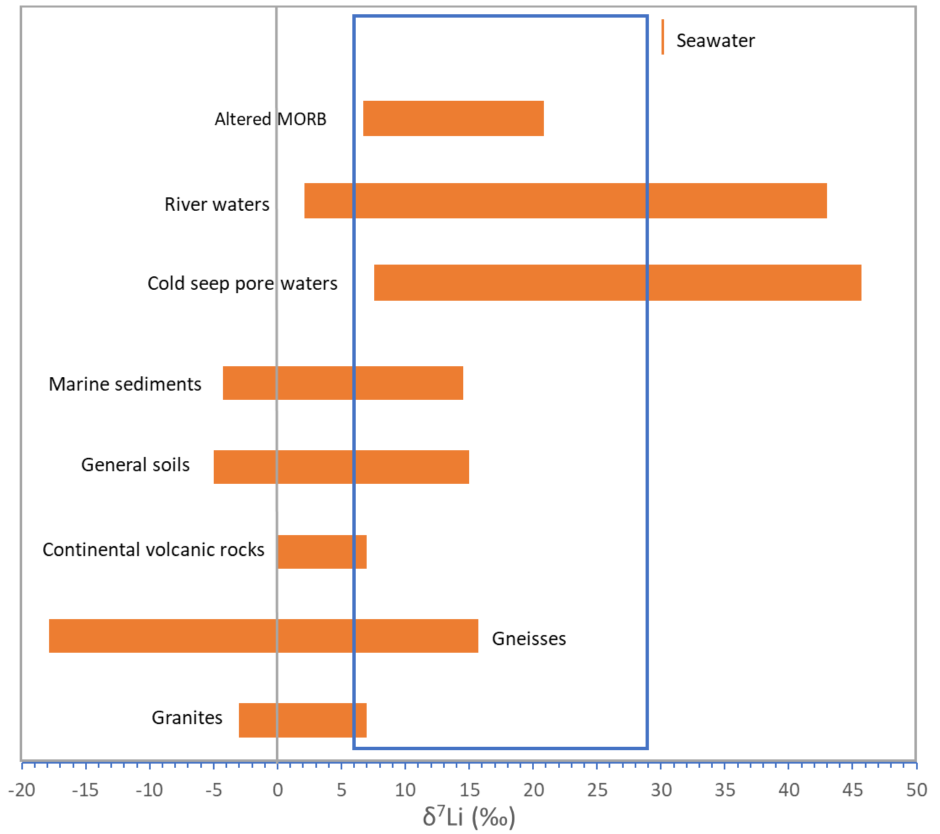

Figure 19. Lithium isotopic composition of various reservoirs: seawater (Brand et al., 2014), altered mid-ocean ridge basalt (MORB; Chan et al., 2002a), river waters (Huh et al., 1998; Dellinger et al., 2015; Murphy et al., 2019), cold seep pore waters (Scholz et al., 2010), marine sediments (Chan et al., 2006), general soils (Penniston-Dorland et al., 2017), continental volcanic rocks (Meixner et al., 2020), gneisses (Teng, 2005), granites (Teng et al., 2006). The blue contoured box represents the δ^7Li range identified in Devonian oil brines from the Alberta Basin (from this study and Eccles and Berhane, 2011).

Residual evaporitic brines, which could potentially be a source of B, are characterized by δ^{11}B values that are higher than those in modern seawater due to the retention of ^{10}B by coexisting salts (Vengosh et al., 1992). Several studies conclude that Paleozoic oceans were depleted in ^{11}B by up to 10‰ (Joachimski and van Geldern, 2005; Ma et al., 2011), compared to modern values (~40‰). Assuming that the effect of evaporation on B isotopes was comparable to what is observed in modern environments, values above those of the theoretical Devonian seawater (~30‰) suggest that evaporitic sources of B are present in the Devonian formations investigated (Figure 20; Appendix 1, Table 3).

Multiple studies have documented high B concentrations (~100 ppm) in marine clay sediments and have shown that the uptake of B by sediments can significantly affect the B isotope composition and concentration of the oceans (Ishikawa and Nakamura, 1993). Furthermore, it is widely accepted that, as in the case of ^{6}Li, ^{10}B is preferentially taken up into clays, which is an output flux of both elements in the oceans, resulting in enriched ^{11}B seawater (Schwarcz et al., 1969; Spivack et al., 1987). Figure 20 depicts a negative correlation between Li concentrations and isotopic compositions, as brines with high Li contents tend to have lower δ^7Li and δ^{11}B values, indicating the influence of Li and B desorbed from clays and marine sediments on the isotopic composition of the Devonian oil brines.

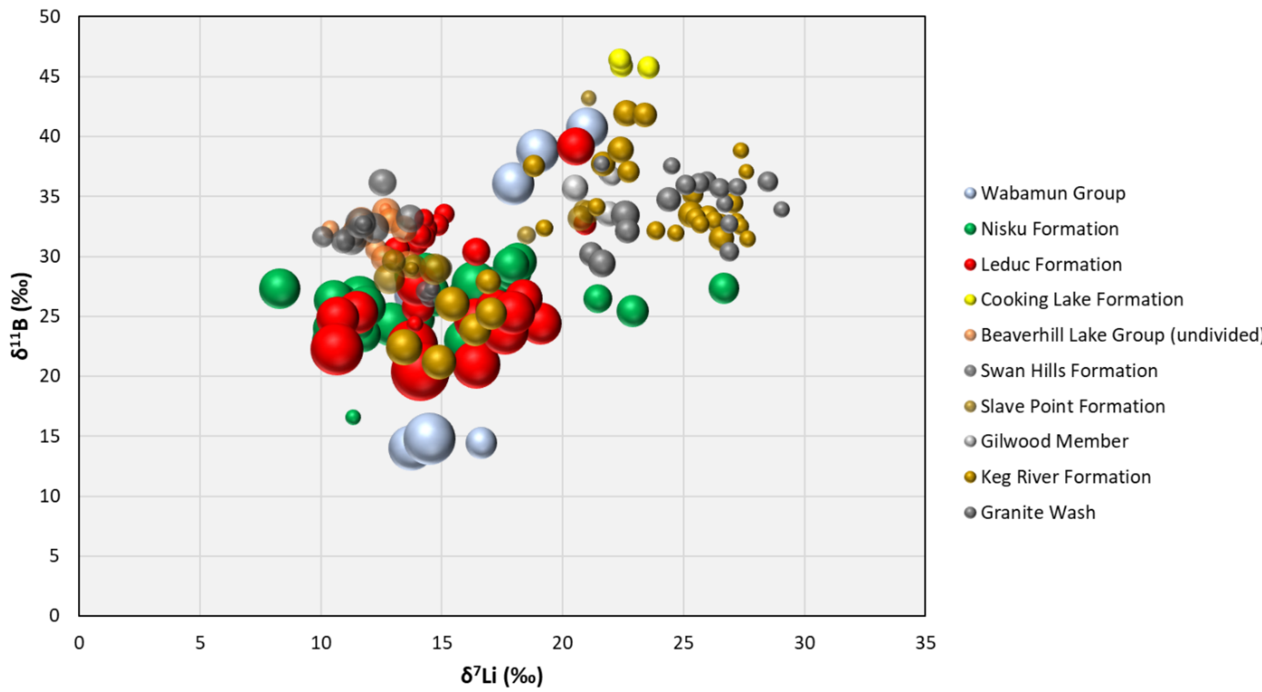

Figure 20. The δ^7Li versus $\delta^{11}B$ composition of Devonian oil brines in Alberta. The bubble size is proportional to the concentration of Li.

The Li mass balance in seawater is primarily determined by two main factors: inputs from continental weathering and marine hydrothermal systems, and outputs resulting from Li removal by clays (Hindshaw et al., 2019). Establishing the secular variations of seawater δ^7Li has proven to be a challenging task. The most extensive record of seawater δ^7Li was obtained from foraminifera (Misra and Froelich, 2012) and brachiopods (Dellinger et al., 2020). Those samples, spanning the Cretaceous to Pleistocene systems, had δ^7Li values of ~30‰ and 31‰, respectively. Even though the endmembers of the seawater δ^7Li suggest a constant composition, a trend towards lower values was detected between the Paleocene and the Eocene (~20‰ to ~25‰) by Misra and Froelich (2012). This variation was attributed to an increase in weathering and denudation resulting from the uplift of the Himalayas. In a recent study, Liu et al. (2025) measured Li isotopes in Devonian brachiopod samples not affected by diagenesis. They found that starting in the Middle Devonian, δ^7Li in seawater increased from 8‰ to 18‰, suggesting a considerable increase in weathering and regolith thickness during the second half of the Devonian.

During the Devonian, deep marine sediments were deposited to the west in what is currently known as British Columbia (Weissenberger and Potma, 2001). These sediments may have been able to adsorb Li from seawater. The isotopic evolution of Devonian oil brines of Alberta, coupled with their enrichment in Li, strongly suggests that isotope fractionation was involved. The wide variation in δ^7Li values (5.8‰ to 29.1‰) suggests that Li was recycled and concentrated as it moved from seawater to clays and marine sediments, and ultimately to products of diagenesis and dolomitization. Extensive field and experimental studies have shown that clays and marine sediments can adsorb Li. It is known that ^6Li will preferentially incorporate into clay structures, which results in a fluid enriched in ^7Li (Tomascak et al., 2016; Penniston-Dorland et al., 2017; Pogge von Strandmann et al., 2020).

The δ^7Li range identified for the Middle–Upper Devonian in the Alberta Basin is not uncommon. Macpherson et al. (2014) reported δ^7Li data from produced water in oil and gas wells of the Appalachian Plateau (Middle to Upper Devonian) and the Gulf Coast Sedimentary Basin (Jurassic to Plio-Pleistocene) reservoirs. These produced waters had δ^7Li values ranging from 4.2‰ to 16.6‰, which is close to the range of brines from the Middle–Upper Devonian in the Alberta Basin (5.8‰ to 26.7‰). Macpherson et al. (2014) note that the water produced from the Appalachian Plateau, an unconventional (tight shale) gas reservoir, is similar in chemistry to water produced from conventional reservoirs and concluded that the source of Li is related to shales and clay minerals.

Experimental work by Li and Liu (2022) has provided insight into the extent of isotope fractionation in diverse types of clay, specifically kaolinite and smectite, at various Li concentrations. The study found that the range of isotope fractionation was up to 30‰ for kaolinite and 5‰ for smectite, resulting from kinetic and equilibrium isotope fractionation, respectively. These δ^7Li values are close to the isotopic compositions of this study's Devonian oil brines (5.8‰ to 29.1‰), suggesting that clays may control Li availability in such fluids. These observations strongly suggest that most of the Li and B present in the analyzed brines were initially sourced from weathering products, such as clays and fine sediments, and Devonian seawater.

However, to explain the presence of Li-enriched brines in carbonate reservoirs, a mechanism that can efficiently extract and mobilize fluids from clays and marine sediments is necessary.

6.3 Flow Paths and Lithium Distribution in the Alberta Basin

Oliver (1986) proposed a hypothesis to explain the migration of fluids over long distances in a foreland basin located on a continental margin. Pore fluids of marine origin were expelled in response to sediments being overridden by thrust sheets. The expelled fluids can reach long distances into adjacent parts of the foreland basin, provided permeable units channelize these fluids. In the Alberta Basin, the existence of channelized flow has been identified in the Upper Devonian (Hitchon, 1969; Hitchon et al., 1990; Bachu, 1995; Drivet and Mountjoy, 1997) as well as in the Middle Devonian (Qing and Mountjoy, 1992). Orogenic tectonic processes influencing southwest to northeast flow near the fold-and-thrust belt were postulated in Bachu (1995, 1997), and those near the Presqu'ile Barrier were postulated in Qing and Mountjoy (1992). Based on ^{87}Sr/^{86}Sr values measured in calcites and dolomite cement, Machel et al. (2000) and Buschkuehle and Machel (2002) proposed a squeegee-type fluid flow for the Alberta Basin. According to these studies, the calcite cement of the Southesk-Cairn carbonate complex, located near the deformation belt (Figure 7), has ^{87}Sr/^{86}Sr values of approximately 0.7320. In contrast, carbonate rocks located approximately 100 km to the northeast have ^{87}Sr/^{86}Sr values as low as 0.7100. This progressive decline in the ^{87}Sr/^{86}Sr isotope values was explained as evidence of the flow of expelled formation fluids away from the fold-and-thrust belt during the Laramide orogeny.

Figure 21 shows the distribution of δ^7Li and ^{87}Sr/^{86}Sr in the samples. In this figure, the estimated isotopic composition of Middle–Upper Devonian seawater (δ^7Li is ~18‰ [Liu et al., 2025] and ^{87}Sr/^{86}Sr is ~0.70800 [Denison et al., 1997]) is shown as a reference.

Figure 21 also shows a fluid in equilibrium with the high ^{87}Sr/^{86}Sr (0.7323) values measured in late calcites of the Southesk-Cairn carbonate complex (SCC; Machel et al., 2000). The red dashed line indicates the maximum Sr isotope ratio of basinal shale (MASIRBAS) defined in Machel and Cavell (1999), which, according to these authors, applies to shales from the Middle Devonian to the Pleistocene.

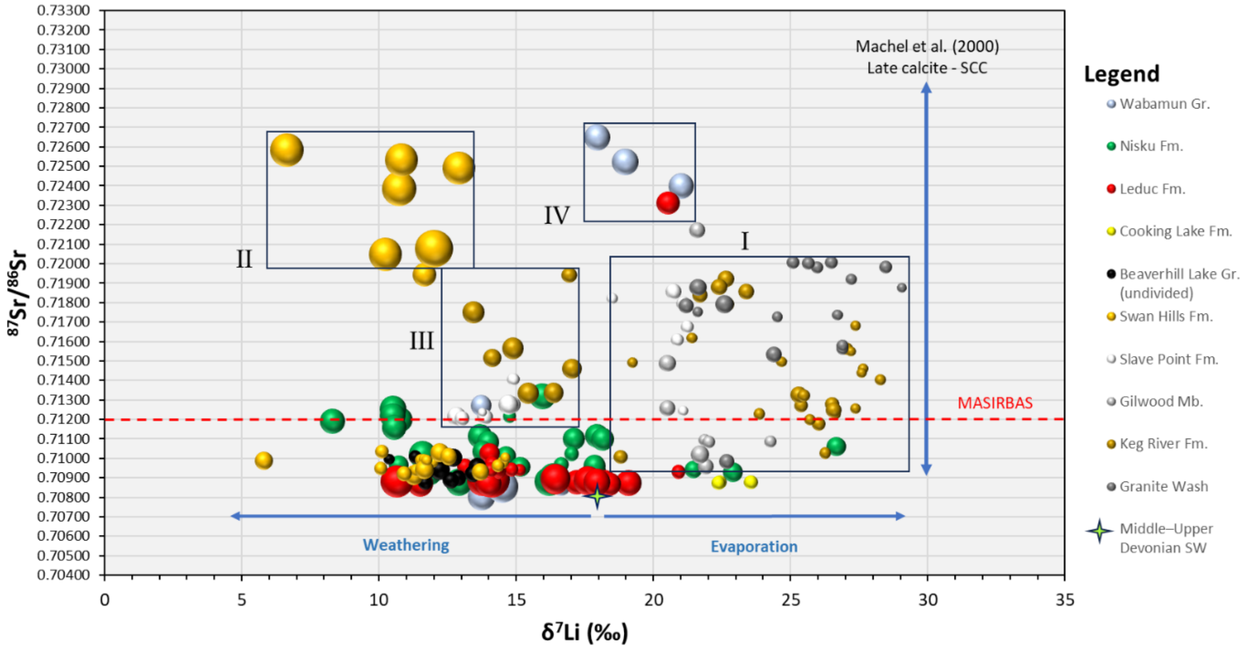

Figure 21. The δ^7Li versus $^{87}Sr/^{86}Sr$ composition of Devonian oil brines in Alberta. The bubble size is proportional to the concentration of Li. The four boxes (I to IV) indicate groups of brine samples with isotopic compositions characteristic of their location in Alberta. The estimated composition for Middle–Upper Devonian seawater is ~18‰ for δ^7Li (Liu et al., 2025) and ~0.70800 for $^{87}Sr/^{86}Sr$ (Denison et al., 1997). Abbreviations: MASIRBAS, maximum Sr isotope ratio of basinal shale; SCC, Southesk-Cairn carbonate complex; SW, seawater.

Box I in Figure 21 includes all the Lower–Middle Devonian oil brines from the Granite Wash, Keg River Formation, Gilwood Member, and Slave Point Formation located east of the PRA area (Figure 9). Box I is defined by $^{87}Sr/^{86}Sr$ values from 0.70957 to 0.72006, representing mixing with a more radiogenic fluid, and a δ^7Li variation from 18.5‰ to 29.1‰, which indicates that these brines underwent extensive isotopic fractionation. Several of these samples plot close to the isotopic value of Devonian seawater (~18‰) and exhibit an increase in δ^7Li. This trend towards higher Li isotope values in Lower–Middle Devonian oil brines may be related to the effects of evaporation, which enriches the brine in ^{7}Li as evaporation progresses (Chan et al., 2002b), resulting in higher δ^7Li values than the estimate for Devonian seawater. The Li concentrations in these samples are in the low range, with a maximum value of 25.1 mg/L. Assuming a fluid with a composition close to Devonian seawater mixed with a radiogenic fluid, it can be concluded that the latter did not contribute much Li to the resulting brine. The trend of Li isotopic fractionation, with lower values correlating to higher Li concentrations, suggests chemical weathering, which can be explained by the progressive accumulation of ^{6}Li in pore fluids from marine sediments and clay minerals.

Based on the available isotopic data, the factors preventing a higher accumulation of Li in the oil brine samples enclosed in box I are not evident. In some of these samples, Li concentrations are about 20 mg/L, and the extent of Li isotopic fractionation is around 10.6‰. This suggests that Li in these brines may have also been adsorbed and desorbed during chemical weathering, albeit at a lower rate.

There is limited data available on the composition of basement rocks near the Lower Devonian geological units in the Alberta Basin. However, Smith et al. (2024) analyzed drillcore containing granite to granodiorite from the Precambrian basement underlying the WCSB in southern Saskatchewan. According to these authors, the upper 100 m of the basement rocks were altered to illite, smectite, and mica by high-temperature hydrothermal fluids. It is tempting to consider a similar process in the PRA area, where argillitic alteration zones of hydrothermal origin may have concentrated alkali metals from seawater in the basement rocks. However, more research needs to be done to better understand the transfer of Li and other metals between the basement and sedimentary basin rocks.

Box II includes $^{87}Sr/^{86}Sr$ values from 0.72047 to 0.72585 and δ^7Li values from 6.6‰ to 12.9‰ measured in oil brines from the Swan Hills Formation (SH01, SH07, SH10, SH11, SH13, and SH14; Appendix 1, Table 3), located south of Fox Creek (Figure 7); these brines are characterized by high Li concentrations up to 112 mg/L (Eccles and Berhane, 2011; Appendix 1, Table 3). The location of these brines, which have high TDS values (Appendix 1, Table 2), coincides with the boundaries of the heavy brine (defined as having TDS values >200 000 mg/L) located updip in the Woodbend–Beaverhill Lake aquifer, defined in Michael et al. (2003). The effects of mixing with meteoric waters and the degree of water-rock interaction could not be estimated in these brines, as water isotopes were not reported in the Eccles and Berhane (2011) study, and it was not possible to access these wells during the 2021–2024 brine sampling program. However, Figure 19 shows that a radiogenic fluid has a strong influence on the Swan Hills Formation brines included in box II, compared to most brines from the same formation. Also, the extent of isotopic fractionation indicates that Li was efficiently concentrated in these brines.

Based on the correlation between Li isotope data measured in basement rocks and the Swan Hills Formation brine samples from the Fox Creek area mentioned above, Eccles and Berhane (2011) proposed that Li-bearing fluids were sourced in the basement and that this fluid may have used the Granite Wash and Gilwood Member as conduits to reach the Devonian aquifers. The data presented here do not support this hypothesis; it is improbable that the Li isotope signature of unaltered basement rocks is preserved in the brines, as the isotopes would fractionate in their journey to Devonian reservoirs. Even brines from the same geological unit are highly fractionated due to chemical weathering. On the other hand, as shown in this study, samples from the Lower–Middle Devonian Granite Wash and Gilwood Member exhibit significantly different isotopic and alkali metal compositions compared to those from Middle–Upper Devonian oil brines (Figures 13 and 18). Therefore, based on the available data for this study, Lower–Middle Devonian geological units near the basement are unlikely to be pathways connecting Li-enriched basement fluids with Middle–Upper Devonian aquifers.

Box III encompasses Middle Devonian oil brines from the Keg River Formation in the Rainbow and Shekilie basins and the Slave Point Formation in the CCSPRC, northwestern Alberta (Figure 11). The isotopic compositions of these samples, $^{87}Sr/^{86}Sr$ values from 0.71204 to 0.71940 and δ^7Li values from 12.8‰ to 17.0‰, indicate that Li isotopic fractionation has been more extensive in these brines relative to other Lower–Middle Devonian oil brines (Figure 21, Box 1). The δ^7Li values of these samples are close to Middle–Upper Devonian oil brines hosted in reef structures. This observation also correlates with the range of Rb/Cs molar ratios measured in the Box III brines, which differ from Rb/Cs molar ratios found in the rest of the Keg River and Slave Point formation brines, as presented in Section 6.1.

Box IV includes $^{87}Sr/^{86}Sr$ values from 0.72311 to 0.72649 and δ^7Li values from 18.0‰ to 21.0‰ measured in brines from the Wabamun Group (WB09, WB10, and WB12) and the Leduc Formation (LD59). These samples are in the LFRC, part of the PRA (Figure 9), and are among the most radiogenic brines measured in this study. The Li concentrations are relatively high, ranging from 51.2 to 56.5 mg/L (Appendix 1, Table 3).

The remaining samples, represented in Figure 21, are Middle–Upper Devonian oil brines with $^{87}Sr/^{86}Sr$ values from 0.70804 to 0.71319 and δ^7Li values from 5.8‰ to 26.7‰. Their $^{87}Sr/^{86}Sr$ composition suggests that mixing with radiogenic fluids was not as pervasive as in other Devonian oil brines. Except for the high Li brines included in box II (Figure 21), the remaining Swan Hills Formation samples and those from the Beaverhill Lake Group are within the isotopic ranges of Upper Devonian oil brines. This implies that the flow paths and water-rock interactions for these brines were similar. On the other hand, the Li isotopes indicate an extensive process of chemical weathering, reflected by the depletion of ^7Li in the brines, and high Li concentrations found in samples not affected by dilution, such as in the case of the Leduc Formation brines in the HGR and BRC. Other Leduc Formation brine samples with high $^{87}Sr/^{86}Sr$ values and relatively high Li concentrations were reported by Huff et al. (2019) in the Sturgeon Lake area

(LD12, LD35, and LD36; Appendix 1, Table 3), however, Figure 21 does not include these samples, as δ^7Li was not analyzed for that study.

7 Conceptual Model

The geochemical results presented in this study can be summarized in a schematic model that provides insights into the accumulation and transport of Li and other species in the brines of the Devonian sequence of Alberta (Figure 22). During the Devonian period, marine deposits were accumulated in what is now western Alberta, parts of British Columbia, and the Northwest Territories (Weissenberger and Potma, 2001). The Li and B isotopes indicate that these deep fine-grained sediments may have contained Li but also adsorbed Li and other alkali metals from seawater, which were later concentrated in the products of chemical weathering, including clay minerals. From the Devonian to the Cretaceous periods, the chemistry of pore fluids in these deposits may have been somewhat modified by burial and diagenesis, as indicated by stable isotopes of B and Li. During the Cretaceous, the Laramide orogeny led to increased pore-pressure buildup in sediments containing modified seawater. Due to increasing pressure, this fluid migrated both vertically and horizontally to areas of enhanced permeability created by diagenetic processes, fracture zones, and reef structures. At that time, diagenesis and dolomitization were already well underway in the reef structures of the carbonate platforms to the east. Due to increasing subsidence, temperatures rose rapidly in the deepest parts of the basin, increasing the capacity of fluids to remove Li from clays and other sediments (Chan et al., 1994). This led to the expulsion of fluids from pores and hydrated minerals during orogenic processes, as described by Oliver (1986). The now Li-enriched fluid, mixed with oil, began migrating upwards in channelized, preferential flow pathways facilitated by dolomitized carbonate rocks of the Swan Hills Formation and the Cooking Lake Platform (Drivet and Mountjoy, 1997), and perhaps through some basement structures (Machel et al., 2000).

The data, shown in Figure 21, suggest that most Devonian oil brines have a radiogenic component. However, they also indicate that Li in these brines fractionated from the initial composition of Devonian seawater. The ^{87}Sr/^{86}Sr and δ^7Li data suggest that a radiogenic fluid (i.e., ^{87}Sr-enriched) is dominant in the Lower–Middle Devonian oil brines and in some samples from the Swan Hills Formation (Middle–Upper Devonian), more specifically, in brines from the Fox Creek area. A highly radiogenic fluid was also detected in samples collected from the Leduc Formation and the Wabamun Group in the PRA area. Lower ^{87}Sr/^{86}Sr values dominate in brines from the Swan Hills Formation and the Beaverhill Lake Group in west-central Alberta, and the Leduc and Nisku formations and Wabamun Group in central Alberta.

Analysis of hydrodynamic data (Wendte et al., 1998) and stratigraphic observations (Buschkuehle and Machel, 2002) suggest that close to the deformation belt, the Upper Devonian Swan Hills, Leduc, and Nisku formations and the Wabamun Group constituted a mega-aquifer. This is confirmed by the chemistry and isotopic composition of brines from wells in the Fox Creek–PRA corridor (Figure 1). The Li-enriched fluid moved updip and mixed with residual evaporitic brines in all Upper Devonian formations. However, the Na-Cl-Br systematics of the Swan Hills Formation brines indicate that the Li-enriched fluid from the west did not contribute considerable amounts of halogens to the Upper Devonian formations.

The Keg River Formation well samples that are located in the west-central part of the province have intermediate ^{87}Sr/^{86}Sr values and Rb/Cs molar ratios. Based on its radiogenic character, it has been proposed that the fluid in the Southesk-Cairn paleoaquifer interacted with metasedimentary Precambrian rocks (Machel et al., 2000). If so, most Devonian oil brines should contain a solute contribution from the basement, reflected in brines with ^{87}Sr/^{86}Sr values higher than Devonian seawater. However, as concluded from high Rb/Cs molar ratios, low Li concentrations, and high δ^7Li values detected in the Granite Wash brines, a significant Li contribution to Middle–Upper Devonian oil brines from the basement in the Fox Creek–PRA corridor is unlikely. In addition, according to δ^{18}O and δ^2H isotopes, the brines from the Granite Wash, Gilwood Member, and Keg River and Slave Point formations (Lower–Middle Devonian) did not mix with brines from the Beaverhill Lake Group, Swan Hills, Cooking Lake, Leduc, and Nisku formations, and Wabamun Group (Middle–Upper Devonian). Water interactions with radiogenic shales at high temperatures appear to be a more viable explanation for the $^{87}Sr/^{86}Sr$ values found in Devonian oil brines. If that is the case, Sr, Li, and B isotopes could be used to identify alkali metal sources in shales and other fine-grained rocks.

In the northwestern corner of Alberta, the migration of a Li-enriched fluid occurred in the reef buildups of the Rainbow Basin, Comet Platform, and Marlowe Field of the Keg River Formation. This is supported by the brines' alkali metal composition. A large-scale fluid flow was documented in the Presqu'ile Barrier north of these reef build-ups, characterized by decreasing $^{87}Sr/^{86}Sr$ values and homogenization temperatures in a northeastern direction (Qing and Mountjoy, 1992). However, alkali metals and stable isotope compositions of the other Lower–Middle Devonian oil brines indicate they were isolated from the Li-enriched fluid.

Previous studies have identified oil migration pathways and estimated the temperature history of the WCSB (Stoakes and Creaney, 1984; Buschkuehle and Machel, 2002; Stacey et al., 2021). These findings coincide with the spatial distribution of high Li brines in Devonian reservoirs and fluid temperatures estimated in this work. Therefore, it is possible that both Li-enriched fluids and oil migrated simultaneously from the west to eventually occupy Devonian reservoirs in the east.

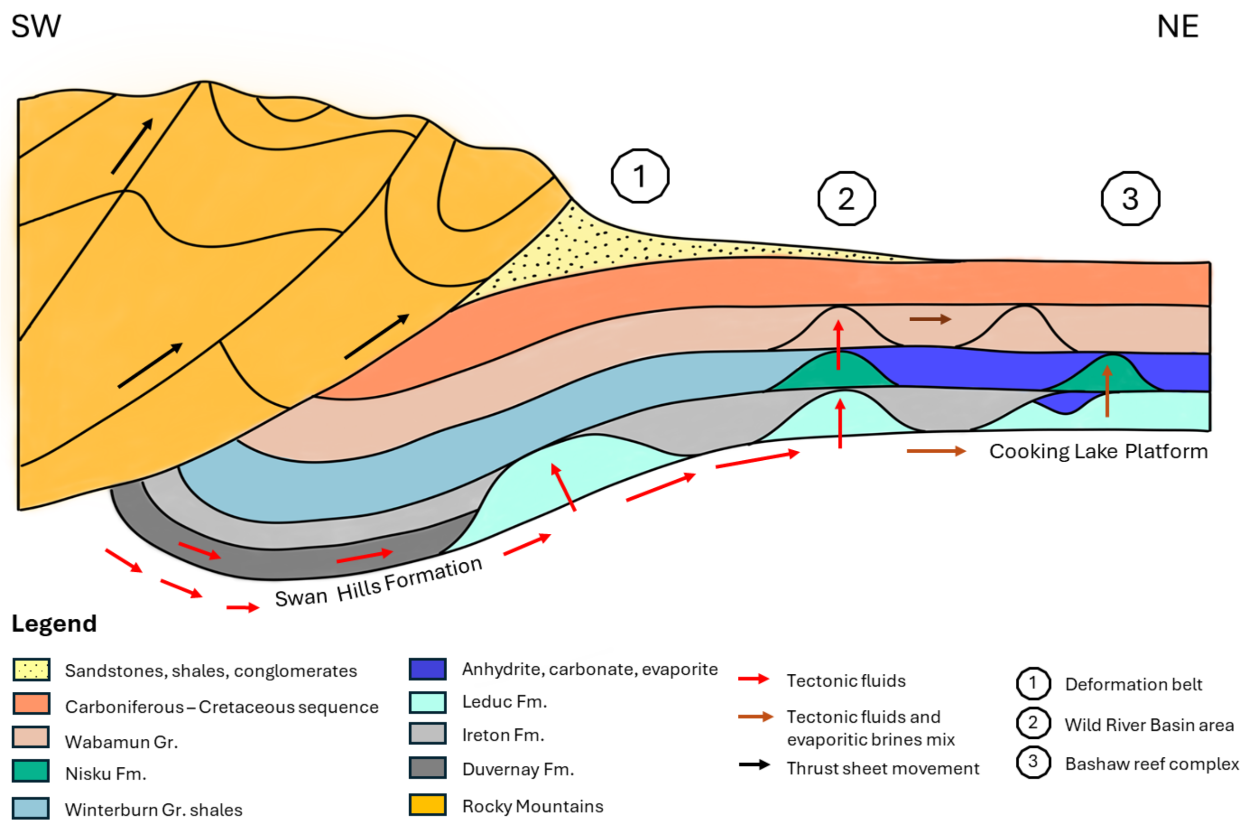

Figure 22. Schematic model representing the effects of the Laramide orogeny on pore water and hydrated minerals, which were subjected to high pressures and temperatures. Enriched in Li, these tectonic fluids may have been channelized by carbonate platforms such as Beaverhill Lake (Swan Hills) and Cooking Lake, where they found residual evaporitic brines in the Leduc, Nisku, and Wabamun reservoirs. High-temperature fluids (red arrows) migrated both horizontally and vertically, interacting with the rocks and losing heat, while mixing with resident evaporitic brines and meteoric water (brown arrows). Abbreviations: NE, northeast; SW, southwest.

8 Conclusions

- Weathering of continental rocks contributed material to Devonian deep-marine sediments, which may have also adsorbed lithium and alkali metals from seawater; these elements were later concentrated in clays and fine-grained sediments. Burial and diagenesis from the Devonian to Cretaceous periods altered pore-fluid chemistry, as evidenced by stable isotopes of boron and lithium.
- The Laramide orogeny during the Cretaceous period increased pore pressure, leading to fluid migration through permeable zones, such as fractures and reef structures. Elevated temperatures in deep basin areas enhanced lithium release from clays and sediments. Lithium-enriched fluids were expelled and migrated upwards through dolomitized carbonate rocks (e.g., Swan Hills Formation, Cooking Lake Platform), possibly mixing with oil and travelling through basement structures.
- The strontium isotope ($^{87}Sr/^{86}Sr$) and lithium isotope (δ^7Li) data indicate radiogenic fluids are dominant in Lower–Middle Devonian oil brines and parts of the Swan Hills Formation, especially near Fox Creek. Brines from central Alberta units (e.g., Leduc Formation, Nisku Formation, Wabamun Group) exhibit lower $^{87}Sr/^{86}Sr$ values, indicating distinct fluid histories.
- Stratigraphic and hydrodynamic data confirm that geological units like the Swan Hills, Leduc, and Nisku formations, and the Wabamun Group formed a mega-aquifer near the deformation belt. Lithium-enriched fluids mixed with residual evaporitic brines in Upper Devonian formations, but their halogen contribution was minimal. Oxygen and hydrogen isotopic data ($\delta^{18}O$, δ^2H) confirm no mixing between Lower–Middle and Middle–Upper Devonian oil brines.
- Keg River Formation samples show intermediate isotopic values, possibly due to interaction with Precambrian rocks. However, high δ^7Li, low lithium, and high rubidium/cesium ratios in Granite Wash brines suggest limited basement contribution to Middle–Upper Devonian oil brines in the Fox Creek–Peace River Arch corridor.

9 Further Work

To confirm or refute the hypotheses proposed in this report, further investigation is recommended on the isotopic and chemical compositions of shale formations in the basin that may have accumulated Li and other metals of economic value. This would help in understanding potential rock sources of Li, the effects of weathering, and the mechanisms of Li accumulation, adsorption, and desorption in natural environments. Specifically, further research is needed on the role of organic matter in enhancing or reducing Li adsorption, as well as on the impact of fluid chemistry, including pH and alkalinity, in facilitating Li release from minerals. Such insights could provide valuable information for optimizing extraction processes and maximizing the economic benefits of these resources.

The data presented here provide a regional overview of the geochemical processes that affected some of the fluids in the Alberta Basin. However, the role of the gas phase and its effects on the chemistry of the brines must be integrated into this knowledge. This information is also fundamental for assessing the potential of other commodities in the province, such as helium and hydrogen.

Throughout Alberta's geological history, hydrothermal fluids have significantly contributed to the mineralization of economic deposits. Although the interaction of high-temperature fluids with basement rocks has been postulated as a source of metals, the transfer mechanisms and flow paths in some areas remain to be defined. The geochemical characterization of basement rocks and fluids would provide vital information to help answer these questions.

10 References

Alberta Geological Survey (2019): Alberta Table of Formations; Alberta Energy Regulator / Alberta Geological Survey, URL <https://ags.aer.ca/publications/Table_of_Formations_2019.html> [August 2023].

Amthor, J.E., Mountjoy, E.W. and Machel, H.G. (1994): Thermochemical sulfate reduction in the Upper Devonian Nisku platform carbonates, Western Canada Sedimentary Basin; Geochimica et Cosmochimica Acta, v. 58, no. 1, p. 119–137.

Araoka, D., Kawahata, H., Takagi, T., Watanabe, Y., Nishimura, K. and Nishio, Y. (2014): Lithium and strontium isotopic systematics in playas in Nevada, USA: constraints on the origin of lithium; Mineralium Deposita, v. 49, p. 371–379, doi:10.1007/s00126-013-0495-y.

Bachu, S. (1995): Synthesis and model of formation water flow in the Alberta Basin, Canada; AAPG Bulletin, v. 79, p. 1159–1178.

Bachu, S. (1997): Flow of formation water, aquifer characteristics, and their relation to hydrocarbon accumulations, northern Alberta Basin; AAPG Bulletin, v. 81, p. 712–733.

Bachu, S., Yuan, L.P. and Brulotte, M. (1995): Resource estimates of industrial minerals in Alberta formation waters; Alberta Research Council, Alberta Geological Survey, Open File Report 1995-01, 59 p., URL <https://ags.aer.ca/publications/all-publications/ofr-1995-01> [April 2023].

Bernal, N.F., Gleeson, S.A., Dean, A.S., Liu, X. and Hoskin, P. (2014): The source of halogens in geothermal fluids from the Taupo Volcanic Zone, North Island, New Zealand; Geochimica et Cosmochimica Acta, v. 126, p. 265–283.

Billings, G.K., Hitchon, B. and Shaw, D.R. (1969): Geochemistry and origin of formation waters in the Western Canada Sedimentary Basin, 2. Alkali metals; Chemical Geology, v. 4, p. 211–223.

Bradley, D.C., Stillings, L.L., Jaskula, B.W., Munk, L. and McCauley, A.D. (2017): Lithium; Chapter K *in* Critical mineral resources of the United States—economic and environmental geology and prospects for future supply, K.J. Schulz, J.H. DeYoung, R.R. Seal II and D.C. Bradley (ed.), U.S. Geological Survey, Professional Paper 1802-K, p. K1–K21.

Brand, W.A., Coplen, T.B., Vogl, J., Rosner, M. and Prohaska, T. (2014): Assessment of international reference materials for isotope-ratio analysis (IUPAC Technical Report); Pure and Applied Chemistry, v. 86, no. 3, p. 425–467, doi:10.1515/pac-2013-1023.

Burton, K. and Vigier, N. (2011): Lithium isotopes as tracers in marine and terrestrial environments; Chapter 4 *in* Handbook of environmental isotope geochemistry, M. Baskaran (ed.), Springer, Berlin, Heidelberg, Germany, p. 41–59.

Buschkuehle, B.E. and Machel, G.M. (2002): Diagenesis and paleofluid flow in the Devonian Southesk-Cairn carbonate complex in Alberta, Canada; Marine and Petroleum Geology, v. 19, p. 219–227.

Chan, L.H., Gieskes, J.M., You, C.F. and Edmond, J.M. (1994): Lithium isotope geochemistry of sediments and hydrothermal fluids of the Guaymas Basin, Gulf of California; Geochimica et Cosmochimica Acta, v. 58, p. 4443–4454.

Chan, L.-H., Alt, J.C. and Teagle, D.A.H. (2002a): Lithium and lithium isotope profiles through the upper oceanic crust: a study of seawater–basalt exchange at ODP Sites 504B and 896A; Earth and Planetary Science Letters, v. 201, no. 1, p. 187–201, doi:10.1016/S0012-821X(02)00707-0.

Chan, L., Starinski, A. and Katz, A. (2002b): The behaviour of lithium and its isotopes in oilfield brines: evidence from the Heletz–Kokhav field, Israel; Geochimica et Cosmochimica Acta, v. 66, no. 4, p. 615–623.

Chan, L.H., Leeman, W.P. and Plank, T. (2006): Lithium isotopic composition of marine sediments; Geochemistry, Geophysics, Geosystems, v. 7, no. 6, Q06005, doi:10.1029/2005GC001202.

Clark, I.D. and Fritz, P. (1997): Environmental isotopes in hydrogeology; CRC Press, Boca Raton, Florida, 342 p.

Clayton, R.N., Friedman, I., Graf, D.L., Mayeda, T.K., Meents, W.F. and Shimp, N.F. (1966): The origin of saline formation waters: 1. isotopic composition; Journal of Geophysical Research, v. 71, no. 16, p. 3869–3882.

Cole, D.M. and Machel, H.G. (1994): Fluid flow and thermochemical sulfate reduction in the Leduc reef complex, Rimbey-Meadowbrook, Alberta; Geological Society of America, Annual Meeting, October 24–28, 1994, Seattle, Washington, Abstracts with Programs, v. 26, no. 7, abstract A-477.

Connolly, C.A., Walter, L.M., Baadsgaard, H. and Longstaff, F.J. (1990a): Origin and evolution of formation waters, Alberta Basin, Western Canada Sedimentary Basin. I. Chemistry; Applied Geochemistry, v. 5, no. 4, p. 375–395.

Connolly, C.A., Walter, L.M., Baadsgaard, H. and Longstaff, F.J. (1990b): Origin and evolution of formation waters, Alberta Basin, Western Canada Sedimentary Basin. II. Isotope systematics and water mixing; Applied Geochemistry, v. 5, no. 4, p. 397–413.

Davies, G.R. and Smith, L.B. (2006): Structurally controlled hydrothermal dolomite reservoir facies: an overview; AAPG Bulletin, v. 90, no. 11, p. 1641–1690.

Decarreau, A., Vigier, N., Palkova, H., Petit, S., Vieillard, P. and Fontaine, C. (2012): Partitioning of lithium between smectite and solution: an experimental approach; Geochimica et Cosmochimica Acta, v. 85, p. 314–325, doi:10.1016/j.gca.2012.02.018.

Dellinger, M., Gaillardet, J., Bouchez, J., Calmels, D., Louvat, P., Dosseto, A., Gorge, C., Alanoca, L. and Maurice, L. (2015): Riverine Li isotope fractionation in the Amazon River basin controlled by the weathering regimes; Geochimica et Cosmochimica Acta, v. 164, p. 71–93, doi:10.1016/j.gca.2015.04.042.

Dellinger, M., Hardisty, D.S., Planavsky, N.J., Gill, B.C., Kalderon-Asael, B., Asael, D., Croissant, T., Swart, P.K. and West, A.J. (2020): The effects of diagenesis on lithium isotope ratios of shallow marine carbonates; American Journal of Science, v. 320, no. 2, p. 150–184, doi:10.2475/02.2020.03.

Denison, R., Koepnick, R., Burke, W., Hetherington, E. and Fletcher, A. (1997): Construction of the Silurian and Devonian seawater $^{87}Sr/^{86}Sr$ curve; Chemical Geology, v. 140, no. 1–2, p. 109–121.

Dix, G. (1993): Patterns of burial- and tectonically controlled dolomitization in an Upper Devonian fringing-reef complex; Leduc Formation, Peace River Arch area, Alberta, Canada; Journal of Sedimentary Research, v. 63, no. 4, p. 628–640.

Drivet, E. and Mountjoy, E.W. (1997): Dolomitization of the Leduc Formation (Upper Devonian), southern Rimbey-Meadowbrook reef trend, Alberta; Journal of Sedimentary Research, v. 67, no. 3, p. 411–423.

Eccles, D.R. and Berhane, H. (2011): Geological introduction to lithium-rich formation water with emphasis on the Fox Creek area of west-central Alberta (NTS 83F and 83K); Energy Resources Conservation Board, ERCB/AGS Open File Report 2011-10, 22 p.

Eccles, D.R. and Jean, G.M. (2010): Lithium groundwater and formation water geochemical data; Energy Resources Conservation Board, ERCB/AGS Digital Data 2010-0001.

Eliuk, L.S. (1984): A hypothesis for the origin of hydrogen sulphide in Devonian Crossfield Member dolomite, Wabamun Formation, Alberta, Canada; *in* Carbonates in subsurface and outcrop, L.S. Eliuk (ed.), Canadian Society of Petroleum Geologists, 1984 C.S.P.G. Core Conference, October 18–19, 1984, Calgary, Alberta, p. 245–289.

Eliuk, L.S. and Hunter, D.F. (1987): Wabamun Group structural thrust fault fields: the Limestone-Burnt Timber example; *in* Devonian lithofacies and reservoir styles in Alberta, F.F. Krause and O.G. Burrowes (ed.), Canadian Society of Petroleum Geologists, Core Conference Notes associated with the Second International Symposium on the Devonian System, August 17–20, 1987, Calgary, Alberta, p. 39–62.

Flexer, V., Baspineiro, C.F. and Galli, C.I. (2018): Lithium recovery from brines: a vital raw material for green energies with a potential environmental impact in its mining and processing; Science of The Total Environment, v. 639, p. 1188–1204.

Gibson, J.J., Birks, S.J., Moncur, M., Yi, Y., Tattrie, K., Jasechko, S., Richardson, K. and Eby, P. (2011): Isotopic and geochemical tracers for fingerprinting process-affected waters in the oil sands industry: a pilot study; Oil Sands Research and Information Network, University of Alberta, School of Energy and the Environment, OSRIN Report No. TR-12, 109 p.

Gonfiantini, R. (1965): Effetti isotopici nell'evaporazione di acque salate; Atti della Società Toscana di Scienze Naturali, Serie A, v. LXXII, p. 3–22.

Green, D.G. and Mountjoy, E.W. (2005): Fault and conduit controlled burial dolomitization of the Devonian west-central Alberta Deep Basin; Bulletin of Canadian Petroleum Geology, v. 53, no. 2, p. 101–129.

Grosjean, C., Herrera Miranda, P., Perrin, M. and Poggi, P. (2012): Assessment of world lithium resources and consequences of their geographic distribution on the expected development of the electric vehicle industry; Renewable and Sustainable Energy Reviews, v. 16, no. 3, p. 1735–1744, doi:10.1016/j.rser.2011.11.023.

Gunter, W.D., Bach, S., Palombi, D., Lakeman, B., Sawchuk, W. and Bonner, D. (2009): Heartland Area Redwater reef saline aquifer CO_2 storage project; Energy Procedia, v. 1, no. 1, p. 3943–3950.

Hay, W., Migdisov, A., Balukhovsky, A., Wold, C., Flögel, S. and Söding, E. (2006): Evaporites and the salinity of the ocean during the Phanerozoic: implications for climate, ocean circulation and life; Palaeogeography, Palaeoclimatology, Palaeoecology, v. 240, issues 1–2, p. 3–46, doi:10.1016/j.palaeo.2006.03.044.

Hindshaw, R.S., Tosca, R., Goût, T.L., Farnan, I., Tosca, N.J. and Tipper, E.T. (2019): Experimental constraints on Li isotope fractionation during clay formation; Geochimica et Cosmochimica Acta, v. 250, p. 219–237.

Hitchon, B. (1969): Fluid flow in the Western Canada Sedimentary Basin: 1. Effect of topography; Water Resources Research, v. 5, p. 186–195.

Hitchon, B. and Friedman, I. (1969): Geochemistry and origin of formation waters in the Western Canada Sedimentary Basin—I. Stable isotopes of hydrogen and oxygen; Geochimica et Cosmochimica Acta, v. 33, p. 1321–1349.

Hitchon, B., Billings, G. and Klovan, J.E. (1971): Geochemistry and origin of formation waters in the Western Canada Sedimentary Basin—III. Factors controlling chemical composition; Geochimica et Cosmochimica Acta, v. 35, no. 6, p. 567–598.

Hitchon, B., Bachu, S. and Underschultz, J.R. (1990): Regional subsurface hydrogeology, Peace River Arch area, Alberta and British Columbia; Bulletin of Canadian Petroleum Geology, v. 38A, p. 196–217.

Hitchon, B., Bachu, S., Underschultz, J.R. and Yuan, L.P. (1995): Industrial mineral potential of Alberta formation waters; Alberta Research Council, Alberta Geological Survey, Bulletin 62, 64 p.

Holser, W. (1979): Trace elements and isotopes in evaporites; *in* Marine minerals, R.G. Burns (ed.), Mineralogical Society of America, Reviews in Mineralogy, v. 6, p. 295–346.

Huff, G.F. (2016): Evolution of Li-enriched oilfield brines in Devonian carbonates of the south-central Alberta Basin, Canada; Bulletin of Canadian Petroleum Geology, v. 64, no. 3, p. 438–448.

Huff, G.F. (2019): Origin and Li-enrichment of selected oilfield brines in the Alberta Basin, Canada; Alberta Energy Regulator / Alberta Geological Survey, Open File Report 2019-01, 35 p.

Huff, G.F., Stewart, S.A., Riddell, J.T.F. and Chisholm, S. (2011): Water geochemical data, saline aquifer project (tabular data, tab-delimited format); Energy Resources Conservation Board, ERCB/AGS Digital Data 2011-0007.

Huff, G.F., Bechtel, D.J., Stewart, S.A., Brock, E. and Heikkinen, C. (2012): Water geochemical data, saline aquifer project, 2011 (tabular data, tab-delimited format); Energy Resources Conservation Board, ERCB/AGS Digital Data 2012-0001.

Huff, G.F., Lopez, G.P. and Weiss, J.A. (2019): Water geochemistry of selected formation brines in the Alberta Basin, Canada (tabular data, tab-delimited format); Alberta Energy Regulator / Alberta Geological Survey, AER/AGS Digital Data 2019-0002.

Huh, Y., Chan, L.-H., Zhang, L. and Edmond, J.M. (1998): Lithium and its isotopes in major world rivers: implications for weathering and the oceanic budget; Geochimica et Cosmochimica Acta, v. 62, p. 2039–2051.

International Energy Agency (2021): The role of critical minerals in clean energy transitions; International Energy Agency, World Energy Outlook Special Report, 284 p.

Ishikawa, T. and Nakamura, E. (1993): Boron isotope systematics of marine sediments; Earth and Planetary Science Letters, v. 117, no. 3–4, p. 567–580.

ISO Committee on Conformity Assessment (2017): ISO/IEC 17025:2017 general requirements for the competence of testing and calibration laboratories (Edition 3); International Organization for Standardization, Geneva, Switzerland.

Jiang, S., Zhang, L., Li, F., Hua, H., Liu, X., Yuan, Z. and Wu, H. (2020): Environmental impacts of lithium production showing the importance of primary data of upstream process in life-cycle assessment; Journal of Environmental Management, v. 262, art. 110253.

Joachimski, M. and van Geldern, R. (2005): Boron isotope geochemistry of Paleozoic brachiopod calcite: implications for a secular change in the boron isotope geochemistry of seawater over the Phanerozoic; Geochimica et Cosmochimica Acta, v. 69, no. 16, p. 4035–4044, doi:10.1016/j.gca.2004.11.017.

Kaunda, R.B. (2020): Potential environmental impacts of lithium mining; Journal of Energy & Natural Resources Law, v. 38, no. 3, p. 237–244.

Kesler, S.E., Appold, M.S., Martini, A.M., Walter, L.M., Huston, T.J. and Kyle, R. (1995): Na-Cl-Br systematics of mineralizing brines in Mississippi Valley–type deposits; Geology, v. 23, no. 7, p. 641–644.

Kharaka, Y.K. and Mariner, R.H. (1989): Chemical geothermometers and their application to formation waters from sedimentary basins; Chapter 6 *in* Thermal history of sedimentary basins, methods and case histories, N.D. Naeser and T.H. McCulloh (ed.), Springer-Verlag, New York, New York, p. 99–117.

Krause, H.R., Viau, C.A., Eliuk, L.S., Ueda, A. and Halas, S. (1988): Chemical and isotopic evidence of thermochemical sulphate reduction by light hydrocarbon gases in deep carbonate reservoirs; Nature, v. 333, p. 415–419.

Lewchuk, M.T., Al-Aasm, I.S., Symons, D.T.A. and Gillen, K.P. (2000): Late Laramide dolomite recrystallization of the Husky Rainbow "A" hydrocarbon Devonian reservoir, northwestern Alberta, Canada: paleomagnetic and geochemical evidence; Canadian Journal of Earth Sciences, v. 37, no. 1, p. 17–29.

Li, W. and Liu, X. (2022): Mineralogy and fluid chemistry controls on lithium isotope fractionation during clay adsorption; Science of The Total Environment, v. 851, pt. 1, art. 158138, doi:10.1016/j.scitotenv.2022.158138.

Liu, X., Krause, A., Wilson, D., Fraser, W., Joachimski, M., Brand, U., Stigall, A., Qie, W., Chen, B., Yang, X. and Pogge von Strandmann, P. (2025): Lithium isotope evidence shows Devonian afforestation may have significantly altered the global silicate weathering regime; Geochimica et Cosmochimica Acta, v. 396, p. 107–121, doi:10.1016/j.gca.2025.02.036.

Lyster, S., Lopez, G.P. and Poulette, S. (2022): Geochemistry data of lithium-bearing groundwater in the Alberta Basin compiled from multiple sources (tabular data, tab-delimited format); Alberta Energy Regulator / Alberta Geological Survey, AER/AGS Digital Data 2021-0021.

Ma, Y., Xiao, Y., He, M., Xiao, J., Shen, Q. and Jiang, S. (2011): Boron isotopic composition of Paleozoic brachiopod and coeval coral calcites in Yunnan-Guizhou Plateau, China; Science China Earth Sciences, v. 54, p. 1912–1925, doi:10.1007/s11430-011-4263-5.

Machel, H.G. (2004): Concepts and models of dolomitization: a critical reappraisal; *in* The geometry and petrogenesis of dolomite hydrocarbon reservoirs, C.J.R. Braithwaite, G. Rizzi and G. Darke (ed.), Geological Society, Special Publication 235, p. 7–63.

Machel, H.G. and Cavell, P.A. (1999): Low-flux, tectonically-induced squeegee fluid flow ("hot flash") into the Rocky Mountain Foreland Basin; Bulletin of Canadian Petroleum Geology, v. 47, no. 4, p. 510–533.

Machel, H.G., Krouse, H.R. and Sassen, R. (1995): Products and distinguishing criteria of bacterial and thermochemical sulfate reduction; Applied Geochemistry, v. 10, no. 4, p. 373–389.

Machel, H.G., Cavell, P.A., Buschkuehle, B.E. and Michael, K. (2000): Tectonically induced fluid flow in Devonian carbonate aquifers of the Western Canada Sedimentary Basin; Journal of Geochemical Exploration, v. 69–70, p. 213–217.

Macpherson, G.L., Capo, R.C., Stewart, B.W., Phan, T.T., Schroeder, K. and Hammack, R.W. (2014): Temperature-dependent Li isotope ratios in Appalachian Plateau and Gulf Coast Sedimentary Basin saline water; Geofluids, v. 14, p. 419–429.

McCaffrey, M.A., Lazar, B. and Holland, H.D. (1987): The evaporation path of seawater and the coprecipitation of Br (super -) and K (super +) with halite; Journal of Sedimentary Research, v. 57, no. 5, p. 928–937, doi:10.1306/212F8CAB-2B24-11D7-8648000102C1865D.

Meixner, A., Sarchi, C. and Lucassen, F. (2020): Lithium concentrations and isotope signatures of Palaeozoic basement rocks and Cenozoic volcanic rocks from the Central Andean arc and back-arc; Mineralium Deposita, v. 55, p. 1071–1084, doi:10.1007/s00126-019-00915-2.

Michael, K., Machel, H.G. and Bachu, S. (2003): New insights into the origin and migration of brines in deep Devonian aquifers, Alberta, Canada; Journal of Geochemical Exploration, v. 80, no. 2–3, p. 193–219, doi:10.1016/S0375-6742(03)00191-2.

Misra, S. and Froelich, P.N. (2012): Lithium isotope history of Cenozoic seawater: changes in silicate weathering and reverse weathering; Science, v. 335, no. 6070, p. 818–823.

Munk, L.A., Jochens, H., Jennings, M., Bradley, D., Hynek, S. and Godfrey, L. (2011): Geochemistry of lithium-rich brines in Clayton Valley, Nevada, USA; *in* Proceedings, 11th SGA Biennial Meeting, Society for Geology Applied to Mineral Deposits, September 26–29, 2011, Antofagasta, Chile, p. 217–219.

Munk, L.A., Hynek, S.A., Bradley, D.C., Boutt, D., Labay, K. and Jochens, H. (2016): Lithium brines: a global perspective; *in* Rare earth and critical elements in ore deposits, P.L. Verplanck and M.W. Hitzman (ed.), Society of Economic Geologists, Reviews in Economic Geology, v. 18, p. 339–365.

Murphy, M., Porcelli, D., Pogge von Strandmann, P., Hirst, C., Kutscher, L., Katchinoff, J., Mörth, C., Maximov, T. and Andersson, P. (2019): Tracing silicate weathering processes in the permafrost-dominated Lena River watershed using lithium isotopes; Geochimica et Cosmochimica Acta, v. 245, p. 154–171, doi:10.1016/j.gca.2018.10.024.

Oliver, J. (1986): Fluids expelled tectonically from orogenic belts: their role in hydrocarbon migration and other geologic phenomena; Geology, v. 14, no. 2, p. 99–102, doi:10.1130/0091-7613(1986)14<99:FETFOB>2.0.CO;2.

Orr, W.L. (1974): Changes in sulphur content and isotopic ratios of sulphur during petroleum maturation study of Big Horn Basin Palaeozoic oils; AAPG Bulletin, v. 58, p. 2295–2318.

Paul, D. (1994): Hydrogeology of the Devonian Rimbey-Meadowbrook reef trend of central Alberta; M.Sc. thesis, University of Alberta.

Penniston-Dorland, S., Liu, X.M. and Rudnick, R.L. (2017): Lithium isotope geochemistry; Reviews in Mineralogy and Geochemistry, v. 82, p. 165–217.

Pierre, C., Ortlieb, L. and Person, A. (1984): Supratidal evaporitic dolomite at Ojo de Liebre lagoon: mineralogical and isotopic arguments for primary crystallization; Journal of Sedimentary Petrology, v. 54, p. 1049–1061.

Pogge von Strandmann, P.A., Kasemann, S.A. and Wimpenny, J.B. (2020): Lithium and lithium isotopes in Earth's surface cycles; Elements, v. 16, p. 253–258.

Potma, K., Weissenberger, J.A., Wong, P.K. and Gilhooly, M.G. (2001): Toward a sequence stratigraphic framework for the Frasnian of the Western Canada Basin; Bulletin of Canadian Petroleum Geology, v. 49, no. 1, p. 37–85.

Qing, H. and Mountjoy, E. (1992): Large-scale fluid flow in the Middle Devonian Presqu’ile barrier, Western Canada Sedimentary Basin; Geology, v. 20, p. 903–906.

Reimert, C., Lyster, S., Hauck, T.E., Palombi, D., Playter, T.L., Lopez, G.P. and Schultz, S.K. (2022): Water geochemical data, Lithium Prospectivity Project, 2021 (tabular data, tab-delimited format); Alberta Energy Regulator / Alberta Geological Survey, AER/AGS Digital Data 2021-0022.

Reimert, C., Lyster, S., Palombi, D. and Bernal, N. (2025): Brine geochemical data, mineral mapping program, 2021–2024 (tabular data, tab-delimited format); Alberta Energy Regulator / Alberta Geological Survey, AER/AGS Digital Data 2023-0019.

Reinson, G.E., Lee, J.P., Warters, W., Osadet, K.G., Bell, L.L., Price, P.R., Trollope, F., Campbell, R.I. and Barclay, J.E. (1993): Devonian gas resources of the Western Canada Sedimentary Basin. Part 1: Geological play analysis and resource assessment; Geological Survey of Canada, Bulletin 452, 157 p.

Riciputi, L.R., Cole, D.R. and Machel, H.G. (1996): Sulfide-mineral isotope thermometry and the genesis of high-temperature hydrogen sulfide in the Upper Devonian Leduc Formation, Alberta, Canada; Geology, v. 24, no. 8, p. 733–736.

Rostron, B.J. and Tóth, J. (1997): Cross-formational fluid flow and the generation of a saline plume of formation waters in the Mannville Group, west-central Alberta; *in* Petroleum geology of the Cretaceous Mannville Group, western Canada, Canadian Society of Petroleum Geologists, Memoir 18, p. 169–190.

Scholz, F., Hensen, C., De Lange, G.J., Haeckel, M., Liebetrau, V., Meixner. A., Reitz, A. and Romer, R.L. (2010): Lithium isotope geochemistry of marine pore waters: insights from cold seep fluids; Geochimica et Cosmochimica Acta, v. 74, p. 3459–3475, doi:10.1016/j.gca.2010.03.026.

Schwarcz, H.P., Agyei, E.K. and McMullen, C.C. (1969): Boron isotopic fractionation during clay adsorption from seawater; Earth and Planetary Science Letters, v. 6, p. 1–5.

Smith, T., Awolayo, A.N., Grasby, S.E. and Tutolo, B.M. (2024): Investigation of geochemically induced permeability alteration in geothermal reservoirs and its implications for sustainable geothermal energy production; Applied Geochemistry, v. 175, art. 106193, doi:10.1016/j.apgeochem.2024.106193.

Spencer, R.J. (1987): Origin of Ca-Cl brines in Devonian formations, Western Canada Sedimentary Basin; Applied Geochemistry, v. 2, p. 373–384.

Spivack, A.J., Palmer, M.R. and Edmond, J.M. (1987): The sedimentary cycle of the boron isotopes; Geochimica et Cosmochimica Acta, v. 51, p. 1939–1949.

Stacey, J., Hollis, C., Corlett, H. and Koeshidayatullah, A. (2021): Burial dolomitization driven by modified seawater and basal aquifer-sourced brines: insights from the Middle and Upper Devonian of the Western Canadian Sedimentary Basin; Basin Research, v. 33, p. 648–680, doi:10.1111/bre.12489.

Standard Methods Committee of the American Public Health Association, American Water Works Association and Water Environment Federation (2023a): 3125B metals by inductively coupled plasma-mass spectrometry; *in* Standard methods for the examination of water and wastewater (24th edition), R.B. Baird, A.D Eaton, L.S. Clesceri and E.W. Rice (ed.), APHA Press, Washington, D.C.

Standard Methods Committee of the American Public Health Association, American Water Works Association and Water Environment Federation (2023b): 4110 determination of anions by ion chromatography; *in* Standard methods for the examination of water and wastewater (24th edition). W.C. Lipps, T. E. Baxter and E. Braun-Howland (ed.), APHA Press, Washington, D.C.

Stoakes, F.A. and Creaney, S. (1984): Sedimentology of a carbonate source rock: the Duvernay Formation of Alberta, Canada; *in* Carbonates in subsurface and outcrop, L. Eliuk (ed.), Canadian Society Petroleum Geology, 1984 C.S.P.G. Core Conference, October 18–19, 1984, Calgary, Alberta, p. 132–147.

Sun, S.Q. (1994): A reappraisal of dolomite abundance and occurrence in the Phanerozoic; Journal of Sedimentary Research, v. 64, no. 2a, p. 396–404.

Taylor, H.L., Kell Duivestein, I.J., Farkas, J., Dietzel, M. and Dosseto A. (2019): Technical note: lithium isotopes in dolostone as a palaeo-environmental proxy – an experimental approach; Climate of the Past, v. 15, p. 635–646.

Teng, F.-Z. (2005): Lithium isotopic systematics of the continental crust; Ph.D. thesis, University of Maryland, 199 p., URL <http://hdl.handle.net/1903/3215> [September 2025].

Teng, F.-Z., McDonough W.F., Rudnick R.L., Walker, R.J. and Sirbescu, M.-L.C. (2006): Lithium isotopic systematics of granites and pegmatites from the Black Hills, South Dakota; American Mineralogist, v. 91, no. 10, p. 1488–1498, doi:10.2138/am.2006.2083.

Tomascak, P.B., Magna, T. and Dohmen, R. (2016): Advances in lithium isotopes geochemistry; Springer-Verlag, Berlin.

U.S. Environmental Protection Agency (1994): Method 200.7: determination of metals and trace elements in water and wastes by inductively coupled plasma-atomic emission spectrometry (Revision 4.4); U.S. Environmental Protection Agency, 58 p.

U.S. Environmental Protection Agency (1996): Method 1669: sampling ambient water for trace metals at EPA water quality criteria levels; U.S. Environmental Protection Agency, URL <https://www.epa.gov/sites/production/files/2015-10/documents/method_1669_1996.pdf> [June 2025].

Vengosh, A., Starinsky, A., Kolodny, Y., Chivas, A.R. and Raab, M. (1992): Boron isotope variations during fractional evaporation of sea water: new constraints on the marine vs. nonmarine debate; Geology, v. 20, no. 9, p. 799.

Walter, L., Stueber, A. and Huston, T. (1990): Br-Cl systematics in Illinois basin fluids: constrains on fluid origin and evolution; Geology, v. 18, p. 315–318.

Weissenberger, J.A.W. and Potma, K. (2001): The Devonian of western Canada – aspects of a petroleum system: introduction; Bulletin of Canadian Petroleum Geology, v. 49, no. 1, p. 1–6.

Weldeghebriel, M.F. and Lowenstein, T.K. (2023): Seafloor hydrothermal systems control long-term changes in seawater [Li+]: evidence from fluid inclusions: Science Advances, v. 9, no. 30, art. eadf1605, doi:10.1126/sciadv.adf1605.

Wendte, J., Qing, H., Dravis, J.J., Moore, S., Stasiuk, L. and Ward, G. (1998): High-temperature saline (thermoflux) dolomitization of Devonian Swan Hills platform and bank carbonates, Wild River area, west-central Alberta; Bulletin of Canadian Petroleum Geology, v. 46, no. 2, p. 210–265.

Appendix 1 – Geochemical Data

Table 2. Analytical results for major ions and halogens in Devonian oil brines in Alberta.

UWI	BH_Lat 83	BH_Long 83	Label	Geological Unit	Vertical Depth* (m)	TDS (mg/L)	pH*	Density* (kg/L)	Cl (mg/L)	Br* (mg/L)	HCO_3* (mg/L)	SO_4* (mg/L)	Na (mg/L)	K (mg/L)	Ca (mg/L)	Mg (mg/L)	Source
100/06-13-038-23W4/00	52.26578	-113.16408	WB01	Wabamun Group	-9999	104042	6.5	1.07	52341	235	1963	2345	32087	256	2718	714	DIG 2012-0001
100/09-30-080-23W5/00	55.96463	-117.58261	WB02	Wabamun Group	-9999	243000	6.5	1.16	172691	549	129	985	80551	2318	25266	4300	DIG 2012-0001
100/10-28-032-02W5/00	51.77504	-114.22317	WB03	Wabamun Group	2767	79877	7.5	1.06	44207	280	2031	1278	28321	2409	2304	360	DIG 2023-0019
100/10-32-076-01W6/00	55.63044	-118.11551	WB04	Wabamun Group	-9999	277000	6.3	1.18	193192	622	124	836	91059	3133	29803	4406	DIG 2011-0007
100/12-35-051-27W4/03	53.44829	-113.88205	WB06	Wabamun Group	1835	125608	7.2	1.09	75500	1080	417	134	38400	1585	8150	1634	DIG 2023-0019
102/13-16-029-26W4/00	51.48532	-113.61388	WB07	Wabamun Group	2160	98485	6.6	1.07	55800	117	195	2410	36500	1690	1415	574	DIG 2023-0019
100/12-02-055-27W4/00	53.72406	-113.91462	WB08	Wabamun Group	-9999	111592	6.9	1.07	65560	280	540	107	34229	687	4120	1105	OFR 2011-10
100/08-28-078-24W5/00	55.78538	-117.65347	WB09	Wabamun Group	1918	257871	6.5	1.17	163470	419	287	531	65700	2600	21700	3730	DIG 2023-0019
100/12-36-077-01W6/00	55.71892	-118.02198	WB10	Wabamun Group	2224	264171	6.2	1.17	174130	491	118	394	60550	2640	22900	3500	DIG 2023-0019
100/14-22-032-02W5/00	51.76532	-114.20817	WB11	Wabamun Group	2808	93549	7.1	1.06	54700	216	2074	1386	31500	2380	2210	353	DIG 2023-0019
103/04-20-078-01W6/00	55.76719	-118.12755	WB12	Wabamun Group	2180	283207	6.4	1.18	178370	542	122	338	72400	2530	25800	3710	DIG 2023-0019
100/02-04-057-03W5/00	53.89380	-114.38048	WB13	Wabamun Group	1334	102000	7.1	1.07	62600	244	-9999	56	33200	714	3890	1292	Connolly et al., 1990
100/03-07-057-01W5/00	53.90782	-114.13909	WB14	Wabamun Group	1247	108000	6.9	1.07	66100	269	-9999	151	33600	992	4810	1498	Connolly et al., 1990
100/09-16-057-03W5/00	53.93024	-114.37939	WB15	Wabamun Group	1340	93000	7.0	1.06	55900	467	-9999	87	30700	714	3550	1051	Connolly et al., 1990
100/01-03-049-25W4/00	53.19353	-113.56339	NK01	Nisku Formation	1607	123562	6.9	1.10	76300	380	453	898	34000	2316	8100	1725	DIG 2023-0019
100/01-34-036-20W4/02	52.13020	-112.77000	NK02	Nisku Formation	1626	118945	6.7	1.09	69488	611	639	858	32011	3502	10800	1973	DIG 2023-0019
100/03-02-038-24W4/00	52.32148	-113.32779	NK04	Nisku Formation	-9999	239514	6.1	1.15	143250	940	691	15929	56154	6956	22232	3885	DIG 2012-0001
100/05-23-038-24W4/00	52.28014	-113.33489	NK05	Nisku Formation	-9999	247320	5.9	1.15	144270	985	690	1489	56792	7099	22328	3985	DIG 2012-0001
100/07-10-056-24W4/00	53.82364	-113.48099	NK06	Nisku Formation	1201	109734	6.5	1.08	67100	574	586	1166	31900	2000	5790	1490	DIG 2023-0019
100/07-31-036-23W4/00	52.13338	-113.27798	NK07	Nisku Formation	2001	199706	6.4	1.13	127800	928	167	484	48080	4010	16500	2750	DIG 2023-0019
100/08-29-051-26W4/00	53.43141	-113.79203	NK09	Nisku Formation	1532	136189	7.1	1.10	85000	342	358	822	37240	2404	8810	1738	DIG 2023-0019
100/08-33-066-08W5/02	54.75526	-115.14007	NK10	Nisku Formation	-9999	225000	6.5	1.14	149733	352	79	983	77381	949	17259	3063	DIG 2019-0002
100/09-26-050-10W5/02	53.34719	-115.34322	NK11	Nisku Formation	2641	79132	7.3	1.05	46300	430	183	1880	28100	867	1650	245	DIG 2023-0019
100/12-22-031-24W4/00	51.67273	-113.33010	NK13	Nisku Formation	2114	157568	6.9	1.10	95900	772	279	1822	53730	2510	2950	520	DIG 2023-0019
102/10-29-035-22W4/00	52.03715	-113.11173	NK14	Nisku Formation	1963	211061	6.0	1.15	130000	985	104	464	54255	2813	20427	3051	DIG 2023-0019
100/03-07-035-22W4/00	51.98457	-113.13585	NK15	Nisku Formation	1922	226481	6.0	1.16	139800	1160	87	360	59244	3104	20766	3164	DIG 2023-0019
100/14-14-035-20W4/00	52.01010	-112.75808	NK16	Nisku Formation	1628	109229	6.6	1.08	68700	430	582	963	25700	3170	8470	1940	DIG 2023-0019
100/15-28-049-25W4/00	53.26243	-113.59400	NK17	Nisku Formation	1546	171177	6.8	1.12	106000	519	168	725	48800	3000	10500	2070	DIG 2023-0019

UWI	BH_Lat 83	BH_Long 83	Label	Geological Unit	Vertical Depth* (m)	TDS (mg/L)	pH*	Density* (kg/L)	Cl (mg/L)	Br* (mg/L)	HCO_3* (mg/L)	SO_4* (mg/L)	Na (mg/L)	K (mg/L)	Ca (mg/L)	Mg (mg/L)	Source
100/16-06-042-23W4/00	52.59170	-113.29429	NK18	Nisku Formation	-9999	251680	6.1	1.14	140712	938	667	15558	55827	6921	21736	3844	DIG 2012-0001
100/16-28-042-23W4/00	52.64976	-113.24615	NK19	Nisku Formation	-9999	225666	6.2	1.13	131544	885	628	19278	53978	5897	19391	3368	DIG 2011-0007
100/11-19-031-09W4/00	51.67132	-111.27111	NK21	Nisku Formation	1137	32608	7.1	1.03	15710	75	1255	4100	9741	524	1403	514	DIG 2023-0019
102/06-05-037-21W4/00	52.14757	-112.97159	NK22	Nisku Formation	1881	194364	6.2	1.13	120000	2160	108	541	58770	2970	10250	1781	DIG 2023-0019
102/09-34-049-26W4/00	53.27493	-113.70971	NK23	Nisku Formation	1565	152186	6.9	1.12	97400	382	303	659	40000	2604	9530	1845	DIG 2023-0019
102/10-23-050-26W4/00	53.33187	-113.69429	NK24	Nisku Formation	1529	143597	7.1	1.11	86900	365	395	684	41100	2470	10270	1980	DIG 2023-0019
102/13-01-036-20W4/00	52.06700	-112.74197	NK25	Nisku Formation	1680	72826	6.9	1.06	44000	240	1224	605	19200	2000	5310	1110	DIG 2023-0019
102/14-35-052-26W4/00	53.54048	-113.72655	NK26	Nisku Formation	-9999	41400	6.7	1.10	86522	598	277	1098	40187	1757	14054	2295	DIG 2019-0002
102/15-33-036-22W4/00	52.14146	-113.08454	NK27	Nisku Formation	1893	166215	5.9	1.12	103000	1740	236	668	46860	1990	11480	2102	DIG 2023-0019
103/02-10-051-26W4/00	53.38408	-113.74490	NK29	Nisku Formation	1535	153571	7.2	1.11	92976	601	230	849	43207	2985	11327	2115	DIG 2023-0019
100/02-17-049-25W4/00	53.22323	-113.61995	NK30	Nisku Formation	-9999	209808	6.3	1.13	118440	680	166	970	55498	2606	13423	2459	DIG 2011-0007
100/07-20-049-25W4/00	53.24140	-113.62115	NK31	Nisku Formation	-9999	206570	6.5	1.14	127120	740	188	999	57318	2701	13961	2463	DIG 2011-0007
100/14-13-050-27W4/00	53.32088	-113.82139	NK32	Nisku Formation	-9999	187656	6.1	1.12	111030	490	298	11170	50712	2971	12287	2279	DIG 2019-0002
102/03-11-053-26W4/00	53.55773	-113.72973	NK33	Nisku Formation	-9999	119880	6.3	1.08	69228	380	793	3888	33588	1901	7096	1598	DIG 2011-0007
102/04-21-057-24W4/00	53.93616	-113.51760	NK34	Nisku Formation	-9999	116316	6.5	1.08	71190	330	794	1400	31448	1497	6160	1497	DIG 2012-0001
103/16-10-056-24W4/00	53.83141	-113.47711	NK35	Nisku Formation	-9999	120848	6.6	1.08	76177	310	511	1403	33449	1597	6927	1705	OFR 2011-10
100/01-08-039-26W4/00	52.33433	-113.70173	NK36	Nisku Formation	2137	64859	6.7	1.05	37800	174	1407	1320	19600	1130	3749	569	DIG 2023-0019
100/04-31-038-26W4/00	52.30482	-113.71564	NK37	Nisku Formation	2199	120781	7.7	1.09	70900	355	1385	1100	41030	1930	4434	706	DIG 2023-0019
100/04-36-038-27W4/00	52.30466	-113.73878	NK38	Nisku Formation	2190	97350	7.9	1.07	58000	255	1429	1210	31800	1409	3624	604	DIG 2023-0019
100/03-27-049-25W4/00	53.25168	-113.57556	NK39	Nisku Formation	1562	187186	6.5	1.12	122700	502	124	785	48200	2290	11200	1950	DIG 2023-0019
100/08-10-049-25W4/00	53.21150	-113.56357	NK40	Nisku Formation	1592	179747	6.8	1.11	115200	508	191	933	48400	2550	10600	1970	DIG 2023-0019
100/12-04-038-04W5/02	52.24086	-114.52444	NK41	Nisku Formation	2949	196790	6.8	1.15	117411	888	504	370	59188	4239	13374	1961	DIG 2023-0019
100/14-08-051-26W4/00	53.39504	-113.80135	NK42	Nisku Formation	1559	174885	6.7	1.12	103000	643	140	636	53200	2840	13200	1940	DIG 2023-0019
100/14-23-049-25W4/00	53.24948	-113.55397	NK43	Nisku Formation	1568	133339	7.0	1.10	77000	229	405	920	41300	2560	9460	1900	DIG 2023-0019
100/15-16-049-25W4/00	53.23488	-113.59666	NK44	Nisku Formation	1588	169759	6.5	1.12	99400	590	63	668	52800	2320	12500	2040	DIG 2023-0019
100/16-20-049-25W4/00	53.24950	-113.61229	NK45	Nisku Formation	1597	203886	6.4	1.13	131300	604	85	784	54200	2390	13000	2170	DIG 2023-0019
100/16-35-049-26W4/00	53.27715	-113.68535	NK46	Nisku Formation	1563	172859	6.4	1.11	105400	447	665	862	48900	3000	12200	2170	DIG 2023-0019
102/01-33-050-26W4/00	53.35591	-113.73428	NK47	Nisku Formation	1549	76429	7.5	1.06	44700	211	236	864	20500	1320	7730	1200	DIG 2023-0019
102/05-18-039-20W4/00	52.35395	-112.88229	NK48	Nisku Formation	1584	203168	6.6	1.13	127200	900	641	613	46900	4690	20100	3350	DIG 2023-0019

UWI	BH_Lat 83	BH_Long 83	Label	Geological Unit	Vertical Depth* (m)	TDS (mg/L)	pH*	Density* (kg/L)	Cl (mg/L)	Br* (mg/L)	HCO_3* (mg/L)	SO_4* (mg/L)	Na (mg/L)	K (mg/L)	Ca (mg/L)	Mg (mg/L)	Source
102/08-02-050-26W4/00	53.28423	-113.68700	NK49	Nisku Formation	1585	138765	6.3	1.10	79700	413	73	659	39700	2410	13700	2560	DIG 2023-0019
102/15-26-049-26W4/00	53.26236	-113.69409	NK50	Nisku Formation	1562	206620	6.2	1.13	134900	795	94	794	50900	2630	14200	3150	DIG 2023-0019
103/04-30-050-26W4/00	53.33865	-113.80086	NK51	Nisku Formation	1544	153855	6.7	1.11	87100	513	112	650	48600	2690	12600	2160	DIG 2023-0019
103/16-24-039-21W4/00	52.37377	-112.88582	NK52	Nisku Formation	1585	230066	6.6	1.15	141900	848	667	598	61200	4790	18200	3050	DIG 2023-0019
104/13-16-050-26W4/00	53.32316	-113.75357	NK53	Nisku Formation	1549	77495	7.1	1.06	43500	191	157	939	23400	1410	6730	1440	DIG 2023-0019
100/11-10-038-20W4/00	52.25389	-112.78080	NK54	Nisku Formation	1573	97462	5.9	1.06	50966	394	495	1383	21280	2479	9672	1809	DIG 2012-0001
100/12-33-040-24W4/02	52.48610	-113.40778	NK55	Nisku Formation	1811	229743	5.8	1.14	142875	914	422	14402	56350	6744	21946	3600	DIG 2012-0001
100/16-10-056-24W4/00	53.83080	-113.47446	NK56	Nisku Formation	1170	111000	6.0	1.08	67000	335	-9999	1000	32700	1840	6400	1768	Connolly et al., 1990
100/01-30-055-25W4/00	53.77579	-113.69996	LD01	Leduc Formation	-9999	138000	5.9	1.08	72509	380	809	3777	33125	1899	7424	1705	DIG 2011-0007
100/02-05-044-01W5/00	52.75794	-114.10756	LD02	Leduc Formation	2297	236776	6.2	1.16	147600	1800	250	273	54100	4240	27000	3440	DIG 2023-0019
100/02-17-055-25W4/00	53.74715	-113.67929	LD03	Leduc Formation	1416	108164	7.1	1.08	64200	1020	557	1340	31700	2120	6900	1630	DIG 2023-0019
100/15-10-034-26W4/00	51.90788	-113.60621	LD04	Leduc Formation	2320	203009	7.2	1.15	131710	1024	950	427	28321	2409	2304	360	DIG 2023-0019
100/03-08-055-25W4/00	53.73294	-113.68244	LD05	Leduc Formation	-9999	133000	6.0	1.08	74186	390	775	3899	34873	2025	7841	1798	DIG 2011-0007
100/04-05-058-21W4/00	53.97979	-113.09666	LD06	Leduc Formation	-9999	110000	6.3	1.08	70436	250	564	1292	33495	829	4922	1702	DIG 2011-0007
100/04-21-057-24W4/00	53.93616	-113.51737	LD07	Leduc Formation	-9999	110000	6.2	1.08	72267	310	844	1002	32202	1605	6397	1497	DIG 2011-0007
100/04-22-044-01W5/00	52.80211	-114.05921	LD08	Leduc Formation	-9999	311055	5.6	1.17	160770	1398	227	350	51843	5476	27844	4520	DIG 2012-0001
100/05-05-044-22W4/00	52.76026	-113.16958	LD09	Leduc Formation	-9999	247320	6.0	1.15	144270	996	652	23244	62059	7202	24045	4111	DIG 2012-0001
100/05-35-051-27W4/00	53.44583	-113.88313	LD10	Leduc Formation	-9999	220000	6.0	1.17	150414	1300	257	303	57251	3067	26118	3731	DIG 2011-0007
100/05-36-038-04W5/00	52.30961	-114.45150	LD11	Leduc Formation	3098	225160	5.9	1.16	139000	1050	283	291	52300	4900	25170	3360	DIG 2023-0019
100/07-26-069-23W5/00	55.00273	-117.39209	LD12	Leduc Formation	-9999	264000	7.0	1.17	181896	489	546	9223	76140	6355	32648	4163	DIG 2019-0002
100/07-35-052-26W4/B0	53.53222	-113.72387	LD14	Leduc Formation	-9999	137000	6.6	1.10	86381	670	248	1319	34619	1649	15606	2506	DIG 2019-0002
100/09-05-038-04W5/00	52.24050	-114.52600	LD15	Leduc Formation	-9999	297728	5.9	1.16	155842	1163	385	8257	62453	5675	30238	3989	DIG 2012-0001
100/09-06-038-23W4/00	52.23999	-113.27222	LD16	Leduc Formation	1845	201029	6.6	1.14	123000	1003	656	527	48800	6430	18900	3050	DIG 2023-0019
100/09-08-050-26W4/02	53.30307	-113.76003	LD17	Leduc Formation	-9999	198000	6.0	1.15	136493	1300	266	505	43701	2776	25463	4106	DIG 2019-0002
100/09-16-057-21W4/00	53.92897	-113.05347	LD18	Leduc Formation	-9999	109000	6.4	1.07	71206	220	496	1181	33401	698	4790	1600	OFR 2011-10
100/10-01-043-02W5/00	52.67769	-114.15692	LD19	Leduc Formation	-9999	279360	5.7	1.16	161796	1280	304	349	53660	6204	33756	4528	OFR 2011-10
100/10-01-043-02W5/00	52.67771	-114.15793	LD20	Leduc Formation	2358	229626	6.2	1.16	145600	1630	250	293	51800	4190	24400	3220	DIG 2023-0019
100/10-11-053-26W4/00	53.56474	-113.72363	LD21	Leduc Formation	1583	136500	6.7	1.10	83700	1480	167	791	33600	1837	14260	2230	DIG 2023-0019
100/11-13-054-26W4/00	53.66843	-113.70486	LD22	Leduc Formation	-9999	191000	6.1	1.14	129846	900	360	399	49547	2494	20730	3178	DIG 2019-0002

UWI	BH_Lat 83	BH_Long 83	Label	Geological Unit	Vertical Depth* (m)	TDS (mg/L)	pH*	Density* (kg/L)	Cl (mg/L)	Br* (mg/L)	HCO_3* (mg/L)	SO_4* (mg/L)	Na (mg/L)	K (mg/L)	Ca (mg/L)	Mg (mg/L)	Source
100/11-14-042-02W5/00	52.62012	-114.18392	LD23	Leduc Formation	2387	245310	6.2	1.16	152600	1900	285	301	56700	4820	27100	3650	DIG 2023-0019
100/12-02-045-01W5/00	52.85211	-114.04709	LD24	Leduc Formation	2330	236364	6.0	1.16	147200	1950	155	288	52300	3900	28800	3800	DIG 2023-0019
100/12-18-056-20W4/00	53.84163	-112.97265	LD25	Leduc Formation	-9999	101000	6.4	1.07	64320	230	481	2680	31195	632	5028	1597	DIG 2019-0002
100/14-07-038-04W5/00	52.25731	-114.56505	LD26	Leduc Formation	3075	226979	5.9	1.16	140400	1080	317	263	51900	4950	26000	3310	DIG 2023-0019
100/14-11-033-26W4/00	51.82128	-113.58527	LD27	Leduc Formation	2264	200124	6.2	1.14	128000	893	972	401	45200	5990	19800	255	DIG 2023-0019
100/14-16-079-22W5/00	55.85290	-117.38447	LD28	Leduc Formation	-9999	268000	6.5	1.17	189540	615	121	1170	86229	2504	29250	4469	DIG 2012-0001
100/14-33-041-22W4/00	52.57612	-113.11642	LD29	Leduc Formation	-9999	227457	6.0	1.14	139446	960	665	5486	55321	6915	21946	3795	DIG 2012-0001
102/08-26-039-21W4/00	52.38275	-112.90920	LD30	Leduc Formation	-9999	335485	6.2	1.15	139690	996	594	16030	55991	6721	23587	4099	DIG 2012-0001
102/10-18-039-03W5/00	52.35703	-114.41997	LD31	Leduc Formation	2943	219743	6.1	1.16	139000	1060	279	267	48800	4680	23700	3160	DIG 2023-0019
102/10-28-038-20W4/00	52.29797	-112.79898	LD32	Leduc Formation	-9999	141700	5.6	1.09	72376	600	896	872	30302	3793	10802	2442	DIG 2011-0007
102/14-02-049-27W4/00	53.20413	-113.84203	LD33	Leduc Formation	-9999	216000	5.9	1.17	151580	1600	286	396	53869	3416	31365	4699	DIG 2019-0002
102/14-35-052-26W4/00	53.54048	-113.72655	LD34	Leduc Formation	-9999	41400	6.7	1.10	86522	598	277	1098	40187	1757	14054	2295	DIG 2019-0002
102/16-29-071-23W5/02	55.18287	-117.49027	LD35	Leduc Formation	-9999	140000	6.9	1.17	184386	498	417	8776	75738	5963	33143	3863	DIG 2019-0002
103/05-05-072-23W5/02	55.20485	-117.51294	LD36	Leduc Formation	-9999	264000	6.9	1.17	185712	460	472	15184	71949	5828	31886	3703	DIG 2019-0002
103/09-20-055-25W4/00	53.77045	-113.67253	LD37	Leduc Formation	-9999	114000	6.1	1.08	73440	380	793	3888	32184	1901	7225	1598	DIG 2011-0007
100/02-22-058-22W4/00	54.02350	-113.18336	LD38	Leduc Formation	995	107498	6.8	1.08	64500	130	559	1250	33800	974	4940	1760	DIG 2023-0019
100/03-19-056-20W4/00	53.84882	-112.96644	LD39	Leduc Formation	992	98081	6.9	1.07	59300	163	423	2270	29700	603	4436	1564	DIG 2023-0019
100/04-12-057-21W4/00	53.90712	-112.99746	LD40	Leduc Formation	981	102509	6.9	1.08	62700	137	478	1120	31800	716	4238	1700	DIG 2023-0019
100/04-20-057-21W4/00	53.93627	-113.09649	LD41	Leduc Formation	1005	103576	7.1	1.08	62100	141	484	1140	33450	708	4400	1540	DIG 2023-0019
100/04-35-056-21W4/00	53.87833	-113.02204	LD42	Leduc Formation	981	63300	6.7	1.05	38700	157	179	3	21900	119	1725	766	DIG 2023-0019
100/05-16-056-21W4/00	53.83818	-113.07155	LD43	Leduc Formation	994	59613	6.8	1.05	33900	87	681	2620	19070	437	2370	882	DIG 2023-0019
100/05-31-056-20W4/00	53.88167	-112.97258	LD44	Leduc Formation	981	93375	6.9	1.07	55500	175	453	1560	29800	610	4100	1582	DIG 2023-0019
100/07-09-057-21W4/00	53.91078	-113.05949	LD45	Leduc Formation	999	105322	6.8	1.08	62600	164	649	1340	33900	737	4740	1686	DIG 2023-0019
100/09-02-058-22W4/00	53.98714	-113.15249	LD46	Leduc Formation	998	96623	7.0	1.07	57100	116	630	2360	30200	761	4507	1385	DIG 2023-0019
100/10-22-057-21W4/00	53.94348	-113.03480	LD47	Leduc Formation	1014	103013	6.7	1.08	61200	114	521	952	34100	778	4120	1607	DIG 2023-0019
100/11-13-056-21W4/00	53.84168	-112.99108	LD48	Leduc Formation	991	94751	6.9	1.07	57300	144	427	2740	27900	605	4486	1510	DIG 2023-0019
100/11-33-057-21W4/00	53.97243	-113.06567	LD49	Leduc Formation	1014	100484	6.9	1.08	60300	135	492	990	32300	795	4278	1580	DIG 2023-0019
100/12-07-058-21W4/00	54.00152	-113.12133	LD50	Leduc Formation	991	114359	6.9	1.08	64500	158	492	1280	33300	8620	4718	1700	DIG 2023-0019
102/06-19-058-22W4/00	54.02617	-113.26402	LD51	Leduc Formation	987	101000	6.7	1.08	60800	151	630	1160	31400	1040	4720	1570	DIG 2023-0019

UWI	BH_Lat 83	BH_Long 83	Label	Geological Unit	Vertical Depth* (m)	TDS (mg/L)	pH*	Density* (kg/L)	Cl (mg/L)	Br* (mg/L)	HCO_3* (mg/L)	SO_4* (mg/L)	Na (mg/L)	K (mg/L)	Ca (mg/L)	Mg (mg/L)	Source
103/09-22-039-26W4/00	52.37115	-113.65714	LD52	Leduc Formation	2203	186566	6.0	1.14	118000	659	486	392	40800	4976	19480	2680	DIG 2023-0019
100/03-13-039-21W4/00	52.34872	-112.89902	LD53	Leduc Formation	1650	193435	6.2	1.13	122200	795	401	669	44000	4590	18600	3180	DIG 2023-0019
100/06-20-038-04W5/00	52.28083	-114.54221	LD55	Leduc Formation	3231	228225	5.9	1.15	149000	1120	264	359	49300	4266	22400	2770	DIG 2023-0019
100/06-36-033-26W4/02	51.87342	-113.56144	LD56	Leduc Formation	2230	224572	6.9	1.14	136700	900	968	552	54697	7052	22116	2980	DIG 2023-0019
100/09-26-039-21W4/00	52.38416	-112.90972	LD57	Leduc Formation	1706	227093	6.5	1.15	145300	868	517	460	49400	5640	22400	3640	DIG 2023-0019
100/15-13-039-21W4/00	52.35993	-112.89320	LD58	Leduc Formation	1657	191393	6.4	1.13	118100	872	490	522	44300	4500	20300	3430	DIG 2023-0019
100/16-08-079-22W5/00	55.83903	-117.39798	LD59	Leduc Formation	2090	267520	6.0	1.17	172880	524	77	348	67700	2310	23900	345	DIG 2023-0019
100/06-20-057-21W4/00	53.93988	-113.09037	LD60	Leduc Formation	978	99000	6.5	1.07	60000	227	-9999	1280	31100	842	4260	1582	Connolly et al., 1990
100/06-23-052-26W4/00	53.50308	-113.72875	LD61	Leduc Formation	1536	129000	6.7	1.09	78300	485	-9999	837	34500	1560	11100	2109	Connolly et al., 1990
100/07-06-058-21W4/00	53.98348	-113.10914	LD62	Leduc Formation	979	108000	6.1	1.07	65100	258	-9999	1170	33000	1000	4850	1862	Connolly et al., 1990
100/07-35-052-26W4/00	53.53222	-113.72387	LD63	Leduc Formation	1523	151386	6.5	1.10	86115	668	245	1316	37627	1755	16345	2600	DIG 2019-0002
100/07-35-052-26W4/B	53.53222	-113.72387	LD64	Leduc Formation	1525	150563	6.6	1.10	86381	670	248	1319	34619	1649	15606	2506	DIG 2019-0002
100/11-12-058-22W4/00	54.00157	-113.13990	LD65	Leduc Formation	985	111000	6.0	1.07	66100	274	-9999	1240	34900	1080	5220	1987	Connolly et al., 1990
100/11-14-057-21W4/00	53.92901	-113.01608	LD66	Leduc Formation	972	106000	6.2	1.07	63100	241	-9999	880	34200	896	4380	1870	Connolly et al., 1990
100/11-15-050-26W4/00	53.31823	-113.72400	LD67	Leduc Formation	1623	235000	6.2	1.16	144000	1260	-9999	294	50000	3640	30000	5035	Connolly et al., 1990
100/09-29-057-19W4/00	53.95818	-112.78047	CO01	Cooking Lake Formation	1128	160586	6.5	1.11	97200	338	207	874	50223	700	8101	3386	DIG 2023-0019
100/13-28-057-19W4/00	53.96167	-112.77430	CO02	Cooking Lake Formation	1143	157553	7.3	1.11	95000	337	187	907	49466	659	8143	3287	DIG 2023-0019
102/04-28-057-19W4/00	53.95193	-112.77623	CO03	Cooking Lake Formation	1144	160373	7.3	1.11	98000	423	222	648	49887	660	7710	3359	DIG 2023-0019
100/12-28-057-19W4/00	53.95929	-112.77643	CO04	Cooking Lake Formation	1121	169677	6.5	1.11	105022	301	251	4547	49351	632	8395	3072	DIG 2011-0007
100/01-18-060-18W5/00	54.18408	-116.68133	SH01	Swan Hills Formation	-9999	225200	6.6	1.16	141956	413	752	15	63600	4260	10900	2250	OFR 2011-10
100/02-17-071-18W5/00	55.14382	-116.72828	SH02	Swan Hills Formation	-9999	187656	6.7	1.12	106785	303	170	972	56297	1106	9997	1340	DIG 2019-0002
100/02-19-067-10W5/00	54.80870	-115.51082	SH03	Swan Hills Formation	-9999	45000	-9999	1.03	24100	82	-9999	-9999	12800	218	1910	319	DIG 2021-0022
100/02-30-071-18W5/00	55.17291	-116.75462	SH04	Swan Hills Formation	-9999	136000	7.1	1.09	77466	208	255	1197	45805	729	6593	968	DIG 2019-0002
100/06-19-067-10W5/00	54.81216	-115.51635	SH05	Swan Hills Formation	-9999	45200	-9999	1.03	23800	101	-9999	-9999	13400	252	1940	399	DIG 2021-0022
100/04-30-065-13W5/00	54.64882	-115.96385	SH06	Swan Hills Formation	-9999	201000	3.4	-9999	126000	280	-9999	640	64200	2720	9960	1260	OFR 2011-10
100/05-23-059-18W5/00	54.11475	-116.59624	SH07	Swan Hills Formation	-9999	215544	7.0	1.15	135958	378	469	55	59900	4720	11700	2930	OFR 2011-10
100/09-11-061-12W5/00	54.26319	-115.67870	SH09	Swan Hills Formation	-9999	207015	6.3	1.12	123090	386	159	560	74078	1902	3894	615	DIG 2011-0007
100/09-27-059-18W5/00	54.13184	-116.60504	SH10	Swan Hills Formation	-9999	228619	7.0	1.16	142956	377	423	70	64500	5070	12500	3270	OFR 2011-10
100/10-02-059-18W5/00	54.07475	-116.58438	SH11	Swan Hills Formation	-9999	216885	6.8	1.15	131959	-9999	733	78	54700	3098	24400	2210	OFR 2011-10

UWI	BH_Lat 83	BH_Long 83	Label	Geological Unit	Vertical Depth* (m)	TDS (mg/L)	pH*	Density* (kg/L)	Cl (mg/L)	Br* (mg/L)	HCO_3* (mg/L)	SO_4* (mg/L)	Na (mg/L)	K (mg/L)	Ca (mg/L)	Mg (mg/L)	Source
100/10-04-067-18W5/00	54.77219	-116.67970	SH12	Swan Hills Formation	-9999	77900	7.1	-9999	46400	100	225	990	29200	668	2140	299	OFR 2011-10
100/10-15-059-18W5/00	54.10297	-116.61168	SH13	Swan Hills Formation	-9999	209093	7.2	1.15	130959	412	687	63	57600	5610	11100	3350	OFR 2011-10
100/10-21-059-18W5/00	54.11769	-116.63771	SH14	Swan Hills Formation	-9999	213288	7.1	1.15	134958	353	616	51	57300	5290	12200	3120	OFR 2011-10
100/11-27-064-13W5/00	54.56804	-115.88113	SH15	Swan Hills Formation	-9999	62953	7.3	1.04	35705	49	327	1775	23803	449	1545	240	DIG 2011-0007
100/12-10-064-19W5/00	54.52521	-116.79563	SH16	Swan Hills Formation	-9999	114000	7.0	-9999	70700	200	377	300	44600	1420	1870	298	OFR 2011-10
100/12-17-067-18W5/00	54.80144	-116.71810	SH17	Swan Hills Formation	-9999	83556	7.1	1.06	46737	127	248	1161	28907	696	2363	327	DIG 2011-0007
100/12-18-063-10W5/00	54.45262	-115.51019	SH18	Swan Hills Formation	-9999	74269	7.5	1.05	42485	113	381	1888	28113	472	2150	325	DIG 2019-0002
100/12-21-067-18W5/03	54.81534	-116.68995	SH19	Swan Hills Formation	-9999	86381	7.3	1.06	47837	140	289	1162	29251	708	2429	338	DIG 2011-0007
S0/04-03-060-18W5/02	54.15241	-116.62528	SH20	Swan Hills Formation	-9999	233957	7.0	1.16	147954	364	523	70	68000	4530	10200	2890	OFR 2011-10
100/02-28-063-10W5/00	54.47421	-115.44738	SH21	Swan Hills Formation	2687	63054	7.8	1.05	37000	54	242	1620	22180	351	1540	245	DIG 2023-0019
100/04-07-061-12W5/00	54.25608	-115.79819	SH22	Swan Hills Formation	2580	188064	6.5	1.13	115000	120	201	821	66480	1365	3761	538	DIG 2023-0019
100/04-17-063-11W5/00	54.44513	-115.63654	SH23	Swan Hills Formation	2702	94291	7.4	1.05	55500	78	256	1340	34420	649	1930	326	DIG 2023-0019
100/06-06-064-11W5/00	54.50522	-115.65234	SH24	Swan Hills Formation	2760	91399	7.6	1.07	56000	59	218	1550	30950	620	1878	295	DIG 2023-0019
100/08-09-064-11W5/00	54.52263	-115.59181	SH25	Swan Hills Formation	2706	65712	7.4	1.05	39800	62	254	1020	22770	363	1396	239	DIG 2023-0019
100/10-19-063-11W5/00	54.46681	-115.64897	SH26	Swan Hills Formation	2689	118945	7.1	1.09	73400	65	222	1260	40760	806	2259	351	DIG 2023-0019
100/12-27-063-11W5/00	54.48173	-115.58511	SH27	Swan Hills Formation	2743	65820	7.6	1.05	38000	69	281	1540	23880	392	1606	264	DIG 2023-0019
100/13-03-065-10W5/02	54.60263	-115.43585	SH28	Swan Hills Formation	2497	180967	6.4	1.13	109000	193	90	543	64500	1149	5136	596	DIG 2023-0019
100/13-13-061-13W5/00	54.28112	-115.82290	SH29	Swan Hills Formation	2585	184878	6.3	1.13	112000	121	181	813	65740	1264	4361	612	DIG 2023-0019
100/14-01-063-12W5/00	54.42772	-115.68047	SH30	Swan Hills Formation	2688	184196	6.4	1.13	115000	115	222	921	62030	914	4582	640	DIG 2023-0019
100/14-30-063-10W5/00	54.48578	-115.50323	SH31	Swan Hills Formation	2648	65693	7.7	1.05	38900	53	222	1560	22970	380	1511	263	DIG 2023-0019
100/01-32-063-09W5/00	54.48786	-115.31391	SH32	Swan Hills Formation	2511	215183	5.6	1.15	130000	310	26	399	72600	1577	9700	894	DIG 2023-0019
100/04-08-065-23W5/00	54.60439	-117.45264	SH33	Swan Hills Formation	3478	59018	6.7	1.04	35238	27	380	248	21900	753	621	71	DIG 2023-0019
100/15-29-064-23W5/00	54.57395	-117.43610	SH34	Swan Hills Formation	3527	63612	7.7	1.04	38345	42	671	246	23400	813	400	79	DIG 2023-0019
102/10-32-064-23W5/00	54.58298	-117.43863	SH35	Swan Hills Formation	3432	43052	6.4	1.03	25897	41	437	274	15600	516	494	57	DIG 2023-0019
100/07-06-087-14W5/00	56.51216	-116.21874	SP01	Slave Point Formation	1610	163266	6.8	1.12	102520	306	157	188	46800	532	10800	2350	DIG 2023-0019
100/09-09-083-14W5/00	56.18170	-116.13747	SP02	Slave Point Formation	1851	253736	5.3	1.18	164940	842	12	342	53200	924	33000	1324	DIG 2023-0019
100/10-19-076-10W5/00	55.60144	-115.53646	SP03	Slave Point Formation	1913	167057	6.1	1.12	102780	235	138	585	51000	625	10200	1800	DIG 2023-0019
100/13-04-085-09W5/00	56.34590	-115.36746	SP04	Slave Point Formation	1560	110991	2.6	1.08	68920	251	-9999	910	26800	340	8650	1720	DIG 2023-0019
100/14-07-087-14W5/00	56.53372	-116.22731	SP05	Slave Point Formation	1637	166951	6.8	1.12	101360	281	118	4897	46400	566	11100	2570	DIG 2023-0019

UWI	BH_Lat 83	BH_Long 83	Label	Geological Unit	Vertical Depth* (m)	TDS (mg/L)	pH*	Density* (kg/L)	Cl (mg/L)	Br* (mg/L)	HCO_3* (mg/L)	SO_4* (mg/L)	Na (mg/L)	K (mg/L)	Ca (mg/L)	Mg (mg/L)	Source
100/16-01-087-15W5/00	56.51985	-116.24071	SP06	Slave Point Formation	1629	165163	6.7	1.12	102760	300	134	202	47800	536	11200	2600	DIG 2023-0019
100/16-22-083-14W5/00	56.21725	-116.11081	SP08	Slave Point Formation	1825	211341	5.8	1.15	136040	421	35	521	53900	804	17650	2410	DIG 2023-0019
100/01-28-097-09W6/00	57.44201	-119.38584	SP09	Slave Point Formation	2511	96528	6.0	1.07	58780	245	120	204	32300	381	4280	525	DIG 2023-0019
100/08-08-096-10W6/00	57.31283	-119.57343	SP10	Slave Point Formation	2510	116631	6.2	1.08	70800	286	187	220	36500	480	7750	790	DIG 2023-0019
100/09-21-097-09W6/00	57.43502	-119.38830	SP11	Slave Point Formation	2480	133063	6.0	1.07	81580	328	153	306	44500	527	5369	707	DIG 2023-0019
100/11-25-097-09W6/00	57.44840	-119.31767	SP12	Slave Point Formation	2409	38931	6.3	1.03	23657	89	146	877	12000	118	1960	247	DIG 2023-0019
100/12-08-096-10W6/00	57.31594	-119.59324	SP13	Slave Point Formation	2523	147712	6.0	1.10	90780	370	96	280	46300	520	8800	986	DIG 2023-0019
100/16-32-097-08W6/00	57.46719	-119.24912	SP14	Slave Point Formation	2390	136150	5.8	1.09	83570	320	75	431	43460	332	7450	871	DIG 2023-0019
100/14-17-077-10W5/00	55.67675	-115.51650	SP15	Slave Point Formation	1854	183114	6.2	1.13	110950	266	132	638	58500	632	10600	1730	DIG 2023-0019
100/03-21-066-13W5/00	54.71980	-115.90590	BL01	Beaverhill Lake Group	2953	163444	6.2	1.12	99500	102	73	406	51460	875	10270	897	DIG 2023-0019
100/04-33-063-09W5/00	54.48955	-115.30992	BL02	Beaverhill Lake Group	2450	172243	6.0	1.12	107000	119	108	246	53210	968	9870	897	DIG 2023-0019
100/05-07-064-10W5/02	54.52227	-115.51078	BL03	Beaverhill Lake Group	2606	68061	7.5	1.05	40200	64	252	1500	23980	387	1608	262	DIG 2023-0019
100/07-17-064-10W5/00	54.53553	-115.47493	BL04	Beaverhill Lake Group	2582	204219	6.7	1.14	121000	160	218	702	73100	1427	7290	594	DIG 2023-0019
100/08-15-064-11W5/00	54.53598	-115.56652	BL05	Beaverhill Lake Group	2725	91519	6.7	1.07	54900	72	250	1290	32450	543	1884	329	DIG 2023-0019
100/09-06-063-14W5/02	54.42449	-116.09483	BL06	Beaverhill Lake Group	2845	185436	6.6	1.12	115260	271	179	84	63600	1930	4000	475	DIG 2023-0019
100/11-34-064-10W5/02	54.58372	-115.42650	BL07	Beaverhill Lake Group	2432	194091	5.2	1.13	117000	233	140	527	67800	1180	6810	705	DIG 2023-0019
100/12-20-061-12W5/00	54.29384	-115.77595	BL08	Beaverhill Lake Group	2606	152612	6.5	1.10	92800	75	161	1200	53660	960	3436	477	DIG 2023-0019
100/16-29-063-09W5/00	54.48582	-115.31610	BL10	Beaverhill Lake Group	2531	209322	5.5	1.14	125000	223	31	497	73800	1620	7630	760	DIG 2023-0019
102/04-09-064-10W5/00	54.51649	-115.46189	BL11	Beaverhill Lake Group	2559	70509	7.7	1.05	42300	54	250	1430	24480	379	1544	253	DIG 2023-0019
102/16-05-061-12W5/00	54.25061	-115.75529	BL12	Beaverhill Lake Group	2577	200764	6.4	1.14	123000	124	136	825	70700	1422	4187	563	DIG 2023-0019
100/10-14-063-11W5/00	54.45273	-115.54837	BL13	Beaverhill Lake Group	2733	70149	7.6	1.05	41600	62	283	1810	24200	391	1745	264	DIG 2023-0019
100/16-18-064-11W5/00	54.54317	-115.64131	BL14	Beaverhill Lake Group	2656	179254	6.4	1.12	105000	128	90	677	67100	1730	4195	509	DIG 2023-0019
102/05-36-065-13W5/02	54.66760	-115.83922	BL15	Beaverhill Lake Group	2769	185905	6.5	1.13	111000	205	81	467	62200	1296	10130	772	DIG 2023-0019
100/03-34-063-10W5/02	54.48848	-115.42855	BL16	Beaverhill Lake Group	2815	74164	7.6	1.05	41960	114	298	1574	27064	451	2004	325	DIG 2019-0002
100/12-19-070-11W5/00	55.07799	-115.67611	BL17	Beaverhill Lake Group	2281	25552	7.5	1.02	14252	34	303	1252	7696	80	1313	237	DIG 2019-0002
100/12-19-070-11W5/B	55.07799	-115.67611	BL18	Beaverhill Lake Group	2281	25348	7.5	1.02	13743	35	300	1252	7910	83	1344	242	DIG 2019-0002
102/02-23-077-21W5/00	55.68009	-117.14303	BL19	Beaverhill Lake Group	2302	289912	6.2	1.17	184702	573	68	818	88610	1087	21977	2338	DIG 2019-0002
100/07-31-067-10W5/00	54.84146	-115.51312	BL20	Beaverhill Lake Group	-9999	44500	-9999	1.03	25800	78	-9999	-9999	14100	196	1390	294	DIG 2021-0022
100/04-14-078-08W5/00	55.75408	-115.13631	GL01	Gilwood Member	-9999	199000	-9999	1.13	117000	427	-9999	-9999	52900	682	17000	2710	DIG 2021-0022

UWI	BH_Lat 83	BH_Long 83	Label	Geological Unit	Vertical Depth* (m)	TDS (mg/L)	pH*	Density* (kg/L)	Cl (mg/L)	Br* (mg/L)	HCO_3* (mg/L)	SO_4* (mg/L)	Na (mg/L)	K (mg/L)	Ca (mg/L)	Mg (mg/L)	Source
100/09-19-078-11W5/00	55.77604	-115.68372	GL02	Gilwood Member	1945	204955	5.4	1.14	132330	368	87	498	51400	1170	17800	1714	DIG 2023-0019
100/13-18-076-10W5/00	55.58928	-115.54858	GL03	Gilwood Member	1986	212623	5.8	1.15	131270	351	100	454	61600	1440	16000	1810	DIG 2023-0019
100/15-25-077-08W5/00	55.70625	-115.09615	GL04	Gilwood Member	-9999	220000	-9999	1.15	135000	564	-9999	-9999	54600	637	20500	3190	DIG 2021-0022
100/02-07-080-08W5/00	55.91449	-115.23725	GL05	Gilwood Member	1757	140036	6.4	1.09	88040	309	155	1127	35500	574	12900	1820	DIG 2023-0019
100/04-30-076-10W5/00	55.60897	-115.54873	GL06	Gilwood Member	1994	207667	5.8	1.14	126770	35	114	412	61400	1370	15900	1760	DIG 2023-0019
100/10-23-079-08W5/00	55.86291	-115.13272	GL07	Gilwood Member	1739	138242	6.5	1.09	86440	284	163	1078	35900	534	12500	1710	DIG 2023-0019
103/10-29-079-08W5/00	55.87809	-115.20985	GL08	Gilwood Member	1715	129437	6.7	1.09	80750	286	189	1175	33200	489	12200	1530	DIG 2023-0019
100/01-03-096-06W5/00	57.29719	-114.87238	KR01	Keg River Formation	1278	218797	6.4	1.15	140650	474	75	664	57700	1006	15700	3040	DIG 2023-0019
100/01-34-089-04W5/00	56.75759	-114.53770	KR02	Keg River Formation	1491	321352	5.2	1.22	209530	1308	18	173	70600	1330	35700	4010	DIG 2023-0019
100/02-23-081-10W5/00	56.02993	-115.44655	KR03	Keg River Formation	1776	236017	5.1	1.16	151060	703	24	375	57000	1220	24500	1850	DIG 2023-0019
100/03-05-095-03W5/00	57.20715	-114.44878	KR04	Keg River Formation	1303	245846	6.2	1.16	157070	620	77	609	66900	1450	16780	3000	DIG 2023-0019
100/04-04-093-05W5/00	57.03554	-114.74958	KR05	Keg River Formation	1346	272654	6.0	1.19	174550	827	57	376	69300	1280	23500	3620	DIG 2023-0019
100/04-10-092-05W5/00	56.96280	-114.72042	KR06	Keg River Formation	1323	296591	5.4	1.20	186330	1100	20	281	69000	1130	35900	3940	DIG 2023-0019
100/05-27-122-22W5/00	59.62468	-117.70713	KR07	Keg River Formation	1353	113082	6.3	1.09	68500	316	596	1160	31200	1450	8720	1760	DIG 2023-0019
100/06-01-094-02W5/02	57.12449	-114.17856	KR08	Keg River Formation	1291	243921	6.1	1.17	158760	593	85	528	66200	1400	16700	292	DIG 2023-0019
100/06-18-094-03W5/00	57.15384	-114.47219	KR09	Keg River Formation	1325	261092	6.2	1.18	167310	624	90	478	72350	1320	16480	3110	DIG 2023-0019
100/06-23-082-09W5/00	56.12168	-115.29530	KR10	Keg River Formation	1789	248054	5.1	1.17	158040	748	39	335	61000	1220	25300	2140	DIG 2023-0019
100/07-34-092-04W5/00	57.02203	-114.54708	KR11	Keg River Formation	1274	301405	5.9	1.20	192350	948	61	295	77000	1320	26300	4110	DIG 2023-0019
100/08-05-082-09W5/02	56.07773	-115.36313	KR12	Keg River Formation	1753	253891	5.3	1.17	161330	688	43	401	62400	1230	26400	2110	DIG 2023-0019
100/09-10-089-03W5/00	56.70678	-114.37894	KR13	Keg River Formation	1540	311778	5.3	1.21	203450	1251	26	239	70000	1516	32100	4460	DIG 2023-0019
100/09-28-082-10W5/00	56.14059	-115.49434	KR14	Keg River Formation	1757	287773	5.2	1.20	185710	1122	35	217	59000	1080	40700	1050	DIG 2023-0019
100/10-03-090-03W5/00	56.77764	-114.38386	KR15	Keg River Formation	1480	296651	5.7	1.20	194390	941	55	275	73600	1280	23500	3580	DIG 2023-0019
103/10-32-110-07W6/00	58.59565	-119.12569	KR17	Keg River Formation	1799	147134	6.4	1.11	90000	404	437	540	44000	1920	9020	1440	DIG 2023-0019
100/13-06-111-06W6/03	58.61397	-119.00892	KR18	Keg River Formation	1705	180782	6.5	1.13	111300	854	236	437	53800	2360	11400	1370	DIG 2023-0019
100/14-32-093-03W5/00	57.11711	-114.44953	KR19	Keg River Formation	1270	254370	6.4	1.17	159620	630	116	598	73500	1255	16280	3060	DIG 2023-0019
100/14-36-092-05W5/00	57.03011	-114.65988	KR20	Keg River Formation	1345	299309	5.6	1.20	189460	912	33	323	82200	1270	22100	3940	DIG 2023-0019
100/15-30-089-03W5/00	56.75191	-114.46513	KR21	Keg River Formation	1490	312157	5.3	1.21	198050	1241	29	289	72000	1445	35700	4660	DIG 2023-0019
100/16-05-081-09W5/00	55.99697	-115.36040	KR22	Keg River Formation	1778	258454	5.0	1.18	167490	721	22	313	61700	1350	25600	1990	DIG 2023-0019
100/16-13-081-10W5/00	56.02603	-115.41151	KR23	Keg River Formation	1773	244562	4.9	1.17	157390	692	24	341	58600	1210	25000	2010	DIG 2023-0019

UWI	BH_Lat 83	BH_Long 83	Label	Geological Unit	Vertical Depth* (m)	TDS (mg/L)	pH*	Density* (kg/L)	Cl (mg/L)	Br* (mg/L)	HCO_3* (mg/L)	SO_4* (mg/L)	Na (mg/L)	K (mg/L)	Ca (mg/L)	Mg (mg/L)	Source
100/16-27-096-06W5/00	57.36307	-114.87305	KR24	Keg River Formation	1194	219774	6.2	1.15	141370	587	69	604	55500	1396	17000	3870	DIG 2023-0019
102/10-07-112-05W6/00	58.71125	-118.82865	KR25	Keg River Formation	1580	166102	6.0	1.12	101300	659	250	569	50700	2030	9600	1780	DIG 2023-0019
102/14-13-090-03W5/00	56.81139	-114.33926	KR26	Keg River Formation	1404	289934	5.9	1.20	191850	870	57	326	72000	1260	24100	370	DIG 2023-0019
102/15-19-094-03W5/02	57.17555	-114.47020	KR27	Keg River Formation	1290	288781	5.8	1.19	185400	769	59	362	75600	1280	22300	3810	DIG 2023-0019
100/10-22-122-21W5/00	59.61247	-117.52087	KR28	Keg River Formation	1155	192835	5.8	1.14	121000	1020	242	457	35200	1040	31500	3520	DIG 2023-0019
102/13-08-089-03W5/00	56.71112	-114.44710	KR29	Keg River Formation	1529	297039	5.8	1.20	193640	1069	104	338	67800	1570	29600	4040	DIG 2023-0019
100/10-32-081-09W5/02	56.06752	-115.36495	KR30	Keg River Formation	1721	154293	5.6	1.11	97650	314	112	826	38200	764	14930	1868	DIG 2023-0019
100/12-23-087-07W5/00	56.56098	-115.00877	KR31	Keg River Formation	1531	296974	5.5	1.18	184790	1033	29	327	71540	1043	35640	3620	DIG 2023-0019
100/14-30-087-07W5/02	56.57751	-115.10514	KR32	Keg River Formation	1570	259190	6.1	1.16	161910	789	39	406	68200	994	27370	291	DIG 2023-0019
102/05-05-110-04W6/00	58.52121	-118.63840	KR33	Keg River Formation	1645	188103	6.1	1.13	117900	626	157	437	55100	2070	10700	1820	DIG 2023-0019
102/10-32-111-05W6/03	58.68277	-118.80168	KR34	Keg River Formation	1542	171215	6.0	1.12	104800	317	246	574	52100	2140	9720	1760	DIG 2023-0019
100/01-16-087-08W5/00	56.53912	-115.19998	GW01	Granite Wash	1508	222743	5.5	1.16	138940	609	37	466	57800	940	22200	2380	DIG 2023-0019
100/01-36-086-11W5/00	56.49506	-115.58689	GW02	Granite Wash	1555	191809	6.3	1.14	120490	399	49	648	50000	807	17700	2140	DIG 2023-0019
100/03-11-087-09W5/00	56.52517	-115.32202	GW03	Granite Wash	1451	198416	5.4	1.14	124280	444	22	625	52000	841	18600	2060	DIG 2023-0019
100/05-11-088-09W5/00	56.61615	-115.32817	GW04	Granite Wash	1444	207226	6.2	1.15	131960	534	59	536	51900	761	19500	2540	DIG 2023-0019
100/06-12-087-10W5/00	56.52810	-115.45110	GW05	Granite Wash	1442	201608	6.0	1.15	126900	510	37	620	50500	860	20600	2110	DIG 2023-0019
100/06-23-086-11W5/00	56.47013	-115.62308	GW06	Granite Wash	1565	188111	6.2	1.13	116190	362	47	699	51300	760	17100	2040	DIG 2023-0019
100/07-30-086-10W5/00	56.48313	-115.56864	GW07	Granite Wash	1531	188056	5.9	1.13	117520	373	26	729	50700	775	16300	2020	DIG 2023-0019
100/08-08-087-09W5/00	56.52772	-115.38473	GW08	Granite Wash	1435	199639	6.2	1.14	124580	488	53	625	52100	709	19500	2100	DIG 2023-0019
102/02-09-085-09W5/02	56.35147	-115.35542	GW09	Granite Wash	1580	261528	5.2	1.18	168420	854	57	350	59400	1130	29300	2900	DIG 2023-0019
100/16-21-087-09W5/00	56.56559	-115.36059	GW11	Granite Wash	1472	205725	5.5	1.15	126740	485	16	660	53800	668	21600	2250	DIG 2023-0019
100/06-24-090-10W5/00	56.81757	-115.45430	GW12	Granite Wash	1474	184175	6.4	1.13	113360	277	45	930	51600	704	15520	2040	DIG 2023-0019
100/07-35-090-10W5/00	56.84809	-115.47543	GW13	Granite Wash	1485	195810	6.4	1.12	123790	370	39	975	53500	700	14800	2026	DIG 2023-0019
100/08-12-090-09W5/00	56.78918	-115.28129	GW14	Granite Wash	1415	216702	6.4	1.14	132680	491	39	880	61000	684	18560	2880	DIG 2023-0019
100/09-03-091-10W5/00	56.86750	-115.50765	GW15	Granite Wash	1505	197589	6.3	1.12	122610	380	35	969	55600	706	15700	1988	DIG 2023-0019
100/09-30-090-09W5/00	56.83687	-115.41694	GW16	Granite Wash	1460	198577	6.4	1.12	122040	389	41	1004	57000	713	15650	2150	DIG 2023-0019
100/10-11-090-09W5/00	56.79346	-115.31151	GW17	Granite Wash	1437	208618	6.4	1.13	126170	404	45	906	60650	680	17560	2630	DIG 2023-0019
100/12-35-090-10W5/00	56.85046	-115.48750	GW18	Granite Wash	1488	192852	6.4	1.12	119710	383	39	1107	53840	700	15460	2017	DIG 2023-0019

[*] -9999 indicates an unrecorded value

Abbreviations: 83, NAD83; BH, borehole; Lat, latitude; Long, longitude; TDS, total dissolved solids

References

Connolly et al., 1990	Connolly, C.A., Walter, L.M., Baadsgaard, H. and Longstaff, F.J. (1990): Origin and evolution of formation waters, Alberta Basin, Western Canada Sedimentary Basin. II. Isotope systematics and water mixing; Applied Geochemistry, v. 5, no. 4, p. 397–413.
DIG 2011-0007	Huff, G.F., Stewart, S.A., Riddell, J.T.F. and Chisholm, S. (2011): Water geochemical data, saline aquifer project (tabular data, tab-delimited format); Energy Resources Conservation Board, ERCB/AGS Digital Data 2011-0007.
DIG 2012-0001	Huff, G.F., Bechtel, D.J., Stewart, S.A., Brock, E. and Heikkinen, C. (2012): Water geochemical data, saline aquifer project, 2011 (tabular data, tab-delimited format); Energy Resources Conservation Board, ERCB/AGS Digital Data 2012-0001.
DIG 2019-0002	Huff, G.F., Lopez, G.P. and Weiss, J.A. (2019): Water geochemistry of selected formation brines in the Alberta Basin, Canada (tabular data, tab-delimited format); Alberta Energy Regulator / Alberta Geological Survey, AER/AGS Digital Data 2019-0002.
DIG 2021-0022	Reimert, C., Lyster, S., Hauck, T.E., Palombi, D., Playter, T.L., Lopez, G.P. and Schultz, S.K. (2022): Water geochemical data, Lithium Prospectivity Project, 2021 (tabular data, tab-delimited format); Alberta Energy Regulator / Alberta Geological Survey, AER/AGS Digital Data 2021-0022.
DIG 2023-0019	Reimert, C., Lyster, S., Palombi, D. and Bernal, N. (2025): Brine geochemical data, mineral mapping program, 2021–2024 (tabular data, tab-delimited format); Alberta Energy Regulator / Alberta Geological Survey, AER/AGS Digital Data 2023-0019.
OFR 2011-10	Eccles, D.R. and Berhane, H. (2011): Geological introduction to lithium-rich formation water with emphasis on the Fox Creek area of west-central Alberta (NTS 83F and 83K); Energy Resources Conservation Board, ERCB/AGS Open File Report 2011-10, 22 p.

Table 3. Analytical results for dissolved species and isotopes in Devonian oil brines in Alberta.

UWI	Label	Li (mg/L)	B* (mg/L)	Si* (mg/L)	S* (mg/L)	Fe* (mg/L)	As* (mg/L)	Rb* (mg/L)	Sr* (mg/L)	Cs* (mg/L)	Ba* (mg/L)	$\delta^{18}O$* (‰)	$\delta^{2}H$* (‰)	$^{87}Sr/^{86}Sr$*	$\delta^{7}Li$* (‰)	$\delta^{11}B$* (‰)	$\delta^{18}O\_SO_4$* (‰)	$\delta^{34}S\_SO_4$* (‰)	Source
100/06-13-038-23W4/00	WB01	14.0	-9999	-9999	-9999	-9999	-9999	-9999	82	-9999	-9999	-3.9	-77.4	0.70974	-9999	-9999	-9999	-9999	DIG 2012-0001
100/09-30-080-23W5/00	WB02	48.4	61.8	-9999	-9999	-9999	-9999	-9999	1071	-9999	4.439	-0.2	-45.0	0.72214	-9999	-9999	-9999	-9999	DIG 2012-0001
100/10-28-032-02W5/00	WB03	61.6	338.0	11.0	1200	-9999	0.40	3.27	86	0.239	0.150	4.8	-46.8	0.70804	13.7	14.0	12.3	24.4	DIG 2023-0019
100/10-32-076-01W6/00	WB04	67.5	63.3	-9999	-9999	-9999	-9999	-9999	1098	-9999	6.667	0.8	-44.0	0.72375	-9999	-9999	-9999	-9999	DIG 2011-0007
100/12-35-051-27W4/03	WB06	32.8	69.0	7.0	68	<1	<0.02	2.58	561	0.294	6.870	-1.6	-75.8	0.71271	13.7	26.7	-9999	-9999	DIG 2023-0019
102/13-16-029-26W4/00	WB07	29.0	999.0	21.0	1160	<5	<0.1	2.93	79	0.221	<0.1	4.1	-55.8	0.70857	16.6	14.4	-9999	-9999	DIG 2023-0019
100/12-02-055-27W4/00	WB08	20.7	-9999	<20	16.1	-9999	-9999	-9999	455	-9999	4.292	-5.5	-83.3	0.71071	-9999	-9999	-9999	-9999	OFR 2011-10
100/08-28-078-24W5/00	WB09	53.3	60.0	14.0	887	<1	<0.02	5.52	725	0.507	2.050	2.3	-42.8	0.72649	18.0	36.1	-9999	-9999	DIG 2023-0019
100/12-36-077-01W6/00	WB10	56.5	64.0	17.0	128	<1	<0.02	7.09	842	0.832	4.620	1.6	-45.6	0.72522	19.0	38.8	-9999	-9999	DIG 2023-0019
100/14-22-032-02W5/00	WB11	81.5	415.0	49.0	1190	<1	<0.02	3.68	94	0.271	0.100	5.0	-52.2	0.70852	14.5	14.8	-9999	-9999	DIG 2023-0019
103/04-20-078-01W6/00	WB12	51.2	51.0	15.0	195	<1	<0.02	6.32	780	0.646	4.600	0.7	-46.8	0.72398	21.0	40.7	-9999	-9999	DIG 2023-0019
100/02-04-057-03W5/00	WB13	22.0	15.0	-9999	-9999	11.9	-9999	-9999	359	-9999	5.000	-6.2	-75.0	0.71062	-9999	-9999	-9999	-9999	Connolly et al., 1990
100/03-07-057-01W5/00	WB14	26.0	43.0	-9999	-9999	0.3	-9999	-9999	393	-9999	2.000	-5.0	-81.0	0.71128	-9999	-9999	-9999	-9999	Connolly et al., 1990
100/09-16-057-03W5/00	WB15	18.0	17.0	-9999	-9999	2.2	-9999	-9999	325	-9999	4.000	-5.6	-82.0	0.71072	-9999	-9999	-9999	-9999	Connolly et al., 1990
100/01-03-049-25W4/00	NK01	58.9	139.0	15.0	538	<1	<0.02	4.99	371	0.550	0.730	-1.2	-71.0	0.71019	11.6	26.5	10.9	20.2	DIG 2023-0019
100/01-34-036-20W4/02	NK02	40.1	97.0	11.0	256	-9999	<0.02	3.50	318	0.294	0.330	-3.2	-75.0	0.70894	13.9	24.8	11.0	23.5	DIG 2023-0019
100/03-02-038-24W4/00	NK04	81.1	-9999	-9999	-9999	-9999	-9999	-9999	755	-9999	2.865	7.5	-50.9	0.70887	-9999	-9999	-9999	-9999	DIG 2012-0001
100/05-23-038-24W4/00	NK05	84.8	-9999	-9999	-9999	-9999	-9999	-9999	752	-9999	2.634	7.1	-49.4	0.70894	-9999	-9999	-9999	-9999	DIG 2012-0001
100/07-10-056-24W4/00	NK06	31.0	65.0	<5	416	<5	<0.1	1.97	199	0.178	0.500	-4.3	-80.3	0.71011	14.6	27.2	13.5	42.2	DIG 2023-0019
100/07-31-036-23W4/00	NK07	46.6	143.0	8.0	197	<1	<0.02	4.84	649	0.620	2.380	5.0	-53.1	0.70922	17.8	25.3	11.2	21.1	DIG 2023-0019
100/08-29-051-26W4/00	NK09	49.6	103.0	9.0	337	<1	<0.02	4.07	330	0.400	0.500	0.3	-67.9	0.71199	10.8	26.0	11.0	26.4	DIG 2023-0019
100/08-33-066-08W5/02	NK10	24.6	40.5	-9999	-9999	5.9	-9999	-9999	534	-9999	0.482	1.5	-37.0	0.71741	-9999	-9999	-9999	-9999	DIG 2019-0002
100/09-26-050-10W5/02	NK11	13.0	61.0	14.0	666	<5	<0.1	0.83	76	0.112	0.100	-5.0	-88.6	0.71216	14.8	25.9	14.6	20.6	DIG 2023-0019
100/12-22-031-24W4/00	NK13	23.6	80.0	10.0	630	<1	0.03	2.84	98	0.438	0.050	3.9	-54.4	0.70943	21.5	26.5	11.5	21.0	DIG 2023-0019
102/10-29-035-22W4/00	NK14	41.2	78.0	12.0	131	2.0	<0.02	4.58	850	0.472	0.810	1.9	-51.6	0.70902	13.8	28.4	-9999	-9999	DIG 2023-0019
100/03-07-035-22W4/00	NK15	39.1	73.0	9.0	122	2.0	<0.02	4.48	825	0.474	0.430	1.9	-51.0	0.70903	14.3	28.8	-9999	-9999	DIG 2023-0019
100/14-14-035-20W4/00	NK16	57.1	141.0	11.0	465	<1	0.13	5.47	329	0.349	0.750	-3.6	-77.8	0.70877	12.9	24.4	10.0	22.7	DIG 2023-0019
100/15-28-049-25W4/00	NK17	50.0	91.0	10.0	185	-9999	<0.02	3.55	358	0.372	0.190	2.8	-58.1	0.71191	8.3	27.3	11.6	20.9	DIG 2023-0019

UWI	Label	Li (mg/L)	B* (mg/L)	Si* (mg/L)	S* (mg/L)	Fe* (mg/L)	As* (mg/L)	Rb* (mg/L)	Sr* (mg/L)	Cs* (mg/L)	Ba* (mg/L)	$\delta^{18}O$* (‰)	$\delta^{2}H$* (‰)	$^{87}Sr/^{86}Sr$*	$\delta^{7}Li$* (‰)	$\delta^{11}B$* (‰)	$\delta^{18}O\_SO_4$* (‰)	$\delta^{34}S\_SO_4$* (‰)	Source
100/16-06-042-23W4/00	NK18	76.0	-9999	-9999	-9999	-9999	-9999	-9999	755	-9999	2.059	7.4	-49.3	0.70888	-9999	-9999	-9999	-9999	DIG 2012-0001
100/16-28-042-23W4/00	NK19	75.3	-9999	-9999	-9999	-9999	-9999	-9999	670	-9999	0.794	5.4	-55.2	0.70919	-9999	-9999	-9999	-9999	DIG 2011-0007
100/11-19-031-09W4/00	NK21	7.4	6.0	10.0	1270	<1	<0.02	0.57	30	0.061	0.024	-14.3	-120.2	0.70851	11.3	16.6	-9999	-9999	DIG 2023-0019
102/06-05-037-21W4/00	NK22	28.8	71.0	6.0	184	<1	0.03	3.46	371	0.330	0.430	2.1	-54.7	0.71061	26.7	27.4	11.4	22.6	DIG 2023-0019
102/09-34-049-26W4/00	NK23	53.8	159.0	9.0	283	<1	0.07	5.28	528	0.679	1.190	2.4	-64.8	0.71253	10.5	23.0	13.3	26.4	DIG 2023-0019
102/10-23-050-26W4/00	NK24	49.3	138.0	9.0	359	<1	<0.02	4.35	413	0.565	0.540	1.6	-67.6	0.71218	10.5	24.0	13.6	26.4	DIG 2023-0019
102/13-01-036-20W4/00	NK25	36.6	90.0	20.0	339	<1	0.07	3.30	225	0.235	4.460	-6.5	-89.8	0.70917	11.8	23.5	11.1	24.2	DIG 2023-0019
102/14-35-052-26W4/00	NK26	30.7	78.7	-9999	-9999	-9999	-9999	-9999	598	-9999	3.426	-5.2	-88.0	0.70946	-9999	-9999	-9999	-9999	DIG 2019-0002
102/15-33-036-22W4/00	NK27	31.0	91.0	7.0	229	4.0	<0.02	1.96	403	0.267	0.580	2.0	-57.3	0.70929	22.9	25.4	11.1	21.1	DIG 2023-0019
103/02-10-051-26W4/00	NK29	47.9	97.0	11.0	256	-9999	<0.02	3.50	318	0.294	0.330	1.2	-65.7	0.71159	10.6	26.3	11.1	24.8	DIG 2023-0019
100/02-17-049-25W4/00	NK30	37.9	-9999	<20	7.896	-9999	-9999	-9999	426	-9999	0.451	3.9	-49.7	0.71126	-9999	-9999	-9999	-9999	DIG 2011-0007
100/07-20-049-25W4/00	NK31	40.7	-9999	<10	38.59	-9999	-9999	-9999	491	-9999	2.043	4.1	-48.9	0.71108	-9999	-9999	-9999	-9999	DIG 2011-0007
100/14-13-050-27W4/00	NK32	39.4	-9999	21.2	240.2	-9999	-9999	-9999	389	-9999	0.447	3.3	-55.7	0.71182	-9999	-9999	-9999	-9999	DIG 2019-0002
102/03-11-053-26W4/00	NK33	30.6	-9999	<20	208.4	-9999	-9999	-9999	178	-9999	0.864	-4.8	-96.8	0.71032	-9999	-9999	-9999	-9999	DIG 2011-0007
102/04-21-057-24W4/00	NK34	33.5	-9999	<20	170.2	-9999	-9999	-9999	216	-9999	0.969	-3.1	-74.7	0.71001	-9999	-9999	-9999	-9999	DIG 2012-0001
103/16-10-056-24W4/00	NK35	41.3	-9999	<20	96.03	-9999	-9999	-9999	236	-9999	0.863	-4.6	-77.0	0.71013	-9999	-9999	-9999	-9999	OFR 2011-10
100/01-08-039-26W4/00	NK36	17.7	96.0	34.0	574	<1	<0.02	1.67	116	0.172	0.250	-10.5	-113.6	0.70912	11.0	23.4	-9999	-9999	DIG 2023-0019
100/04-31-038-26W4/00	NK37	29.6	134.0	26.0	526	<1	<0.02	2.98	169	0.281	0.150	-1.7	-75.5	0.70963	10.7	24.9	-9999	-9999	DIG 2023-0019
100/04-36-038-27W4/00	NK38	21.3	103.0	27.0	533	<1	<0.02	2.10	133	0.174	0.150	-5.5	-92.6	0.70960	11.6	24.2	-9999	-9999	DIG 2023-0019
100/03-27-049-25W4/00	NK39	38.9	86.0	19.0	270	<1	<0.02	3.06	335	0.329	0.360	1.3	-64.8	0.71101	17.1	27.6	-9999	-9999	DIG 2023-0019
100/08-10-049-25W4/00	NK40	43.5	91.0	18.0	324	<1	<0.02	3.52	324	0.365	0.340	1.3	-62.7	0.71114	17.9	28.8	-9999	-9999	DIG 2023-0019
100/12-04-038-04W5/02	NK41	51.4	168.0	14.0	258	-9999	<0.02	6.89	800	0.767	2.270	6.2	-49.6	0.70930	11.8	25.8	-9999	-9999	DIG 2023-0019
100/14-08-051-26W4/00	NK42	45.5	88.0	16.0	226	<1	<0.02	3.87	371	0.441	0.160	3.2	-58.3	0.71114	13.4	-9999	-9999	-9999	DIG 2023-0019
100/14-23-049-25W4/00	NK43	39.2	89.0	16.0	335	<1	<0.02	3.26	252	0.306	0.280	-1.3	-69.0	0.71083	14.0	-9999	-9999	-9999	DIG 2023-0019
100/15-16-049-25W4/00	NK44	39.8	84.0	15.0	228	<1	<0.02	3.14	370	0.364	0.280	-9999	-9999	-9999	-9999	-9999	-9999	-9999	DIG 2023-0019
100/16-20-049-25W4/00	NK45	42.0	89.0	15.0	245	<1	<0.02	3.33	387	0.370	0.330	2.5	-58.5	0.71098	18.2	29.6	-9999	-9999	DIG 2023-0019
100/16-35-049-26W4/00	NK46	53.2	151.0	19.0	1890	<1	0.17	4.98	369	0.628	0.670	2.2	-66.0	0.71319	16.0	23.0	-9999	-9999	DIG 2023-0019
102/01-33-050-26W4/00	NK47	16.2	47.0	15.0	322	<1	<0.02	1.75	252	0.188	0.180	-11.1	-118.2	0.70968	16.6	-9999	-9999	-9999	DIG 2023-0019
102/05-18-039-20W4/00	NK48	66.4	174.0	26.0	241	<1	<0.02	7.10	610	0.259	0.650	3.7	-61.0	0.70880	16.2	26.6	-9999	-9999	DIG 2023-0019

UWI	Label	Li (mg/L)	B* (mg/L)	Si* (mg/L)	S* (mg/L)	Fe* (mg/L)	As* (mg/L)	Rb* (mg/L)	Sr* (mg/L)	Cs* (mg/L)	Ba* (mg/L)	$\delta^{18}O$* (‰)	$\delta^{2}H$* (‰)	$^{87}Sr/^{86}Sr$*	$\delta^{7}Li$* (‰)	$\delta^{11}B$* (‰)	$\delta^{18}O\_SO_4$* (‰)	$\delta^{34}S\_SO_4$* (‰)	Source
102/08-02-050-26W4/00	NK49	30.5	82.0	11.0	228	2.0	<0.02	3.05	443	0.310	0.460	-3.1	-83.3	0.70955	15.2	-9999	-9999	-9999	DIG 2023-0019
102/15-26-049-26W4/00	NK50	38.6	91.0	18.0	267	<1	<0.02	3.06	462	0.276	1.090	1.9	-62.6	0.70959	17.9	29.3	-9999	-9999	DIG 2023-0019
103/04-30-050-26W4/00	NK51	34.3	86.0	18.0	232	<1	<0.02	3.55	369	0.372	0.140	-0.7	-72.9	0.71036	13.8	-9999	-9999	-9999	DIG 2023-0019
103/16-24-039-21W4/00	NK52	63.1	145.0	23.0	207	<1	<0.02	6.91	499	0.437	0.470	5.1	-55.3	0.70902	16.4	27.7	-9999	-9999	DIG 2023-0019
104/13-16-050-26W4/00	NK53	15.8	38.0	16.0	323	<1	0.03	1.73	197	0.159	0.360	-9.7	-110.2	0.71023	17.0	-9999	-9999	-9999	DIG 2023-0019
100/11-10-038-20W4/00	NK54	36.4	-9999.0	-9999	-9999	-9999	-9999	-9999	214	-9999	0.210	-9.7	-104.9	0.70925	-9999	-9999	-9999	-9999	DIG 2012-0001
100/12-33-040-24W4/02	NK55	84.8	-9999.0	-9999	-9999	-9999	-9999	-9999	736	-9999	0.340	6.8	-51.2	0.70883	-9999	-9999	-9999	-9999	DIG 2012-0001
100/16-10-056-24W4/00	NK56	36.0	62.0	-9999	-9999	0.3	-9999	-9999	184	-9999	1.000	-5.3	-77.0	0.71005	-9999	-9999	-9999	-9999	Connolly et al., 1990
100/01-30-055-25W4/00	LD01	37.8	-9999	-9999	-9999	-9999	-9999	-9999	189	-9999	0.540	-4.5	-76.4	0.71031	-9999	-9999	-9999	-9999	DIG 2011-0007
100/02-05-044-01W5/00	LD02	46.7	172.0	12.0	122	<1	0.03	6.30	1210	0.711	5.720	4.6	-53.0	0.70873	17.8	25.0	12.4	20.9	DIG 2023-0019
100/02-17-055-25W4/00	LD03	31.0	69.0	7.0	435	<1	0.03	2.48	178	0.204	0.490	-4.4	-79.5	0.71026	14.0	25.8	12.9	34.4	DIG 2023-0019
100/15-10-034-26W4/00	LD04	68.5	217.0	<1	2400	<1	2.28	9.35	943	0.743	4.910	-9999	-9999	-9999	-9999	-9999	-9999	-9999	DIG 2023-0019
100/03-08-055-25W4/00	LD05	38.9	-9999	-9999	-9999	-9999	-9999	-9999	207	-9999	0.650	-3.1	-74.9	0.71040	-9999	-9999	-9999	-9999	DIG 2011-0007
100/04-05-058-21W4/00	LD06	20.4	-9999	-9999	-9999	-9999	-9999	-9999	205	-9999	0.215	-5.3	-86.4	0.70950	-9999	-9999	-9999	-9999	DIG 2011-0007
100/04-21-057-24W4/00	LD07	32.8	-9999	-9999	-9999	-9999	-9999	-9999	226	-9999	0.862	-3.5	-74.5	0.71001	-9999	-9999	-9999	-9999	DIG 2011-0007
100/04-22-044-01W5/00	LD08	66.4	-9999	-9999	-9999	-9999	-9999	-9999	1293	-9999	9.786	3.8	-55.6	0.70877	-9999	-9999	-9999	-9999	DIG 2012-0001
100/05-05-044-22W4/00	LD09	84.2	-9999	-9999	-9999	-9999	-9999	-9999	614	-9999	1.031	7.3	-51.4	0.70885	-9999	-9999	-9999	-9999	DIG 2012-0001
100/05-35-051-27W4/00	LD10	34.0	-9999	-9999	-9999	-9999	-9999	-9999	1070	-9999	5.947	1.7	-56.8	0.70889	-9999	-9999	-9999	-9999	DIG 2011-0007
100/05-36-038-04W5/00	LD11	53.7	208.0	13.0	126	<1	<0.02	7.24	1260	0.786	8.950	4.9	-55.7	0.70871	11.5	25.3	-9999	-9999	DIG 2023-0019
100/07-26-069-23W5/00	LD12	103.5	184.2	-9999	-9999	-9999	-9999	-9999	1621	-9999	14.692	4.5	-44.0	0.72833	-9999	-9999	-9999	-9999	DIG 2019-0002
100/07-35-052-26W4/B0	LD14	28.8	79.1	-9999	-9999	-9999	-9999	-9999	543	-9999	0.723	-6.8	-97.0	0.70895	-9999	-9999	-9999	-9999	DIG 2019-0002
100/09-05-038-04W5/00	LD15	63.6	-9999	-9999	-9999	-9999	-9999	-9999	1268	-9999	8.025	5.2	-52.6	0.70875	-9999	-9999	-9999	-9999	DIG 2012-0001
100/09-06-038-23W4/00	LD16	77.6	278.0	10.0	309	-9999	0.76	9.51	697	1.190	1.340	7.6	-50.4	0.70887	13.8	22.6	13.4	20.4	DIG 2023-0019
100/09-08-050-26W4/02	LD17	42.9	-9999	-9999	-9999	-9999	-9999	-9999	1150	-9999	4.244	-0.7	-66.2	0.70881	-9999	-9999	-9999	-9999	DIG 2019-0002
100/09-16-057-21W4/00	LD18	18.0	-9999	-9999	-9999	-9999	-9999	-9999	208	-9999	0.215	-5.2	-82.8	0.70945	-9999	-9999	-9999	-9999	OFR 2011-10
100/10-01-043-02W5/00	LD19	74.6	-9999	-9999	-9999	-9999	-9999	-9999	1176	-9999	10.010	4.8	-53.3	0.70879	-9999	-9999	-9999	-9999	OFR 2011-10
100/10-01-043-02W5/00	LD20	47.6	172.0	11.0	112	<1	<0.02	6.47	1190	0.701	8.620	4.8	-53.8	0.70877	18.2	25.1	13.4	22.8	DIG 2023-0019
100/10-11-053-26W4/00	LD21	23.2	67.0	7.0	254	<1	<0.02	2.27	509	0.209	1.180	-5.7	-91.6	0.70923	16.4	30.4	13.3	26.3	DIG 2023-0019
100/11-13-054-26W4/00	LD22	40.0	-9999	-9999	-9999	-9999	-9999	-9999	711	-9999	1.025	-0.1	-66.3	0.70888	-9999	-9999	-9999	-9999	DIG 2019-0002

UWI	Label	Li (mg/L)	B* (mg/L)	Si* (mg/L)	S* (mg/L)	Fe* (mg/L)	As* (mg/L)	Rb* (mg/L)	Sr* (mg/L)	Cs* (mg/L)	Ba* (mg/L)	$\delta^{18}O$* (‰)	$\delta^{2}H$* (‰)	$^{87}Sr/^{86}Sr$*	$\delta^{7}Li$* (‰)	$\delta^{11}B$* (‰)	$\delta^{18}O\_SO_4$* (‰)	$\delta^{34}S\_SO_4$* (‰)	Source
100/11-14-042-02W5/00	LD23	52.9	204.0	12.0	131	<1	0.03	7.39	1270	0.842	10.100	5.4	-52.9	0.70875	19.1	24.4	12.6	21.1	DIG 2023-0019
100/12-02-045-01W5/00	LD24	43.9	153.0	10.0	111	<1	<0.02	5.67	1330	0.600	7.810	3.8	-54.6	0.70869	18.2	26.8	12.9	22.5	DIG 2023-0019
100/12-18-056-20W4/00	LD25	17.0	-9999	-9999	-9999	-9999	-9999	-9999	111	-9999	0.214	-6.9	-90.9	0.70941	-9999	-9999	-9999	-9999	DIG 2019-0002
100/14-07-038-04W5/00	LD26	54.5	213.0	13.0	128	<1	<0.02	7.70	1330	0.812	8.160	5.1	-53.4	0.70873	10.7	24.9	12.8	20.2	DIG 2023-0019
100/14-11-033-26W4/00	LD27	102.0	460.0	28.0	236	<5	<0.1	16.00	1380	1.670	5.340	7.9	-46.6	0.70890	14.1	20.4	13.0	23.5	DIG 2023-0019
100/14-16-079-22W5/00	LD28	47.4	61.3	-9999	-9999	-9999	-9999	-9999	1229	-9999	7.207	-0.1	-44.0	0.72244	-9999	-9999	-9999	-9999	DIG 2012-0001
100/14-33-041-22W4/00	LD29	83.1	-9999	-9999	-9999	-9999	-9999	-9999	680	-9999	1.029	7.8	-49.8	0.70882	-9999	-9999	-9999	-9999	DIG 2012-0001
102/08-26-039-21W4/00	LD30	85.5	-9999	-9999	-9999	-9999	-9999	-9999	753	-9999	0.573	6.5	-50.2	0.70878	-9999	-9999	-9999	-9999	DIG 2012-0001
102/10-18-039-03W5/00	LD31	54.1	193.0	11.0	125	<1	<0.02	7.25	1300	0.758	8.320	5.0	-55.5	0.70869	13.6	27.6	-9999	-9999	DIG 2023-0019
102/10-28-038-20W4/00	LD32	52.0	-9999	-9999	-9999	-9999	-9999	-9999	320	-9999	0.981	-2.0	-71.2	0.70885	-9999	-9999	-9999	-9999	DIG 2011-0007
102/14-02-049-27W4/00	LD33	38.8	-9999	-9999	-9999	-9999	-9999	-9999	1370	-9999	5.597	2.2	-54.3	0.70869	-9999	-9999	-9999	-9999	DIG 2019-0002
102/14-35-052-26W4/00	LD34	30.7	78.7	-9999	-9999	-9999	-9999	-9999	598	-9999	3.426	-5.2	-88.0	0.70946	-9999	-9999	-9999	-9999	DIG 2019-0002
102/16-29-071-23W5/02	LD35	96.5	172.7	-9999	-9999	-9999	-9999	-9999	1575	-9999	17.038	4.8	-42.0	0.72896	-9999	-9999	-9999	-9999	DIG 2019-0002
103/05-05-072-23W5/02	LD36	88.1	156.5	-9999	-9999	-9999	-9999	-9999	1413	-9999	15.768	4.3	-44.0	0.72898	-9999	-9999	-9999	-9999	DIG 2019-0002
103/09-20-055-25W4/00	LD37	39.3	-9999	-9999	-9999	-9999	-9999	-9999	197	-9999	0.540	-3.8	-75.6	0.71035	-9999	-9999	-9999	-9999	DIG 2011-0007
100/02-22-058-22W4/00	LD38	18.9	49.0	8.0	595	<1	<0.02	1.15	215	0.078	0.160	-4.9	-84.6	0.70943	13.9	31.1	-9999	-9999	DIG 2023-0019
100/03-19-056-20W4/00	LD39	12.0	36.0	6.0	922	<1	<0.02	0.71	101	0.053	0.050	-7.3	-96.3	0.70940	15.1	33.5	-9999	-9999	DIG 2023-0019
100/04-12-057-21W4/00	LD40	14.1	42.0	8.0	453	<1	<0.02	0.89	218	0.063	0.280	-5.4	-87.4	0.70930	14.4	32.5	-9999	-9999	DIG 2023-0019
100/04-20-057-21W4/00	LD41	14.2	42.0	7.0	477	<1	<0.02	0.85	207	0.063	0.280	-5.4	-87.9	0.70942	14.8	32.7	-9999	-9999	DIG 2023-0019
100/04-35-056-21W4/00	LD42	4.4	9.0	<1	6	<1	<0.02	0.09	193	<0.005	144.000	-8.4	-93.7	0.70865	12.7	33.9	-9999	-9999	DIG 2023-0019
100/05-16-056-21W4/00	LD43	7.4	25.0	3.0	1130	<1	<0.02	0.57	58	0.062	0.070	-12.3	-70.0	0.70963	13.9	24.4	-9999	-9999	DIG 2023-0019
100/05-31-056-20W4/00	LD44	11.7	35.0	5.0	632	<1	<0.02	0.69	137	0.050	0.140	-7.3	-96.4	0.70934	14.4	32.4	-9999	-9999	DIG 2023-0019
100/07-09-057-21W4/00	LD45	15.1	41.0	9.0	579	<1	<0.02	0.85	170	0.076	0.170	-5.6	-88.2	0.70931	20.9	32.7	-9999	-9999	DIG 2023-0019
100/09-02-058-22W4/00	LD46	15.4	43.0	8.0	901	<1	<0.02	0.88	97	0.063	0.030	-5.7	-87.2	0.70974	14.1	31.8	-9999	-9999	DIG 2023-0019
100/10-22-057-21W4/00	LD47	14.7	44.0	7.0	420	<1	<0.02	0.90	236	0.063	0.290	-5.5	-87.8	0.70940	14.3	32.2	-9999	-9999	DIG 2023-0019
100/11-13-056-21W4/00	LD48	11.9	37.0	6.0	1010	4.0	<0.02	0.75	90	0.052	<0.02	-6.9	-94.0	0.70943	14.3	33.1	-9999	-9999	DIG 2023-0019
100/11-33-057-21W4/00	LD49	15.1	45.0	7.0	504	<1	<0.02	0.95	235	0.072	0.300	-5.6	-87.8	0.70944	14.3	31.6	-9999	-9999	DIG 2023-0019
100/12-07-058-21W4/00	LD50	16.9	45.0	7.0	557	<1	<0.02	1.06	193	0.076	0.160	-5.2	-85.9	0.70940	14.1	31.8	-9999	-9999	DIG 2023-0019
102/06-19-058-22W4/00	LD51	19.5	51.0	9.0	403	<1	<0.02	1.20	198	0.037	0.250	-5.3	-85.7	0.70959	13.1	30.6	-9999	-9999	DIG 2023-0019

UWI	Label	Li (mg/L)	B* (mg/L)	Si* (mg/L)	S* (mg/L)	Fe* (mg/L)	As* (mg/L)	Rb* (mg/L)	Sr* (mg/L)	Cs* (mg/L)	Ba* (mg/L)	$\delta^{18}O$* (‰)	$\delta^{2}H$* (‰)	$^{87}Sr/^{86}Sr$*	$\delta^{7}Li$* (‰)	$\delta^{11}B$* (‰)	$\delta^{18}O\_SO_4$* (‰)	$\delta^{34}S\_SO_4$* (‰)	Source
103/09-22-039-26W4/00	LD52	82.8	361.0	29.0	166	<1	0.50	8.61	876	1.070	0.990	5.3	-56.3	0.70881	10.7	22.2	-9999	-9999	DIG 2023-0019
100/03-13-039-21W4/00	LD53	57.0	182.0	16.0	221	<1	0.02	6.85	545	0.698	0.250	3.4	-57.9	0.70885	16.4	24.7	-9999	-9999	DIG 2023-0019
100/06-20-038-04W5/00	LD55	48.2	176.0	27.0	115	<1	<0.02	6.60	1130	0.756	5.870	5.2	-56.1	0.70877	17.2	25.6	-9999	-9999	DIG 2023-0019
100/06-36-033-26W4/02	LD56	70.0	313.0	27.0	150	<1	<0.02	10.50	943	1.080	5.100	7.5	-45.7	0.70893	16.4	21.0	-9999	-9999	DIG 2023-0019
100/09-26-039-21W4/00	LD57	65.7	245.0	14.0	164	<1	0.03	9.06	634	1.080	0.340	7.3	-52.4	0.70885	17.5	23.7	-9999	-9999	DIG 2023-0019
100/15-13-039-21W4/00	LD58	58.0	166.0	19.0	191	<1	0.02	6.57	563	0.676	0.170	3.5	-57.0	0.70878	17.9	25.3	-9999	-9999	DIG 2023-0019
100/16-08-079-22W5/00	LD59	42.1	53.0	19.0	125	<1	<0.02	5.61	762	0.588	5.640	0.3	-44.9	0.72311	20.5	39.2	-9999	-9999	DIG 2023-0019
100/06-20-057-21W4/00	LD60	19.0	35.0	-9999	-9999	0.3	-9999	-9999	168	-9999	1.000	-7.2	-82.0	0.70975	-9999	-9999	-9999	-9999	Connolly et al., 1990
100/06-23-052-26W4/00	LD61	28.0	56.0	-9999	-9999	0.6	-9999	-9999	397	-9999	3.000	-6.8	-87.0	0.70981	-9999	-9999	-9999	-9999	Connolly et al., 1990
100/07-06-058-21W4/00	LD62	22.0	42.0	-9999	-9999	0.3	-9999	-9999	187	-9999	1.000	-6.1	-82.0	0.70937	-9999	-9999	-9999	-9999	Connolly et al., 1990
100/07-35-052-26W4/00	LD63	29.4	78.6	-9999	-9999	-9999	-9999	-9999	538	-9999	1.560	-6.9	-97.0	0.70895	-9999	-9999	-9999	-9999	DIG 2019-0002
100/07-35-052-26W4/B	LD64	28.8	79.1	-9999	-9999	-9999	-9999	-9999	543	-9999	0.720	-6.8	-97.0	0.70895	-9999	-9999	-9999	-9999	DIG 2019-0002
100/11-12-058-22W4/00	LD65	23.0	48.0	-9999	-9999	0.3	-9999	-9999	198	-9999	1.000	-4.5	-98.0	0.70959	-9999	-9999	-9999	-9999	Connolly et al., 1990
100/11-14-057-21W4/00	LD66	20.0	43.0	-9999	-9999	0.3	-9999	-9999	219	-9999	1.000	-5.4	-88.0	0.70944	-9999	-9999	-9999	-9999	Connolly et al., 1990
100/11-15-050-26W4/00	LD67	50.0	142.0	-9999	-9999	17.5	-9999	-9999	1190	-9999	7.000	2.4	-104.0	0.70872	-9999	-9999	-9999	-9999	Connolly et al., 1990
100/09-29-057-19W4/00	CO01	14.8	29.0	8.0	538	<1	<0.02	0.72	283	0.028	0.740	-4.1	-82.5	0.70878	23.3	46.0	-9999	-9999	DIG 2023-0019
100/13-28-057-19W4/00	CO02	14.6	32.0	8.0	320	<1	<0.02	0.70	260	0.025	0.540	-3.9	-82.0	0.70876	22.4	45.9	-9999	-9999	DIG 2023-0019
102/04-28-057-19W4/00	CO03	15.0	34.0	8.0	307	<1	<0.02	0.68	290	0.026	0.840	-3.7	-81.6	0.70873	22.4	46.4	-9999	-9999	DIG 2023-0019
100/12-28-057-19W4/00	CO04	16.0	-9999.0	-9999	-9999	-9999	-9999	-9999	261	-9999	0.670	-4.3	-80.3	0.70878	-9999	-9999	-9999	-9999	DIG 2011-0007
100/01-18-060-18W5/00	SH01	87.5	140.0	-9999	-9999	5.9	-9999	-9999	510	-9999	538.000	-9999	-9999	0.72584	6.6	-9999	-9999	-9999	OFR 2011-10
100/02-17-071-18W5/00	SH02	29.2	68.4	-9999	-9999	-9999	-9999	-9999	509	-9999	3.720	-2.4	-62.0	0.71832	-9999	-9999	-9999	-9999	DIG 2019-0002
100/02-19-067-10W5/00	SH03	6.9	30.7	32.4	502	<2.40	ND	-9999	107	-9999	0.802	-12.0	-114.0	0.71068	-9999	-9999	-9999	-9999	DIG 2021-0022
100/02-30-071-18W5/00	SH04	19.3	47.1	-9999	-9999	-9999	-9999	-9999	329	-9999	1.752	-4.1	-74.0	0.71577	-9999	-9999	-9999	-9999	DIG 2019-0002
100/06-19-067-10W5/00	SH05	8.3	37.4	42.0	591	<2.39	ND	-9999	134	-9999	1.100	-11.9	-113.0	0.71083	-9999	-9999	-9999	-9999	DIG 2021-0022
100/04-30-065-13W5/00	SH06	42.9	121.0	-9999	-9999	767.0	-9999	-9999	-9999	-9999	5.300	-9999	-9999	0.71942	11.7	-9999	-9999	-9999	OFR 2011-10
100/05-23-059-18W5/00	SH07	93.9	181.0	-9999	-9999	-9999	-9999	-9999	847	-9999	1130.000	-9999	-9999	0.72384	10.7	-9999	-9999	-9999	OFR 2011-10
100/09-11-061-12W5/00	SH09	36.0	157.8	-9999	-9999	-9999	-9999	-9999	300	-9999	3.682	5.0	-50.0	0.70918	-9999	-9999	-9999	-9999	DIG 2011-0007
100/09-27-059-18W5/00	SH10	86.4	158.0	-9999	-9999	5.3	-9999	-9999	-9999	-9999	1400.000	-9999	-9999	0.72532	10.8	-9999	-9999	-9999	OFR 2011-10
100/10-02-059-18W5/00	SH11	112.0	223.0	-9999	-9999	-9999	-9999	-9999	919	-9999	408.000	-9999	-9999	0.72077	12.0	-9999	-9999	-9999	OFR 2011-10

UWI	Label	Li (mg/L)	B* (mg/L)	Si* (mg/L)	S* (mg/L)	Fe* (mg/L)	As* (mg/L)	Rb* (mg/L)	Sr* (mg/L)	Cs* (mg/L)	Ba* (mg/L)	$\delta^{18}O$* (‰)	$\delta^{2}H$* (‰)	$^{87}Sr/^{86}Sr$*	$\delta^{7}Li$* (‰)	$\delta^{11}B$* (‰)	$\delta^{18}O\_SO_4$* (‰)	$\delta^{34}S\_SO_4$* (‰)	Source
100/10-04-067-18W5/00	SH12	14.0	46.5	-9999	-9999	2.9	-9999	-9999	-9999	-9999	1.100	-9999	-9999	0.71035	10.1	-9999	-9999	-9999	OFR 2011-10
100/10-15-059-18W5/00	SH13	85.8	187.0	-9999	-9999	-9999	-9999	-9999	978	-9999	896.000	-9999	-9999	0.72047	10.2	-9999	-9999	-9999	OFR 2011-10
100/10-21-059-18W5/00	SH14	86.8	173.0	-9999	-9999	6.0	-9999	-9999	785	-9999	1390.000	-9999	-9999	0.72490	12.9	-9999	-9999	-9999	OFR 2011-10
100/11-27-064-13W5/00	SH15	9.1	42.1	-9999	-9999	-9999	-9999	-9999	76	-9999	0.573	-11.4	-116.0	0.70936	-9999	-9999	-9999	-9999	DIG 2011-0007
100/12-10-064-19W5/00	SH16	24.0	84.9	-9999	-9999	2.0	-9999	-9999	-9999	-9999	12.000	-9999	-9999	0.70988	5.8	-9999	-9999	-9999	OFR 2011-10
100/12-17-067-18W5/00	SH17	14.0	56.0	-9999	-9999	-9999	-9999	-9999	148	-9999	0.978	-10.8	-112.0	0.71020	-9999	-9999	-9999	-9999	DIG 2011-0007
100/12-18-063-10W5/00	SH18	11.4	43.3	-9999	-9999	-9999	-9999	-9999	111	-9999	0.619	-8.4	-99.0	0.70991	-9999	-9999	-9999	-9999	DIG 2019-0002
100/12-21-067-18W5/03	SH19	13.9	55.5	-9999	-9999	-9999	-9999	-9999	153	-9999	1.109	-10.5	-110.0	0.71039	-9999	-9999	-9999	-9999	DIG 2011-0007
S0/04-03-060-18W5/02	SH20	87.1	154.0	-9999	-9999	-9999	-9999	-9999	869	-9999	1290.000	-9999	-9999	0.72575	-9999	-9999	-9999	-9999	OFR 2011-10
100/02-28-063-10W5/00	SH21	10.1	49.0	34.0	500	<1	<0.02	0.61	78	0.064	0.500	-8.4	-100.6	0.70992	11.5	32.6	-9999	-9999	DIG 2023-0019
100/04-07-061-12W5/00	SH22	28.1	148.0	23.0	315	<1	<0.02	2.13	192	0.237	0.770	2.7	-64.1	0.70913	11.3	31.4	-9999	-9999	DIG 2023-0019
100/04-17-063-11W5/00	SH23	13.0	77.0	34.0	418	<1	<0.02	0.99	114	0.126	0.850	-4.6	-85.6	0.70948	10.1	31.7	-9999	-9999	DIG 2023-0019
100/06-06-064-11W5/00	SH24	13.1	77.0	35.0	485	<1	<0.02	1.02	110	0.115	0.810	-4.7	-86.8	0.70939	11.4	31.6	-9999	-9999	DIG 2023-0019
100/08-09-064-11W5/00	SH25	8.4	41.0	39.0	328	<1	<0.02	0.58	78	0.063	0.940	-8.1	-99.1	0.70994	11.7	32.7	-9999	-9999	DIG 2023-0019
100/10-19-063-11W5/00	SH26	16.7	103.0	33.0	432	<1	<0.02	1.36	138	0.167	1.010	-1.6	-74.0	0.70921	10.9	31.2	-9999	-9999	DIG 2023-0019
100/12-27-063-11W5/00	SH27	9.2	44.0	40.0	491	<1	<0.02	0.63	85	0.068	0.600	-8.0	-98.9	0.70980	12.0	32.8	-9999	-9999	DIG 2023-0019
100/13-03-065-10W5/02	SH28	27.1	119.0	14.0	173	<1	<0.02	2.31	261	0.340	3.770	2.8	-47.4	0.71030	12.2	32.4	-9999	-9999	DIG 2023-0019
100/13-13-061-13W5/00	SH29	27.8	152.0	28.0	314	<1	<0.02	2.04	204	0.236	1.500	4.1	-51.4	0.70941	11.7	32.8	-9999	-9999	DIG 2023-0019
100/14-01-063-12W5/00	SH30	22.7	96.0	17.0	331	<1	<0.02	1.47	188	0.165	1.470	2.6	-53.7	0.71008	12.5	36.2	-9999	-9999	DIG 2023-0019
100/14-30-063-10W5/00	SH31	9.5	46.0	36.0	509	<1	<0.02	0.64	85	0.071	0.570	-7.6	-98.0	0.70991	11.8	32.7	-9999	-9999	DIG 2023-0019
100/01-32-063-09W5/00	SH32	22.9	106.0	15.0	134	10.0	<0.02	2.57	289	0.258	4.690	1.7	-54.9	0.70929	13.7	33.1	-9999	-9999	DIG 2023-0019
100/04-08-065-23W5/00	SH33	11.1	51.0	64.0	108	<1	<0.02	1.37	29	0.190	1.580	-7.7	-105.1	0.70979	14.5	26.6	-9999	-9999	DIG 2023-0019
100/15-29-064-23W5/00	SH34	12.1	58.0	65.0	849	<1	<0.02	1.48	31	0.226	1.470	-6.7	-101.4	0.70962	13.7	27.3	-9999	-9999	DIG 2023-0019
102/10-32-064-23W5/00	SH35	7.6	35.0	66.0	92	<1	<0.02	0.94	23	0.133	1.270	-11.9	-122.4	0.71002	14.6	27.3	-9999	-9999	DIG 2023-0019
100/07-06-087-14W5/00	SP01	12.3	24.0	6.0	72	<1	<0.02	0.64	578	0.023	3.710	-2.2	-44.2	0.71607	20.9	33.9	-9999	-9999	DIG 2023-0019
100/09-09-083-14W5/00	SP02	9.6	20.0	3.0	97	11.0	<0.02	2.68	857	0.119	5.300	-4.0	-41.8	0.71819	18.5	31.8	-9999	-9999	DIG 2023-0019
100/10-19-076-10W5/00	SP03	11.5	23.0	7.0	207	2.0	<0.02	0.84	363	0.060	1.920	-2.6	-49.3	0.71295	14.7	-9999	-9999	-9999	DIG 2023-0019
100/13-04-085-09W5/00	SP04	7.2	14.0	6.0	349	3950.0	<0.02	0.41	270	0.015	0.460	-10.2	-97.3	0.71244	21.1	43.2	-9999	-9999	DIG 2023-0019
100/14-07-087-14W5/00	SP05	15.2	26.0	6.0	207	<1	<0.02	0.71	570	0.025	1.340	-2.3	-43.7	0.71795	21.1	33.7	-9999	-9999	DIG 2023-0019

UWI	Label	Li (mg/L)	B* (mg/L)	Si* (mg/L)	S* (mg/L)	Fe* (mg/L)	As* (mg/L)	Rb* (mg/L)	Sr* (mg/L)	Cs* (mg/L)	Ba* (mg/L)	δ¹⁸O* (‰)	δ²H* (‰)	⁸⁷Sr/⁸⁶Sr*	δ⁷Li* (‰)	δ¹¹B* (‰)	δ¹⁸O_SO₄* (‰)	δ³⁴S_SO₄* (‰)	Source
100/16-01-087-15W5/00	SP06	12.4	23.0	7.0	75	<1	<0.02	0.60	613	0.024	3.240	-2.3	-43.7	0.71675	21.2	-9999	-9999	-9999	DIG 2023-0019
100/16-22-083-14W5/00	SP08	18.9	39.0	5.0	217	<1	<0.02	1.74	698	0.099	2.530	-2.5	-45.1	0.71857	20.7	33.2	-9999	-9999	DIG 2023-0019
100/01-28-097-09W6/00	SP09	21.0	39.0	33.0	75	<1	<0.02	1.00	368	0.205	6.000	0.8	-35.4	0.71274	14.9	29.0	-9999	-9999	DIG 2023-0019
100/08-08-096-10W6/00	SP10	18.0	29.0	16.0	79	7.0	<0.02	1.20	546	0.238	6.800	1.3	-34.5	0.71212	13.9	29.1	-9999	-9999	DIG 2023-0019
100/09-21-097-09W6/00	SP11	29.0	52.0	41.0	113	4.0	<0.02	1.40	490	0.252	7.100	1.2	-34.4	0.71276	14.7	28.9	-9999	-9999	DIG 2023-0019
100/11-25-097-09W6/00	SP12	6.0	15.0	10.0	32	<1	<0.02	0.35	134	0.070	2.000	-2.7	-49.1	0.71237	13.8	29.0	-9999	-9999	DIG 2023-0019
100/12-08-096-10W6/00	SP13	28.0	42.0	38.0	85	6.0	<0.02	1.50	678	0.284	8.400	1.3	-36.4	0.71215	12.8	28.1	-9999	-9999	DIG 2023-0019
100/16-32-097-08W6/00	SP14	16.0	32.0	36.0	141	2.0	<0.02	0.92	425	0.198	3.500	0.5	-34.2	0.71204	13.0	29.6	-9999	-9999	DIG 2023-0019
100/14-17-077-10W5/00	SP15	11.7	27.0	5.0	219	<1	<0.02	0.92	372	0.065	1.770	-2.1	-48.7	0.71405	14.9	-9999	-9999	-9999	DIG 2023-0019
100/03-21-066-13W5/00	BL01	14.6	79.0	20.0	145	5.0	<0.02	1.39	174	0.189	3.400	-1.2	-66.4	0.70944	12.3	30.6	-9999	-9999	DIG 2023-0019
100/04-33-063-09W5/00	BL02	25.1	90.0	20.0	95	103.0	<0.02	1.55	300	0.196	4.590	0.0	-62.3	0.71004	12.7	33.6	-9999	-9999	DIG 2023-0019
100/05-07-064-10W5/02	BL03	9.3	44.0	36.0	470	<1	<0.02	0.65	84	0.077	0.570	-7.7	-97.5	0.70995	10.4	32.3	-9999	-9999	DIG 2023-0019
100/07-17-064-10W5/00	BL04	19.7	116.0	21.0	229	<1	<0.02	2.26	201	0.311	2.640	2.4	-52.7	0.70900	12.9	33.0	-9999	-9999	DIG 2023-0019
100/08-15-064-11W5/00	BL05	13.0	65.0	39.0	415	<1	<0.02	0.91	113	0.098	1.110	-5.6	-87.7	0.71008	11.3	32.1	-9999	-9999	DIG 2023-0019
100/09-06-063-14W5/02	BL06	22.4	133.0	18.0	34	<1	<0.02	2.91	193	0.438	7.840	4.8	-53.0	0.70958	13.6	29.3	-9999	-9999	DIG 2023-0019
100/11-34-064-10W5/02	BL07	31.3	118.0	23.0	191	<1	<0.02	2.38	287	0.326	5.380	2.0	-51.4	0.70940	12.2	-9999	-9999	-9999	DIG 2023-0019
100/12-20-061-12W5/00	BL08	21.4	111.0	22.0	373	<1	<0.02	1.46	139	0.160	0.820	0.5	-66.7	0.70927	11.7	33.0	-9999	-9999	DIG 2023-0019
100/16-29-063-09W5/00	BL10	20.9	108.0	14.0	162	18.0	<0.02	2.68	272	0.225	3.770	1.1	-56.5	0.70920	13.4	32.3	-9999	-9999	DIG 2023-0019
102/04-09-064-10W5/00	BL11	9.4	45.0	38.0	450	<1	<0.02	0.65	85	0.073	0.620	-7.8	-97.6	0.70989	11.6	32.0	-9999	-9999	DIG 2023-0019
102/16-05-061-12W5/00	BL12	26.8	132.0	26.0	294	<1	<0.02	2.12	191	0.238	0.960	3.9	-53.5	0.70930	11.6	32.2	-9999	-9999	DIG 2023-0019
100/10-14-063-11W5/00	BL13	9.9	48.0	37.0	552	<1	<0.02	0.68	89	0.072	0.480	-7.4	-96.1	0.70985	11.9	32.9	-9999	-9999	DIG 2023-0019
100/16-18-064-11W5/00	BL14	20.8	149.0	15.0	215	1.0	<0.02	2.65	223	0.414	3.070	4.6	-47.3	0.70888	12.4	29.8	-9999	-9999	DIG 2023-0019
102/05-36-065-13W5/02	BL15	14.6	84.0	22.0	147	<1	<0.02	2.24	151	0.190	3.200	0.0	-68.0	0.70872	11.7	31.7	-9999	-9999	DIG 2023-0019
100/03-34-063-10W5/02	BL16	10.6	40.5	-9999	-9999	-9999	-9999	-9999	105	-9999	0.700	-8.2	-98.0	0.70992	-9999	-9999	-9999	-9999	DIG 2019-0002
100/12-19-070-11W5/00	BL17	2.0	6.8	-9999	-9999	-9999	-9999	-9999	56	-9999	0.190	-12.5	-114.0	0.71184	-9999	-9999	-9999	-9999	DIG 2019-0002
100/12-19-070-11W5/B	BL18	2.0	6.8	-9999	-9999	-9999	-9999	-9999	55	-9999	0.190	-12.5	-113.0	0.71188	-9999	-9999	-9999	-9999	DIG 2019-0002
102/02-23-077-21W5/00	BL19	23.3	24.9	-9999	-9999	80.5	-9999	-9999	793	-9999	8.550	-3.0	-47.0	0.72037	-9999	-9999	-9999	-9999	DIG 2019-0002
100/07-31-067-10W5/00	BL20	6.1	27.1	32.7	371	<2.41	ND	-9999	98	-9999	1.000	-12.0	-114.0	0.71085	-9999	-9999	-9999	-9999	DIG 2021-0022
100/04-14-078-08W5/00	GL01	16.7	46.6	<13.2	263	66.4	ND	-9999	626	-9999	2.780	-4.8	-59.0	0.72170	-9999	-9999	-9999	-9999	DIG 2021-0022

UWI	Label	Li (mg/L)	B* (mg/L)	Si* (mg/L)	S* (mg/L)	Fe* (mg/L)	As* (mg/L)	Rb* (mg/L)	Sr* (mg/L)	Cs* (mg/L)	Ba* (mg/L)	$\delta^{18}O$* (‰)	$\delta^{2}H$* (‰)	$^{87}Sr/^{86}Sr$*	$\delta^{7}Li$* (‰)	$\delta^{11}B$* (‰)	$\delta^{18}O\_SO_4$* (‰)	$\delta^{34}S\_SO_4$* (‰)	Source
100/09-19-078-11W5/00	GL02	18.9	42.0	6.0	180	17.0	<0.02	2.36	607	0.113	2.670	-2.3	-48.5	0.70957	21.9	33.6	12.4	19.9	DIG 2023-0019
100/13-18-076-10W5/00	GL03	21.3	44.0	5.0	153	34.0	<0.02	1.81	478	0.107	3.130	-1.4	-48.6	0.71486	20.5	35.7	11.2	17.5	DIG 2023-0019
100/15-25-077-08W5/00	GL04	20.9	49.1	<14.7	184	71.9	ND	-9999	770	-9999	3.980	-3.8	-55.0	0.71019	-9999	-9999	-9999	-9999	DIG 2021-0022
100/02-07-080-08W5/00	GL05	10.9	27.0	13.0	343	<1	<0.02	0.41	315	0.008	0.650	-8.6	-84.5	0.71092	21.9	36.9	-9999	-9999	DIG 2023-0019
100/04-30-076-10W5/00	GL06	19.0	43.0	5.0	153	34.0	<0.02	1.83	458	0.096	3.260	-1.7	-49.3	0.71259	20.5	-9999	-9999	-9999	DIG 2023-0019
100/10-23-079-08W5/00	GL07	11.5	30.0	14.0	342	<1	<0.02	0.45	305	0.007	0.630	-8.3	-86.2	0.71085	22.0	36.7	-9999	-9999	DIG 2023-0019
103/10-29-079-08W5/00	GL08	11.3	29.0	15.0	390	<1	<0.02	0.40	306	0.008	0.640	-8.8	-90.4	0.71087	24.3	36.4	-9999	-9999	DIG 2023-0019
100/01-03-096-06W5/00	KR01	11.8	32.0	4.0	250	<1	<0.02	1.05	444	0.031	0.200	-2.6	-44.6	0.71563	27.1	34.4	12.6	20.3	DIG 2023-0019
100/01-34-089-04W5/00	KR02	7.9	28.0	1.0	91	13.0	<0.02	1.77	1430	0.026	4.720	-5.0	-43.4	0.71226	26.6	32.4	-9999	-9999	DIG 2023-0019
100/02-23-081-10W5/00	KR03	20.9	47.0	6.0	183	75.0	<0.02	3.34	1110	0.127	3.820	-2.4	-48.3	0.71922	22.6	42.0	-9999	-9999	DIG 2023-0019
100/03-05-095-03W5/00	KR04	13.3	46.0	1.0	183	<1	<0.02	1.25	367	0.021	0.580	-2.9	-46.0	0.71272	25.4	35.2	-9999	-9999	DIG 2023-0019
100/04-04-093-05W5/00	KR05	8.6	25.0	4.0	143	<1	<0.02	1.23	704	0.013	1.150	-4.4	-44.3	0.71496	24.7	32.0	-9999	-9999	DIG 2023-0019
100/04-10-092-05W5/00	KR06	7.5	27.0	4.0	126	11.0	<0.02	1.40	957	0.021	3.190	-4.6	-41.7	0.71548	27.2	33.0	12.2	17.7	DIG 2023-0019
100/05-27-122-22W5/00	KR07	25.5	75.0	9.0	390	<1	<0.02	2.19	245	0.211	0.420	-5.8	-71.7	0.71517	14.1	24.3	-9999	-9999	DIG 2023-0019
100/06-01-094-02W5/02	KR08	20.8	90.0	4.0	296	<1	<0.02	2.34	692	0.045	1.100	-2.9	-45.2	0.71325	25.3	33.5	-9999	-9999	DIG 2023-0019
100/06-18-094-03W5/00	KR09	14.3	40.0	2.0	208	<1	<0.02	1.30	576	0.024	0.600	-3.7	-42.8	0.71176	26.0	33.3	-9999	-9999	DIG 2023-0019
100/06-23-082-09W5/00	KR10	17.8	37.0	6.0	185	108.0	<0.02	3.77	1300	0.138	4.670	-2.5	-45.2	0.71839	21.7	37.7	12.1	17.0	DIG 2023-0019
100/07-34-092-04W5/00	KR11	12.0	41.0	2.0	151	<1	<0.02	1.76	1000	0.021	0.090	-4.5	-43.4	0.71322	25.5	33.2	-9999	-9999	DIG 2023-0019
100/08-05-082-09W5/02	KR12	14.4	27.0	3.0	147	32.0	<0.02	2.33	891	0.103	2.230	-2.9	-47.1	0.71790	22.7	37.0	-9999	-9999	DIG 2023-0019
100/09-10-089-03W5/00	KR13	9.8	30.0	2.0	92	4.0	<0.02	2.03	1200	0.032	3.710	-4.8	-44.0	0.71227	23.9	32.1	-9999	-9999	DIG 2023-0019
100/09-28-082-10W5/00	KR14	9.1	25.0	4.0	96	21.0	<0.02	4.11	1450	0.115	8.360	-4.7	-42.5	0.71618	21.4	34.1	10.5	12.4	DIG 2023-0019
100/10-03-090-03W5/00	KR15	15.0	48.0	4.0	190	<1	<0.02	2.58	1500	0.042	3.970	-4.6	-44.8	0.71279	26.5	32.6	-9999	-9999	DIG 2023-0019
103/10-32-110-07W6/00	KR17	39.0	138.0	14.0	202	<1	<0.02	3.76	351	0.677	2.060	-2.9	-59.3	0.71750	13.5	22.4	-9999	-9999	DIG 2023-0019
100/13-06-111-06W6/03	KR18	36.2	177.0	14.0	179	<1	<0.02	4.49	475	0.459	4.530	-0.9	-48.7	0.71565	14.9	21.2	-9999	-9999	DIG 2023-0019
100/14-32-093-03W5/00	KR19	10.2	31.0	3.0	207	2.0	<0.02	1.08	430	0.017	0.260	-5.3	-55.1	0.71026	26.3	33.0	13.7	21.4	DIG 2023-0019
100/14-36-092-05W5/00	KR20	9.1	23.0	<1	122	<1	<0.02	1.14	777	0.021	1.310	-4.5	-43.4	0.71404	28.3	-9999	-9999	-9999	DIG 2023-0019
100/15-30-089-03W5/00	KR21	8.2	26.0	2.0	92	4.0	<0.02	1.85	1160	0.031	3.940	-5.1	-45.2	0.71254	27.4	32.5	-9999	-9999	DIG 2023-0019
100/16-05-081-09W5/00	KR22	20.5	40.0	8.0	140	62.0	<0.02	3.23	1160	0.137	3.660	-2.2	-46.8	0.71879	22.4	38.9	12.4	16.5	DIG 2023-0019
100/16-13-081-10W5/00	KR23	17.6	35.0	5.0	135	62.0	<0.02	2.79	1010	0.111	3.450	-2.6	-48.2	0.71856	23.4	41.8	-9999	-9999	DIG 2023-0019

UWI	Label	Li (mg/L)	B* (mg/L)	Si* (mg/L)	S* (mg/L)	Fe* (mg/L)	As* (mg/L)	Rb* (mg/L)	Sr* (mg/L)	Cs* (mg/L)	Ba* (mg/L)	$\delta^{18}O$* (‰)	$\delta^{2}H$* (‰)	$^{87}Sr/^{86}Sr$*	$\delta^{7}Li$* (‰)	$\delta^{11}B$* (‰)	$\delta^{18}O\_SO_4$* (‰)	$\delta^{34}S\_SO_4$* (‰)	Source
100/16-27-096-06W5/00	KR24	8.6	44.0	3.0	205	<1	<0.02	1.06	420	0.025	0.440	-2.4	-42.2	0.71491	19.2	32.4	-9999	-9999	DIG 2023-0019
102/10-07-112-05W6/00	KR25	31.2	125.0	10.0	186	<1	<0.02	3.08	300	0.356	1.720	-2.6	-53.1	0.71337	16.4	23.9	-9999	-9999	DIG 2023-0019
102/14-13-090-03W5/00	KR26	18.4	57.0	4.0	273	<1	<0.02	3.13	1740	0.037	3.760	-4.4	-44.8	0.71247	26.6	31.5	-9999	-9999	DIG 2023-0019
102/15-19-094-03W5/02	KR27	8.3	23.0	3.0	139	2.0	<0.02	1.17	655	0.014	1.340	-4.2	-43.5	0.71460	27.7	31.5	-9999	-9999	DIG 2023-0019
100/10-22-122-21W5/00	KR28	18.2	50.0	5.0	159	<1	<0.02	2.74	743	0.461	2.950	-6.0	-58.3	0.71940	16.9	27.9	-9999	-9999	DIG 2023-0019
102/13-08-089-03W5/00	KR29	9.8	38.0	1.0	148	<1	<0.02	2.12	1250	0.037	3.520	-5.5	-52.2	0.71198	25.7	32.7	-9999	-9999	DIG 2023-0019
100/10-32-081-09W5/02	KR30	14.4	27.0	5.0	261	8.0	<0.02	0.70	388	0.017	1.290	-6.0	-69.7	0.71006	18.8	37.6	-9999	-9999	DIG 2023-0019
100/12-23-087-07W5/00	KR31	7.1	18.0	<1	117	22.0	<0.02	1.48	887	0.044	3.240	-3.4	-43.6	0.71437	27.6	37.0	-9999	-9999	DIG 2023-0019
100/14-30-087-07W5/02	KR32	7.7	19.0	7.0	138	29.0	<0.02	1.50	634	0.041	2.060	-2.7	-44.1	0.71681	27.4	38.9	-9999	-9999	DIG 2023-0019
102/05-05-110-04W6/00	KR33	29.7	133.0	11.0	142	<1	<0.02	3.41	357	0.290	2.630	-2.5	-50.7	0.71459	17.0	25.2	-9999	-9999	DIG 2023-0019
102/10-32-111-05W6/03	KR34	35.5	152.0	11.0	185	<1	<0.02	3.61	339	0.294	1.900	-2.5	-53.2	0.71335	15.5	26.0	-9999	-9999	DIG 2023-0019
100/01-16-087-08W5/00	GW01	8.7	23.0	3.0	175	61.0	<0.02	1.44	705	0.035	1.740	-2.9	-44.2	0.71727	24.5	37.6	13.3	25.4	DIG 2023-0019
100/01-36-086-11W5/00	GW02	25.1	56.0	4.0	428	<1	<0.02	1.70	935	0.033	1.370	-2.6	-48.3	0.71790	22.6	33.4	15.6	38.0	DIG 2023-0019
100/03-11-087-09W5/00	GW03	18.1	49.0	3.0	350	97.0	<0.02	1.49	809	0.040	1.680	-2.7	-47.8	0.71534	24.4	34.8	14.3	27.5	DIG 2023-0019
100/05-11-088-09W5/00	GW04	10.0	32.0	3.0	270	<1	<0.02	1.02	866	0.018	1.140	-2.9	-43.4	0.71562	26.9	32.7	13.2	25.7	DIG 2023-0019
100/06-12-087-10W5/00	GW05	17.2	42.0	3.0	281	38.0	<0.02	1.34	747	0.033	0.950	-2.7	-47.8	0.70985	22.7	32.1	15.5	31.9	DIG 2023-0019
100/06-23-086-11W5/00	GW06	16.7	34.0	2.0	269	7.0	<0.02	1.14	535	0.035	0.800	-2.6	-48.8	0.71782	21.2	30.2	15.8	35.6	DIG 2023-0019
100/07-30-086-10W5/00	GW07	22.3	48.0	3.0	393	41.0	<0.02	1.54	696	0.033	1.020	-2.6	-48.7	0.71879	21.6	29.4	15.1	32.3	DIG 2023-0019
100/08-08-087-09W5/00	GW08	9.0	26.0	2.0	242	<1	<0.02	0.77	575	0.019	0.920	-2.8	-44.5	0.71737	26.7	34.4	14.3	29.5	DIG 2023-0019
102/02-09-085-09W5/02	GW09	7.9	21.0	4.0	115	27.0	<0.02	2.10	771	0.060	3.130	-4.9	-41.3	0.71752	21.6	37.7	-9999	-9999	DIG 2023-0019
100/16-21-087-09W5/00	GW11	10.8	38.0	4.0	399	66.0	<0.02	0.87	878	0.023	1.520	-2.6	-46.6	0.71579	26.9	30.4	12.5	22.1	DIG 2023-0019
100/06-24-090-10W5/00	GW12	11.2	26.0	7.0	300	<1	<0.02	0.70	341	0.012	0.300	-2.0	-44.0	0.71981	26.0	36.3	-9999	-9999	DIG 2023-0019
100/07-35-090-10W5/00	GW13	12.1	29.0	7.0	318	1.0	<0.02	0.70	344	0.012	0.440	-2.1	-43.5	0.72002	25.7	36.1	-9999	-9999	DIG 2023-0019
100/08-12-090-09W5/00	GW14	7.6	22.0	4.0	268	1.0	<0.02	0.55	379	0.007	0.450	-2.4	-43.7	0.71876	29.1	33.9	-9999	-9999	DIG 2023-0019
100/09-03-091-10W5/00	GW15	12.0	28.0	6.0	308	3.0	<0.02	0.73	347	0.013	0.360	-2.0	-43.1	0.72006	26.5	35.7	-9999	-9999	DIG 2023-0019
100/09-30-090-09W5/00	GW16	12.2	30.0	6.0	333	4.0	<0.02	0.74	339	0.012	0.410	-1.9	-44.4	0.71982	28.5	36.2	-9999	-9999	DIG 2023-0019
100/10-11-090-09W5/00	GW17	9.5	26.0	6.0	305	4.0	<0.02	0.64	339	0.008	0.400	-2.2	-44.8	0.71920	27.2	35.8	-9999	-9999	DIG 2023-0019
100/12-35-090-10W5/00	GW18	12.2	29.0	7.0	327	1.0	<0.02	0.69	351	0.009	0.430	-2.2	-43.0	0.72006	24.4	36.0	-9999	-9999	DIG 2023-0019

* -9999 indicates an unrecorded value

Abbreviation: ND, not detected

References

Connolly et al., 1990	Connolly, C.A., Walter, L.M., Baadsgaard, H. and Longstaff, F.J. (1990): Origin and evolution of formation waters, Alberta Basin, Western Canada Sedimentary Basin. II. Isotope systematics and water mixing; Applied Geochemistry, v. 5, no. 4, p. 397–413.
DIG 2011-0007	Huff, G.F., Stewart, S.A., Riddell, J.T.F. and Chisholm, S. (2011): Water geochemical data, saline aquifer project (tabular data, tab-delimited format); Energy Resources Conservation Board, ERCB/AGS Digital Data 2011-0007.
DIG 2012-0001	Huff, G.F., Bechtel, D.J., Stewart, S.A., Brock, E. and Heikkinen, C. (2012): Water geochemical data, saline aquifer project, 2011 (tabular data, tab-delimited format); Energy Resources Conservation Board, ERCB/AGS Digital Data 2012-0001.
DIG 2019-0002	Huff, G.F., Lopez, G.P. and Weiss, J.A. (2019): Water geochemistry of selected formation brines in the Alberta Basin, Canada (tabular data, tab-delimited format); Alberta Energy Regulator / Alberta Geological Survey, AER/AGS Digital Data 2019-0002.
DIG 2021-0022	Reimert, C., Lyster, S., Hauck, T.E., Palombi, D., Playter, T.L., Lopez, G.P. and Schultz, S.K. (2022): Water geochemical data, Lithium Prospectivity Project, 2021 (tabular data, tab-delimited format); Alberta Energy Regulator / Alberta Geological Survey, AER/AGS Digital Data 2021-0022.
DIG 2023-0019	Reimert, C., Lyster, S., Palombi, D. and Bernal, N. (2025): Brine geochemical data, mineral mapping program, 2021–2024 (tabular data, tab-delimited format); Alberta Energy Regulator / Alberta Geological Survey, AER/AGS Digital Data 2023-0019.
OFR 2011-10	Eccles, D.R. and Berhane, H. (2011): Geological introduction to lithium-rich formation water with emphasis on the Fox Creek area of west-central Alberta (NTS 83F and 83K); Energy Resources Conservation Board, ERCB/AGS Open File Report 2011-10, 22 p.